

WL-TR-94-4030

FATIGUE CRACK GROWTH BEHAVIOR OF  
SMALL AND LARGE CRACKS IN TITANIUM ALLOYS AND  
INTERMETALLICS

AD--A278 875



K.S. RAVICHANDRAN, PHD

SYSTRAN CORPORATION  
4126 LINDEN AVENUE  
DAYTON, OH 45432-3068

MARCH 1994

FINAL REPORT FOR 01/21/91-01/29/92

APPROVED FOR PUBLIC RELEASE; DISTRIBUTION IS UNLIMITED.



DTIC  
ELECTE  
MAY 09 1994  
S B D

MATERIALS DIRECTORATE  
WRIGHT LABORATORY  
AIR FORCE MATERIEL COMMAND  
WRIGHT PATTERSON AFB OH 45433-7734

94-13837



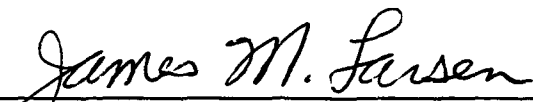
94 5 06 064

## NOTICE

When Government drawings, specifications, or other data are used for any other purpose other than in connection with a definitely Government-related procurement, the United States Government incurs no responsibility or any obligation whatsoever. The fact that the government may have formulated or in any way supplied the said drawings, specifications, or other data, is not to be regarded by implication, or otherwise in any manner construed, as licensing the holder, or any other person or corporation, or as conveying any rights or permission to manufacture, use, or sell any patented invention that may be related thereto.

This report is releasable to the National Technical Information Service (NTIS). At NTIS, it will be available to the general public, including foreign nations.

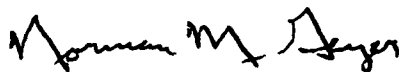
This technical report has been reviewed and is approved for publication.



JAMES M. LARSEN  
Materials Behavior Branch  
Metals and Ceramics Division



ALLAN W. GUNDERSON, Chief  
Materials Behavior Branch  
Metals and Ceramics Division



NORMAN M. GEYER, Acting Chief  
Metals and Ceramics Division  
Materials Directorate

If your address has changed, if you wish to be removed from our mailing list, or if the addressee is no longer employed by your organization please notify WL/MLLN Bldg 655, 2230 Tenth St Ste 1, WPAFB, OH 45433-7817 to help us maintain a current mailing list.

Copies of this report should not be returned unless return is required by security considerations, contractual obligations, or notice on a specific document.

REPORT DOCUMENTATION PAGE			Form Approved OMB No. 0704-0188	
Public reporting burden for this collection of information is estimated to average 1 hour per response, including the time for reviewing instructions, searching existing data sources, gathering and maintaining the data needed, and completing and reviewing the collection of information. Send comments regarding this burden estimate or any other aspect of this collection of information, including suggestions for reducing this burden, to Washington Headquarters Services, Directorate for Information Operations and Reports, 1215 Jefferson David Highway, Suite 1204, Arlington, VA 22202-4302, and to the Office of Management and Budget, Paperwork Reduction Project (0704-0188), Washington, DC 20503.				
1. AGENCY USE ONLY (leave blank)		2. REPORT DATE March 1993		3. REPORT TYPE AND DATES COVERED Final Report 21 January 1991 - 29 January 1992
4. TITLE AND SUBTITLE  Fatigue Crack Growth Behavior of Small and Large Cracks in Titanium Alloys and Intermetallics			5. FUNDING NUMBERS PE 62102F PROJ 2418 TA 04 WU 77 Cont #F33615-90-C-5944	
6. AUTHOR(S)  K.S. Ravichandran, Ph.D.			8. PERFORMING ORGANIZATION REPORT NUMBER	
7. PERFORMING ORGANIZATION NAME(S) AND ADDRESS(ES) SYSTRAN Corporation 4126 Linden Avenue Dayton, OH 45432-3068			10. SPONSORING/MONITORING AGENCY REPORT NUMBER  WL-TR-94-4030	
9. SPONSORING/MONITORING AGENCY NAME(S) AND ADDRESS(ES) Materials Directorate Wright Laboratory Wright-Patterson AFB, OH 45433-7734				
11. SUPPLEMENTARY NOTES				
12a. DISTRIBUTION/AVAILABILITY STATEMENT Approved for public release; distribution is unlimited.			12b. DISTRIBUTION CODE	
13. ABSTRACT (Maximum 200 words)  This report is a compilation of results of research performed on small fatigue cracks in titanium alloys and titanium aluminide intermetallics. The principal theme underlying this investigation is the measurement of surface crack lengths and aspect ratios during the growth of three-dimensional small surface cracks in fatigue using a laser interferometric and photomicroscopic system at the Materials Behavior Branch, Materials Directorate, Wright Laboratory. It has been shown that such measurements could be made accurately on a number of candidate alloys systems comprising titanium alloys and newly developed titanium aluminide intermetallics. Fatigue crack growth rates could be accurately calculated and were correlated to data obtained on large cracks in the corresponding materials. Specific test programs, which were designed to accomplish this task and the corresponding results of the study, are categorically discussed in the following.  Measurements of shapes of three dimensional surface cracks continuously during fatigue crack growth were made in a near-alpha titanium alloy, Ti-6Al-2Sn-4Zr-6Mo. Crack aspect ratio measurements are demonstrated for cracks growing from electro-discharge-machined (EDM) notches of different geometries (shallow or deep). The experimentally determined aspect ratio variations during crack growth are shown to be in good agreement with the expected variations in aspect ratio. The fatigue crack growth rates of surface cracks, after incorporating the variations in aspect ratio in the calculations, agreed with the large-crack growth data.				
14. SUBJECT TERMS  Fatigue Crack Growth TiAl Fatigue Cracks  Small Crack Behavior TiAl Intermetallics Fatigue			15. NUMBER OF PAGES 110	
			16. PRICE CODE	
17. SECURITY CLASSIFICATION OF REPORT Unclassified		18. SECURITY CLASSIFICATION OF THIS PAGE Unclassified		19. SECURITY CLASSIFICATION OF ABSTRACT Unclassified
				20. LIMITATION OF ABSTRACT UL

### 13. Abstract (cont.)

Fatigue crack growth behavior of small surface cracks in  $\alpha_2$  (Ti<sub>3</sub>Al) based titanium aluminide alloys such as Ti-24Al-11Nb (at%) and Ti-25Al-17Nb-1Mo were also investigated in the Widmanstätten basketweave microstructural condition. The continuous variations in crack shape induced by microstructure have been measured and accounted for in crack growth rate calculations. The growth rates of large cracks were found to be similar in both the alloys. The differences in small crack behavior are attributed to the differences in the microstructural environment through which the cracks grew.

A theoretical simulation of crack shape variations in a polycrystalline titanium alloy, Ti-8Al was made. It has been shown that the variations in crack shape and the corresponding errors in stress intensity factor range ( $\Delta K$ ) calculations could be significant in small crack investigations. A large number of experiments were done on a coarse grained (200  $\mu\text{m}$ ) Ti-8Al alloy to measure crack aspect ratios using a laser interferometric system. The experimentally measured aspect ratios were found to agree closely with the expected theoretically simulated pattern of crack aspect ratio variations. After incorporating crack shape data into growth rate calculations, much of the scatter in small crack data could be reduced and the small crack behavior is similar to that of large cracks.

Fatigue crack growth data of large cracks in Ti-24Al-11Nb revealed that crack growth rates are sensitive to stress ratio. Crack growth rates in the three microstructures investigated, show higher crack growth rates at high stress ratios even after closure correction. While the crack growth rates varied little between the microstructures, the variation of crack closure was found to be sensitive to microstructure.

## FOREWORD

This report is a compilation of results of research sponsored by U. S. Air Force through the Materials Behavior Branch (MLLN), Materials Directorate, Wright Laboratory, Wright Patterson Air Force Base under a visiting scientist Contract No. F33615-90-C-5944, "Contributive Research and Development," Task 40. The Air Force program Monitor was Dr. James M. Larsen, Group Leader, Materials Behavior Group. The program manager for Systran Corporation was Mr. Milton E. Zellmer. The principal investigator for this program was Dr. K. S. Ravichandran.

<b>Accession For</b>	
NTIS GRA&I	<input checked="checked" type="checkbox"/>
DTIC TAB	<input type="checkbox"/>
Unannounced	<input type="checkbox"/>
Justification	
By	
Distribution/	
Availability Codes	
Dist	Avail and/or Special
A-1	

## TABLE OF CONTENTS

SECTION	PAGE
Foreword	iii
List of Figures	vii
List of Tables	xii
Summary	1
<b>Chapter 1</b>	
<b>Measurement of the shapes of Three Dimensional Surface Cracks in Ti-6Al-2Sn-4Zr-6Mo</b>	<b>4</b>
1.1 Introduction	4
1.2 A Compliance Expression for Surface Cracks	6
1.3 Measurement of Aspect Ratios of Surface Cracks	10
1.3.1 Material	10
1.3.2 Experimental Procedure	10
1.3.3 Determination of Aspect Ratio of a Surface Crack	13
1.3.4 Calculation of crack growth rates	17
1.4 Results and Discussion	18
1.5 Conclusions	30
1.6 Recommendations	30
Appendix 1.1	31
Appendix 1.2	33
Appendix 1.3	34
<b>Chapter 2</b>	
<b>The Growth Behavior of Small Fatigue Cracks in Titanium Aluminide Alloys</b>	<b>36</b>
2.1 Introduction	36
2.2 Experimental Procedure	36
2.3 Results	37
2.4 Discussion	43
2.5 Conclusions	45
2.6 Recommendations	45

### **Chapter 3**

#### **Simulation of Crack Shape and Crack Growth rates in Polycrystalline**

##### **Ti-8Al Titanium Alloy 46**

##### **3.1 Introduction 46**

##### **3.2 Crack Growth Simulation 45**

##### **3.3 Conclusions 55**

##### **3.4 Recommendations 56**

### **Chapter 4**

#### **Small Crack Growth in Ti-8Al Material with Coarse Grain Size 57**

##### **4.1 Introduction 57**

##### **4.2 Material and Experimental Procedure 57**

##### **4.3 Results and Discussion 59**

##### **4.3.1 Large Crack Data 59**

##### **4.3.2 Small Crack Data 60**

##### **4.3.3 Crack Growth Rates 71**

##### **4.4 Conclusions 77**

### **Chapter 5**

#### **Effects of Microstructure on Large Crack Growth Behavior of**

##### **Ti-24Al-11Nb 78**

##### **5.1 Introduction 78**

##### **5.2 Experimental Procedure 78**

##### **5.3 Results and Discussion 84**

##### **5.4 Conclusions 92**

### **References 93**

## LIST OF FIGURES

<b>Figure</b>	<b>Page</b>
<b>Chapter 1</b>	
1.1. (a) A schematic of the surface crack and (b) the surface profile illustrating the variables defining the crack	7
1.2. The variation of non-dimensional compliance as a function of aspect ratio of the surface crack	9
1.3. Microstructure of the titanium alloy, Ti-6Al-2Sn-4Zr-6Mo	11
1.4. The small crack fatigue specimen used for crack aspect ratio measurements	12
1.5. Micrographs of EDM notches; (a) shallow and (b) deep notch	14
1.6. A schematic of the laser interferometric and photomicroscopic system	15
1.7. Crack shapes after heat tinting of cracks grown from (a) shallow and (b) deep notches	16
1.8. The variation of surface crack length and crack compliance as a function of fatigue cycles in (a) shallow and (b) deep-notch specimens	19
1.9. A comparison of the experimentally and predicted crack aspect ratios for cracks growing from (a) shallow and (b) deep notches	21
1.10. Optical micrographs illustrating crack shapes delineated by heat tinting at various stages of crack growth from the notch; (a) $a/c=2.3$ , $2c=270\text{ }\mu\text{m}$ and (b) $a/c=2.0$ , $2c=300\text{ }\mu\text{m}$	22
1.11. A comparison of fatigue crack growth rates of cracks growing from a shallow notch as a function of $\Delta K$ , without and with aspect ratio correction, (a) and (b) respectively and (c) with aspect ratio correction as a function of $\Delta K_{\text{eff}}$ compared with the large crack growth data	25
1.12. A comparison of fatigue crack growth rates of cracks growing from deep notch as a function of $\Delta K$ , without and with aspect ratio correction, (a) and (b) respectively, and (c) with aspect ratio correction as a function of $\Delta K_{\text{eff}}$ compared with the large crack growth data	26



<b>Figure</b>	<b>Page</b>
1.13. Optical micrograph of a crack grown from a semicircular notch illustrating the two locations of compliance measurement	28
1.14. Variation of crack compliance measured at two locations (Fig. 1.13) when the crack grew from 1.5 mm to 2.5 mm. Also shown are the compliance measurements corrected for the asymmetry in the measurement location as well as the eccentricity (a measure of asymmetry of the measurement location)	29
1.15. A comparison of the aspect ratio calculated from the compliance measured at the center of the crack with that calculated from compliance from the asymmetric location after correction	29
A.1.1.1. An estimation of % error in the calculated aspect ratio due to errors in surface crack length for a range of aspect ratios of crack of 1.0 mm in surface length	32
A.1.2.1. The variation of non-dimensional stress intensity factors at the surface and at the depth of a surface crack as a function of aspect ratio, as calculated using the Newman-Raju formula [25]	33
A.1.3.1. The variation of the ratio of compliance of a surface crack to that of the crack-free specimen as a function of normalized surface crack length	35

## **Chapter 2**

2.1	Microstructures of (a) Ti-24-11 and (b) Ti-25-17-1 alloys	38
2.2	Crack growth rates versus $\Delta K$ ; (a) Ti-24-11 and (b) Ti-25-17-1 (Solid symbols: $da/dN$ vs. $\Delta K_a$ ; Open symbols: $dc/dN$ vs. $\Delta K_c$ )	40
2.3	Crack growth rates versus $\Delta K_{eff}$ ; (a) Ti-24-11 and (b) Ti-25-17-1 (Solid symbols: $da/dN$ vs. $\Delta K_{eff,a}$ ; Open symbols: $dc/dN$ vs. $\Delta K_{eff,c}$ )	41
2.4	Aspect ratio vs. surface crack length in Ti-24-11	42
2.5	Aspect ratio vs. surface crack length in Ti-25-17-1	42
2.6.	Crack path profile of a small crack in Ti-24-11	44
2.7.	Crack path profile of a small crack in Ti-25-17-1	44

<b>Figure</b>		<b>Page</b>
<b>Chapter 3</b>		
3.1	(a) and (b): An illustration of crack growth schemes	49
3.2	The variation of aspect ratio from the simulation of crack growth according to (a) scheme A and (b) scheme B	50
3.3	A comparison of experimentally observed and theoretically simulated variations in aspect ratio, (a) scheme A compared with the data of Wagner et. al [3.11] and (b) scheme B compared with data from Larsen [3.14].	51
3.4	Crack growth rates calculated with aspect ratio variations as well as with assuming $a/c = 1$ for simulations (a) scheme A and (b) scheme B.	52
3.5	The correlation between the grain size parameter and $\Delta K_{th}$ proposed by Taylor and Knott [3.12, 3.13]	53
3.6	Estimations of errors associated with the assumption of $a/c = 1$ in the crack growth simulations; (a) scheme A and (b) scheme B.	54
<b>Chapter 4</b>		
4.1	Crack growth data of large cracks of Ti-8Al as a function of $\Delta K$ and $\Delta K_{eff}$ . PM-constant load, increasing $\Delta K$ and TH-decreasing $\Delta K$ tests.	59
4.2	Crack closure data of large cracks of Ti-8Al as a function of $K_{max}$ . PM-constant load, increasing $\Delta K$ and TH-decreasing $\Delta K$ tests.	60
4.3	The variation of surface crack length and compliance as observed in typical small crack tests in Ti-8Al; (a) for specimen 89483 and (b) for specimen 89487.	61
4.4	Comparison of experimentally observed and theoretically simulated variations in aspect ratio for specimen 89481	62
4.5	Comparison of experimentally observed and theoretically simulated variations in aspect ratio for specimen 89482	63
4.6	Comparison of experimentally observed and theoretically simulated variations in aspect ratio for specimen 89483	63

<b>Figure</b>		<b>Page</b>
4.7	Comparison of experimentally observed and theoretically simulated variations in aspect ratio for specimen 89484	64
4.8	Comparison of experimentally observed and theoretically simulated variations in aspect ratio for specimen 89486	64
4.9	Comparison of experimentally observed and theoretically simulated variations in aspect ratio for specimen 89487	65
4.10	Comparison of experimentally observed and theoretically simulated variations in aspect ratio for specimen 89488	65
4.11	Comparison of experimentally observed and theoretically simulated variations in aspect ratio for specimen 89491	66
4.12	Small crack path profile at surface in specimen 89482	67
4.13	Small crack path profile at depth in specimen 89483	68
4.14	Small crack path profile at surface in specimen 89484	69
4.15	Small crack path profile at surface in specimen 89486	70
4.16	Fatigue crack growth rates of small cracks, deduced by secant method and assuming an aspect ratio of 1.0; as a function of (a) $\Delta K$ and (b) $\Delta K_{eff}$	72
4.17	Fatigue crack growth rates of small cracks, deduced by incremental polynomial method and assuming an aspect ratio of 1.0; as a function of (a) $\Delta K$ and (b) $\Delta K_{eff}$	73
4.18	Fatigue crack growth rates of small cracks, after incorporating the variations in aspect ratio and reduced by incremental polynomial regression; as a function of (a) $\Delta K$ and (b) $\Delta K_{eff}$	74
4.19	The variation of fatigue crack closure levels at the surface $K_{cl,c}$ and at the depth, $K_{cl,a}$ in terms of respective $K_{max}$ levels for all the small crack specimens tested in this study.	75

## **Chapter 5**

5.1	Microstructures after heat treatment (a) $\alpha_2 + \beta$ , (b) fully $\beta$ and (c) equiaxed $\alpha_2$ microstructures	80
5.2	A schematic of the CT specimen used for large crack tests	83

<b>Figure</b>		<b>Page</b>
5.3	Fatigue crack growth rates of large cracks in $\alpha_2+\beta$ microstructure at different stress ratios; (a) in terms of $\Delta K$ and (b) in terms of $\Delta K_{eff}$	86
5.4	The variation of $K_{cl}$ as a function of $K_{max}$ for $R=0.1$ tests for the $\alpha_2+\beta$ microstructure	87
5.5	Fatigue crack growth rates of large cracks in $\beta$ microstructure at different stress ratios; (a) in terms of $\Delta K$ and (b) in terms of $\Delta K_{eff}$	88
5.6	The variation of $K_{cl}$ as a function of $K_{max}$ for $R=0.1$ tests for the $\beta$ microstructure	89
5.7	Fatigue crack growth rates of large cracks in the equiaxed $\alpha_2$ microstructure at different stress ratios; (a) in terms of $\Delta K$ and (b) in terms of $\Delta K_{eff}$	90
5.8	The variation of $K_{cl}$ as a function of $K_{max}$ for $R=0.1$ tests for the equiaxed $\alpha_2$ microstructure	91

## **LIST OF TABLES**

<b><u>Table</u></b>	<b>Page</b>
<b>Chapter 2</b>	
2.1 Microstructure and Mechanical Property Data for Ti-24-11 and Ti-25-17-1	39
<b>Chapter 4</b>	
4.1 Specimen Identification with final crack length and Aspect Ratio Data	58
<b>Chapter 5</b>	
5.1 Heat Treatment and Microstructural Parameters	80
5.2 Specimen Identification and Stress Ratio for Large Crack Tests	85

## SUMMARY

The current research comprises studies on some alloys of titanium and recently developed titanium aluminides to provide an in-depth understanding of the mechanisms of growth of small surface cracks in these materials. These materials are prime candidates for various aerospace applications, and hence an understanding of small crack behavior is of importance both for alloy design by microstructure control and predictions of life in fatigue. The investigations on small crack growth center around a common theme in all the materials considered, namely, the measurement and the effects of variations in crack shape on crack growth. Earlier studies in this area neglected the effects of variations in crack shape for two reasons. Firstly, in most engineering materials in current use, the microstructure is fine enough to consider that the variations in crack shape are only significant at very early stages of growth of surface cracks. Such crack sizes are often very small ( $\leq 200 \mu\text{m}$ ) making it difficult to measure their size in the first place reliably. Secondly, the crack shape variations induced by microstructure and other factors tend to average to reach a equilibrium semicircular shape and hence in data calculations this shape was usually assumed. Nevertheless, the small crack data in literature exhibit large scatter making a consistent interpretation of small crack behavior difficult. The second important theme of study in the materials considered is the measurement of crack closure as a function of crack length. Since the small cracks have a smaller crack wake, closure levels are often low relative to large cracks. Hence, interpretation of small crack growth data must be done after accounting for the different crack closure situations.

Both the objectives of measurement and interpretation of variations in crack shape and crack closure for small cracks have been accomplished in four materials in this study. These materials are a near-alpha titanium alloy, Ti-6Al-2Sn-4Zr-6Mo, a coarse grained alpha titanium alloy, Ti-8Al and recently developed titanium aluminides, viz., Ti-24Al-11Nb and Ti-25Al-17Nb-1Mo. Although the central theme is common for studies in these materials, specific experiments were conducted in different materials to provide answers to the objectives specific to each material under investigation. This is discussed in detail for different materials in the following. In all the small crack tests, crack compliance was measured using a laser interferometric system and surface crack length using a photomicroscopic system as a function of fatigue cycles.

**(1) Ti-6Al-2Sn-4Zr-6Mo**

The Ti-6Al-2Sn-4Zr-6Mo alloy in the equiaxed alpha + Widmanstatten microstructure condition was investigated for crack growth from pre-existing deep and shallow notches introduced by EDM. The prime objective of this part of the study is to validate the procedure for the measurement and calculation of crack aspect ratio from compliance and surface crack length. Continuous measurement of crack aspect ratio as a function of fatigue cycles are demonstrated. The experimentally observed variations in crack shape have been found to agree well with the theoretically predicted variations. The calculated crack growth rates as a function of stress intensity ranges have been found to agree well with the large crack growth data after correcting for crack shape variations and crack closure. The effects of asymmetric growth of crack with respect to original measurement location have been incorporated in crack shape calculations and verified using experiments.

**(2) Coarse Grained Ti-8Al**

Small crack experiments were conducted on coarse grained (200  $\mu\text{m}$ ) Ti-8Al alloy to investigate whether the variations in crack shape are induced by crack front interactions with the grain boundary at the surface and at the depth. The experimentally seen variations in crack shape are compared with theoretically simulated patterns of crack shape variation assuming alternate crack retardation at the surface and at depth. After incorporating the variations in crack shape, the crack growth data were seen to consolidate well with the large crack data. Crack closure was seen to develop as the crack extends and reach the closure levels of large through-cracks at large crack sizes.

**(3) Titanium Aluminides: Ti-24Al-11Nb and Ti-25Al-17Nb-1Mo**

In order to evaluate the small crack growth behavior of Ti-24Al-11Nb alloy with respect to Ti-25Al-17Nb-1Mo, small crack experiments were performed on both materials. Tests were done on naturally initiated small cracks in Ti-24Al-11Nb, while cracks initiated from EDM notches were studied in Ti-25Al-17Nb-1Mo. The crack shape variations were significant in Ti-24Al-11Nb while such variations were absent in Ti-25Al-17Nb-1Mo. In Ti-24Al-11Nb, naturally initiated cracks

encountered certain microstructural features at the grain boundary which influenced the crack shape development, while cracks in Ti-25Al-17Nb-1Mo almost propagated in a single grain maintaining almost a semielliptical crack shape. The crack growth data for both materials were found to agree with the respective large crack data after incorporating the variations in cracks shape and crack closure.

#### **(4) Growth Behavior of Large Cracks in Ti-24Al-11Nb**

A complete investigation of the effects of microstructure and stress ratio on the large crack growth behavior in CT specimens was performed. The microstructures tested were an equiaxed  $\alpha_2$  in a Widmanstatten matrix microstructure, an aligned colony Widmanstatten structure and a completely equiaxed  $\alpha_2$  structure. Tests were conducted at stress ratios of  $R=0.1$ ,  $0.5$  and  $0.8$ . In a given microstructure, pronounced effects of stress ratio were seen. The differences in closure levels could not successfully explain the effect of stress ratio on crack growth in all the microstructures. A strong effect of stress ratio or mean stress on the crack growth is seen. When compared in terms of intrinsic crack growth resistance, the crack growth rates increased with stress ratio, suggesting the presence of static mode of crack advance superimposed on cyclic crack extension.



## CHAPTER 1

### MEASUREMENT OF THE SHAPES OF THREE DIMENSIONAL SURFACE CRACKS IN Ti-6Al-2Sn-4Zr-6Mo

#### 1.1. INTRODUCTION

A knowledge of fatigue crack growth behavior of three-dimensional surface cracks is essential in many engineering applications such as pressure vessels, aerospace structures, turbines for power generation and aircraft engines. Data on fatigue crack growth, generated using through-the-thickness cracks in standard fracture mechanics specimens, have often been used in the life prediction of components having surface cracks or cracks emanating from notches or discontinuities [1.1, 1.2]. However, such a procedure often involves the assumption that cracks grow generally in a nearly semicircular fashion. While this is adequate for isotropic materials loaded in unidirectional tension, many engineering applications experience complex loading conditions such as bending and bi-axial stresses in addition to tension. Surface cracks under such conditions do not grow with shapes predictable by simple tension approximations and often exhibit continuous changes in crack shape dictated by the loading conditions [1.3, 1.4]. Surface cracks at structural inhomogeneities such as weldments [1.5, 1.6] also grow with unpredictable changes in crack shape. The shape of a growing crack is also affected by the presence of deformed layers introduced to improve fatigue life through operations such as shot peening [1.7] as well as by the elongated grains formed by material processing [1.7-1.9]. Surface cracks in these situations were found to develop shallow configurations. In addition, due to coalescence of multiple cracks during fatigue [1.10, 1.11], large changes in crack shape or aspect ratio can occur causing significant variations in crack growth rates at various locations of crack front. It is known [1.12, 1.13] that the shapes of the pre-existing cracks or inclusions or notches also affect the development of crack shape and hence the crack growth rates. For instance, in situations of crack growth from deep notches [1.14, 1.15], the crack tip at the surface rapidly grows at first until the crack shape becomes nearly semicircular, after which the entire crack front grows at constant rate.

Apart from these predominantly large-crack situations, crack shape is also

important during the growth of small surface cracks. Several investigations indicate that cracks at very small sizes may assume arbitrary shapes due to the influence of local microstructure [1.9, 1.10, 1.16-1.20] especially in coarse grained microstructures. The important microstructural variables that affect crack shape are, grain size [1.16, 1.17], the grain shape [1.9, 1.10] and the presence of inclusions [1.19]. The shape of surface cracks is also important [1.21, 1.22] in new classes of intermetallic materials in which strong effects of microstructure and material anisotropy on crack shape development were found during crack growth. The crack shape variations in these cases are unpredictable due to the randomness of the crack tip interactions with microstructural features and must be accounted in the calculations of stress intensity factors at the cracks tips for the accurate description of growth rates all along the crack front. Hence, a knowledge of the continuous variation of crack shape or aspect ratio as a function of surface crack length is required. However, in conventional materials such as steels [1.17], nickel base superalloys [1.23] and titanium alloys [1.24], surface cracks were seen to grow in an almost semicircular shape over the range of crack sizes studied and an assumption of semicircular crack shape is adequate to accurately describe the crack growth behavior.

Measurements of crack shapes are usually made from photomicrographs of fracture surfaces on which the crack fronts are delineated by heat tinting [1.9, 1.23, 1.24] or by using marker loads [1.11, 1.25, 1.26] during fatigue crack growth. Attempts [1.27] were also made to estimate the depths of surface cracks using D. C. electrical potential measurements. However, estimation of crack aspect ratio from the compliance has not been attempted so far. This is partly due to the requirement of a sensitive technique to measure the displacements accurately across the faces of the surface crack, in addition to the lack of analytical expressions relating compliance to aspect ratio and surface crack length. The compliance of a surface crack is related to its crack area [1.23, 1.24], and for a semielliptical crack this would be a function of the surface crack length and the aspect ratio,  $a/c$ , which is the ratio of crack length at the depth to half the surface length. The aspect ratio can be estimated if independent measurements of surface crack length and compliance are available.

In the present study, measurement of aspect ratios of the surface cracks of arbitrary shapes using a combined laser interferometric and photomicroscopic system is demonstrated. The present approach facilitates the continuous measurement of the evolving crack shapes during crack growth of surface cracks as a

function of fatigue cycles. Briefly, this involves independent measurements of crack compliance and the surface crack length continuously during fatigue cycling. The aspect ratios were then calculated from these measurements using a compliance expression. Cracks of arbitrary shapes are approximated to the closest semielliptical configurations, which allows the use of available stress intensity factor solutions. A compliance equation for surface cracks, valid for the crack aspect ratios of practical interest ( $0.2 \leq a/c \leq 2.0$ ), deduced from the literature [1.30], is presented. This expression is used in the present study to determine crack aspect ratios from compliance. The variations in crack shape are accounted for in stress intensity factor calculations, and the crack growth rates at the surface as well as in the crack depth are calculated.

## 1.2. A COMPLIANCE EXPRESSION FOR SURFACE CRACKS

Continuous measurement of the shape of a growing crack requires a compliance equation valid for a range of crack aspect ratios of practical interest ( $0.2 \leq a/c \leq 2.0$ ). The equations for surface crack compliance can be deduced following the work of Fett [1.30], who presented an approach by which crack surface displacements can be expressed in terms of the parameters used to express the stress intensity factor for three-dimensional surface cracks (Newman-Raju equation [1.31]). The crack surface displacements were assumed in the form of a power series:

$$u(\rho, \phi) = \sum_{v=1}^{\infty} C_v(\phi) \left(1 - \frac{\rho}{r}\right)^{v+\frac{1}{2}} \quad \text{.....(1.1)}$$

in which  $u$  is the half crack mouth displacement,  $\phi$  is the parametric angle,  $r$  is the distance from the crack origin to any point on the crack perimeter,  $\rho$  is the distance of any point within the crack from the origin and  $C_v$  ( $v = 1 \rightarrow \infty$ ) are the constants to be determined from certain boundary conditions [1.30]. The crack co-ordinates are illustrated in Fig. 1.1(a). The expression for CMOD from Eqn. (1.1) can be deduced by taking  $\text{CMOD} = 2U = 2u$  ( $\rho=0, \phi=0$ ) and substituting for  $C_0, C_1$  and  $C_2$  (see [1.30]). After some simplification, the resulting equation is:

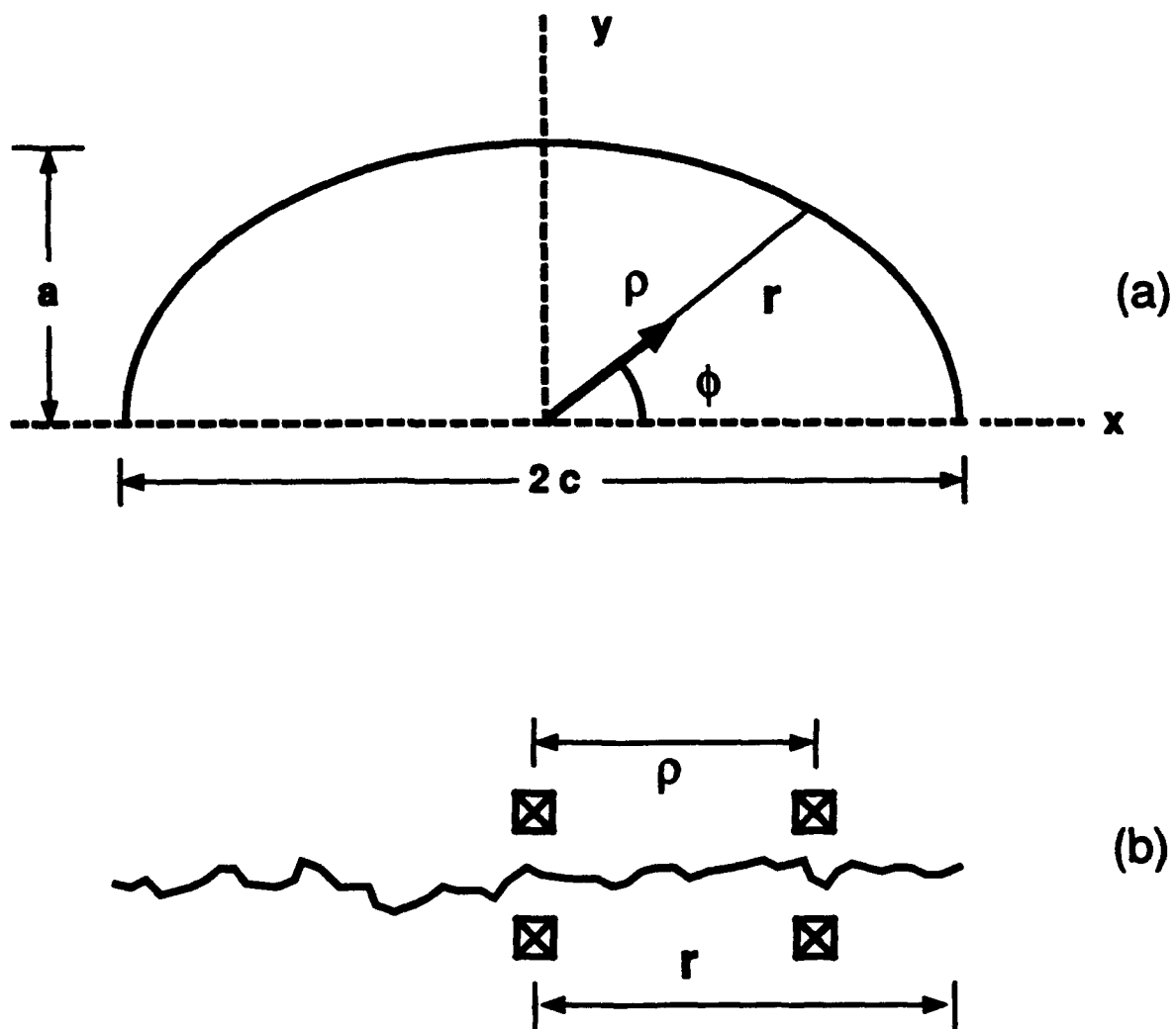


Fig. 1.1 A Schematic of the surface crack (a) and the surface profile illustrating the variables definin crack.

$$\frac{2U}{\sigma} = 1.6 \frac{\sqrt{8}}{\sqrt{\pi} E} c (1-\phi^2) \lambda F f_w g \quad \text{.....(1.2)}$$

where

$$F = [M_1 + M_2 \left(\frac{a}{t}\right)^2 + M_3 \left(\frac{a}{t}\right)^4] \sqrt{\frac{\pi}{Q}}$$

$$f_w = \sqrt{\sec \left( \frac{\pi c}{2w} \sqrt{\frac{a}{t}} \right)}$$

in which for  $a/c \leq 1$

$$\lambda = \frac{a}{c}$$

$$g = 1 + [0.1 + 0.35 \left(\frac{a}{t}\right)^2]$$

$$M_1 = 1.13 - 0.09 \left(\frac{a}{c}\right)$$

$$M_2 = -0.54 + \frac{0.89}{0.2 + \left(\frac{a}{c}\right)}$$

$$M_3 = 0.5 + \frac{1}{0.65 + \left(\frac{a}{c}\right)} + 14 \left(1 - \frac{a}{c}\right)^{24}$$

$$Q = 1 + 1.464 \left(\frac{a}{c}\right)^{1.65}$$

for  $a/c > 1$

$$\lambda = \sqrt{\frac{a}{c}}$$

$$g = 1 + [0.1 + 0.35 \left(\frac{c}{a}\right) \left(\frac{a}{t}\right)^2]$$

$$M_1 = \sqrt{\frac{c}{a}} \left(1 + 0.04 \frac{c}{a}\right)$$

$$M_2 = 0.2 \left(\frac{c}{a}\right)^4$$

$$M_3 = -0.11 \left(\frac{c}{a}\right)^4$$

$$Q = 1 + 1.464 \left(\frac{c}{a}\right)^{1.65}$$

where  $c$  is the half surface length,  $a$  is the crack depth and  $t$  and  $w$  are respectively the specimen thickness and half width. Many of the above equations are identical to those in the Newman-Raju stress intensity factor equation for surface cracks, since Fett used the Newman-Raju equation to formulate the crack surface displacements. The validity of the above equation should then be similar to the validity of the Newman-Raju stress intensity factor formula. The asymptotic behavior of the non-dimensional compliance from Eqn. (1.2) is illustrated for several  $a/t$  values in Fig. 1.2. The surface crack compliance can be seen to be a strong function of the crack aspect ratio. As expected, the non-dimensional compliance approaches that [1.32] of the center, through-crack specimen, (CCT), as  $a/c \rightarrow \infty$  and that of the single edge through crack specimen (SEN), as  $a/c \rightarrow 0$ . Eqn. (1.2) can be rewritten in terms of only two variables,  $a/c$  and  $c$ , a form suitable to determine the aspect ratio if the compliance and surface crack length are known.

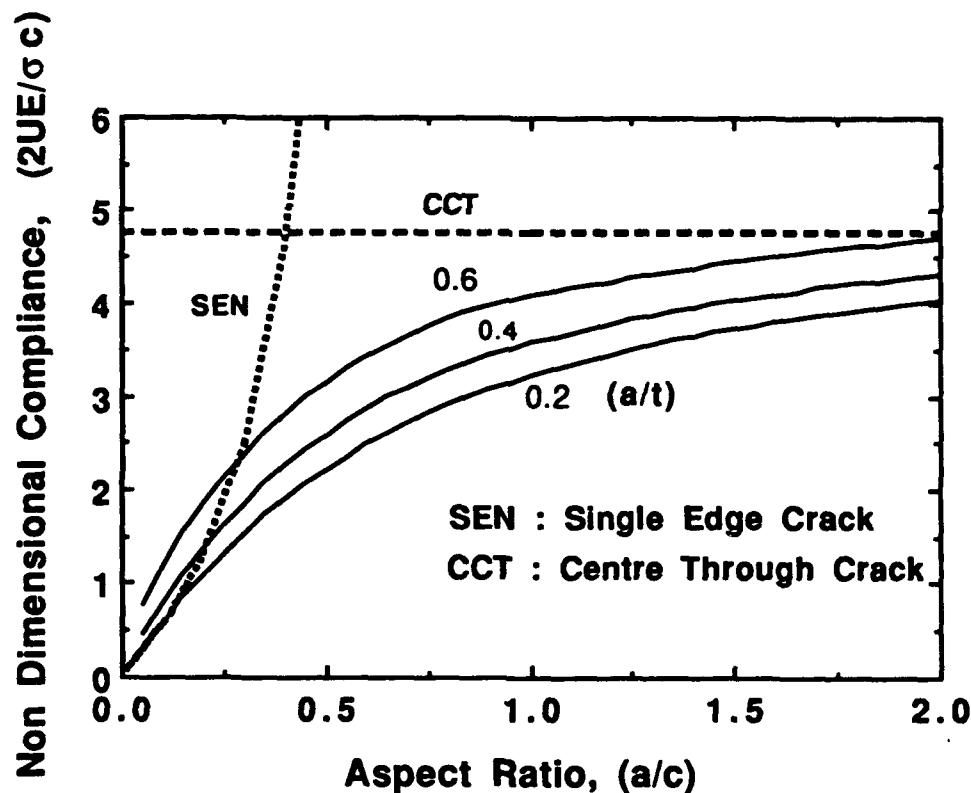


Fig. 1.2 The asymptotic behavior of the non-dimensional compliance from Eqn. (1.2).

Due to microstructural effects, surface cracks in many cases grow asymmetrically [1.21, 1.22] with respect to the original location at which compliance is measured. Hence it is important to correct the compliance ( $2U(\rho/r, 0)$ ) measured at any location along the surface,  $\rho/r$ , to the compliance ( $2U(0, 0)$ ) at the center of the crack through the relationship:

$$2U(0, 0) = \frac{4 (2U(\rho/r, 0))}{5 \left[ (1-\rho/r)^{0.5} - \frac{1}{5} (1-\rho/r)^{2.5} \right]} \quad \text{.....(1.3)}$$

in which  $\rho$  is the distance along the surface (for  $\phi=0$ ) of the measurement location from the center of the crack and  $r$  is equal to the half surface length ( $c$ ) of the crack (Fig. 1.1(b)).

### 1.3 MEASUREMENT OF ASPECT RATIOS OF SURFACE CRACKS

#### 1.3.1 Material

In order to illustrate the approach, experimental measurements of crack aspect ratios of surface cracks in a titanium alloy, Ti-6Al-2Sn-4Zr-6Mo (wt%), will be demonstrated. From previous studies [1.24, 1.33], this alloy was found to exhibit isotropic fatigue crack growth behavior because of its processing history, which resulted in a fine, homogeneous microstructure, shown in Fig. 1.3. Surface cracks in this material grow in a semicircular fashion ( $a/c=1$ ) from small crack sizes (typically  $2c=100\mu\text{m}$ ) to large crack sizes (typically  $2c=2\text{ mm}$ ). A pre-existing crack of aspect ratio other than 1.0 (either a shallow crack,  $a/c < 1.0$  or a deep crack,  $a/c > 1.0$ ) would naturally tend to become semicircular during crack growth. On this basis, experiments to continuously measure evolving crack aspect ratios from pre-existing shallow ( $a/c < 1$ ) and deep ( $a/c > 1$ ) notches were performed in this study. The measured aspect ratios will be compared with the predicted variation of the aspect ratio to illustrate the accuracy of the measurement.

#### 1.3.2 Experimental Procedure

Crack growth tests were performed on specimens of rectangular cross section (Fig. 1.4) with a mild curvature ( $K_t=1.037$ ) containing an electro-discharge-machined

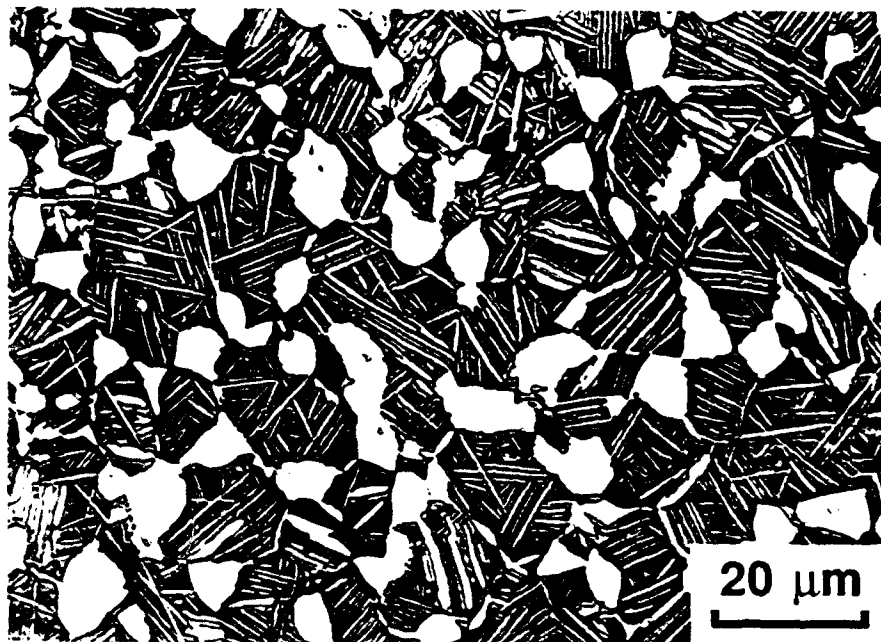


Figure 1.3. Microstructure of the titanium alloy, Ti-6Al-2Sn-4Zr-6Mo



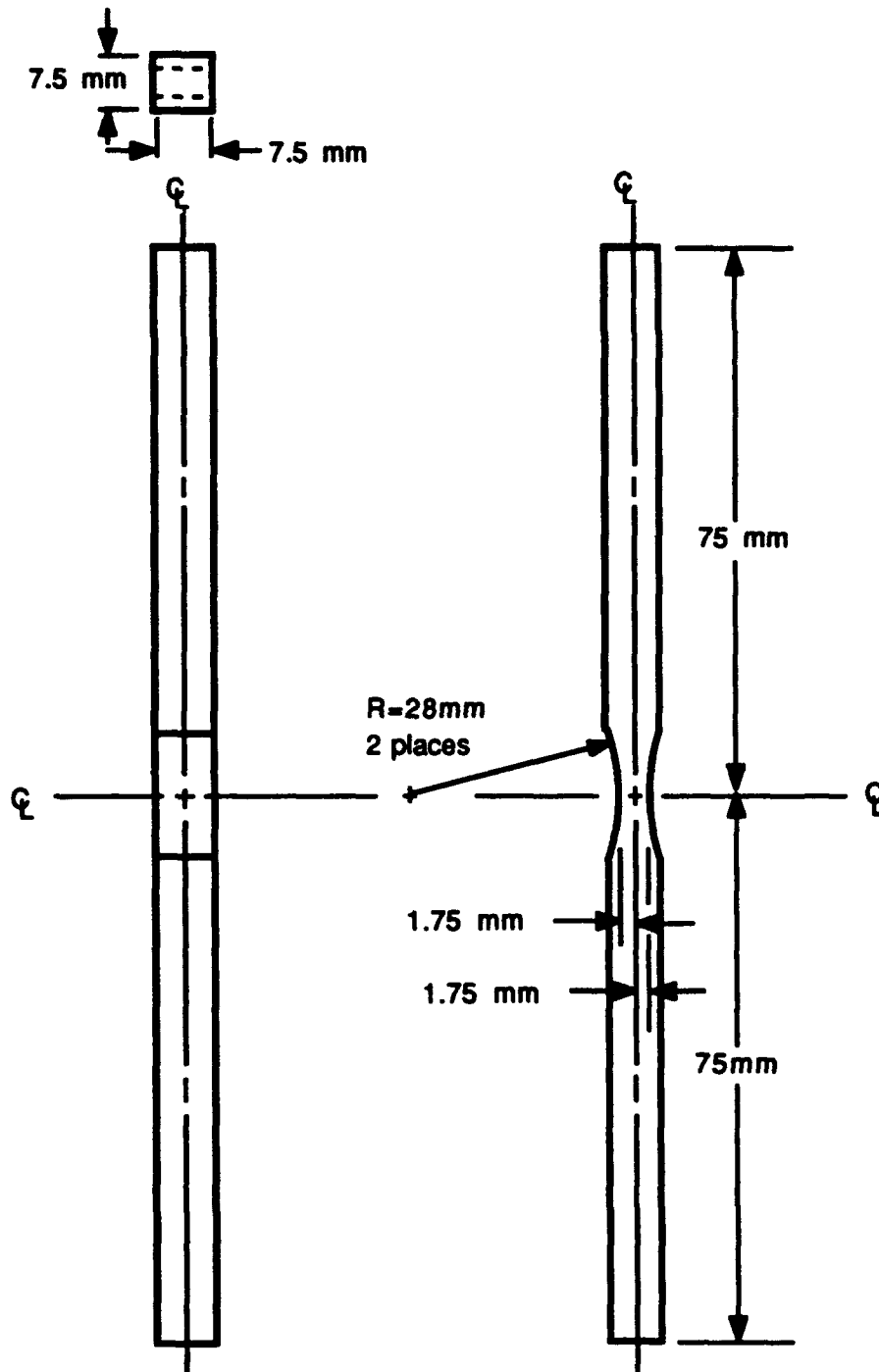


Fig. 1.4 The geometry of specimens used in small crack tests.

(EDM) notch with either a deep ( $a/c \approx 2.8$ ) or a shallow ( $a/c \approx 0.1$ ) configuration at the center of curvature. Optical micrographs of the notches after machining are shown in Figs. 1.5 (a) and (b) for the shallow and deep notch configurations, respectively. The photomicrographs also show the Vickers microhardness indentations placed above and below the notch, usually with a spacing of about 100  $\mu\text{m}$ , for use in measuring crack opening displacements by laser interferometry. Fatigue cracks were generally initiated from the notch root at a net-section stress level of  $0.4 \sigma_y$  ( $\sigma_y$  is the yield stress) under fully tensile cyclic loading ( $R = (\sigma_{\min}/\sigma_{\max}) = 0.1$ ). Cracks initiated at the notch root at the specimen surface typically around 5000 cycles in the case of deep notches while for the shallow notches, cracks quickly initiated at the notch root at the depth in few cycles. Crack initiation at the depth could be readily detected by changes in crack compliance. The surface crack lengths were photographed at periodic intervals, and crack mouth opening displacements (CMOD) were measured as a function of load at the same intervals throughout the duration of the tests. An automated photomicroscopic system was used for photography, and a laser interferometric displacement measurement system was used to obtain CMOD of the surface crack as a function of load. The full details of the system are reported elsewhere [1.24, 1.33]. A schematic of the laser interferometric displacement measurement system is presented in Fig. 1.6. Using surface crack length measurements from the photographic record, an apparent aspect ratio can be estimated from the compliance of the crack using Eqns. (1.2 & 1.3). In a given test, about 200 or more measurements of surface crack length and compliance were acquired to thoroughly document crack growth. At the end of the tests, specimens were heat tinted at 400°C for 1 hr. to reveal the shape of the surface cracks. Figures 1.7(a) and (b) illustrate the shapes of cracks grown from shallow and deep notches, respectively. The profiles of the EDM started notches are also visible.

### 1.3.3 Determination of the Aspect Ratio of a Surface Crack

From the test record, the compliance at various cycle counts was calculated from the load-displacement traces. The surface crack length data were collected by digitizing the optical micrographs taken at the same intervals as compliance. The apparent aspect ratio was then calculated using Eqn. (1.2) by using the surface crack length  $2c$  on the right hand side of the equation and iterating on the aspect ratio until both sides of the Eqn. (1.2) agree within 0.1%. The iteration was usually started with  $a/c = 1.0$ . It is important to note that any measurement error in surface crack

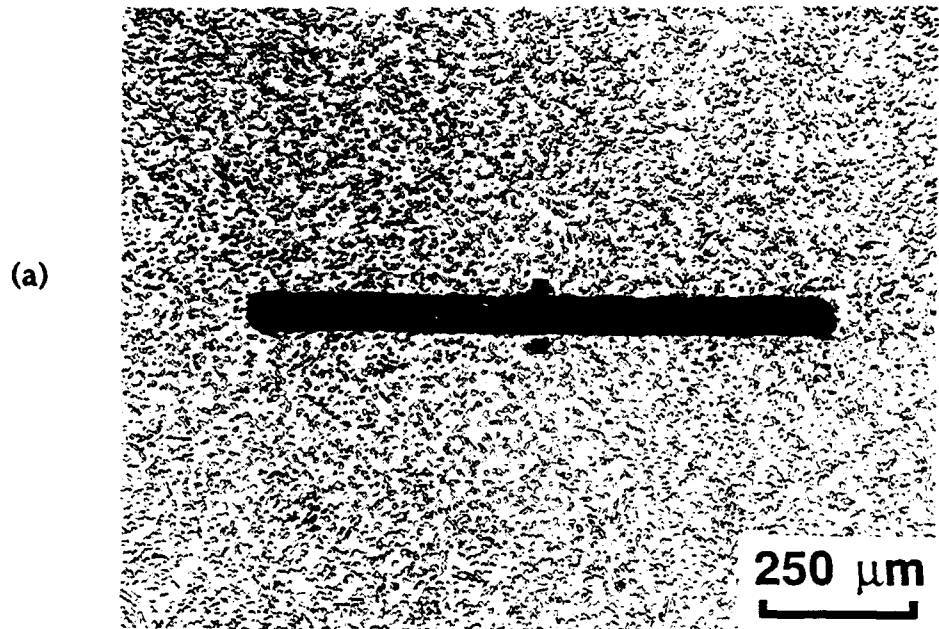


Figure 1.5. Micrographs of EDM notches; (a) shallow and (b) deep notch

# Laser Interferometric Displacement Gage

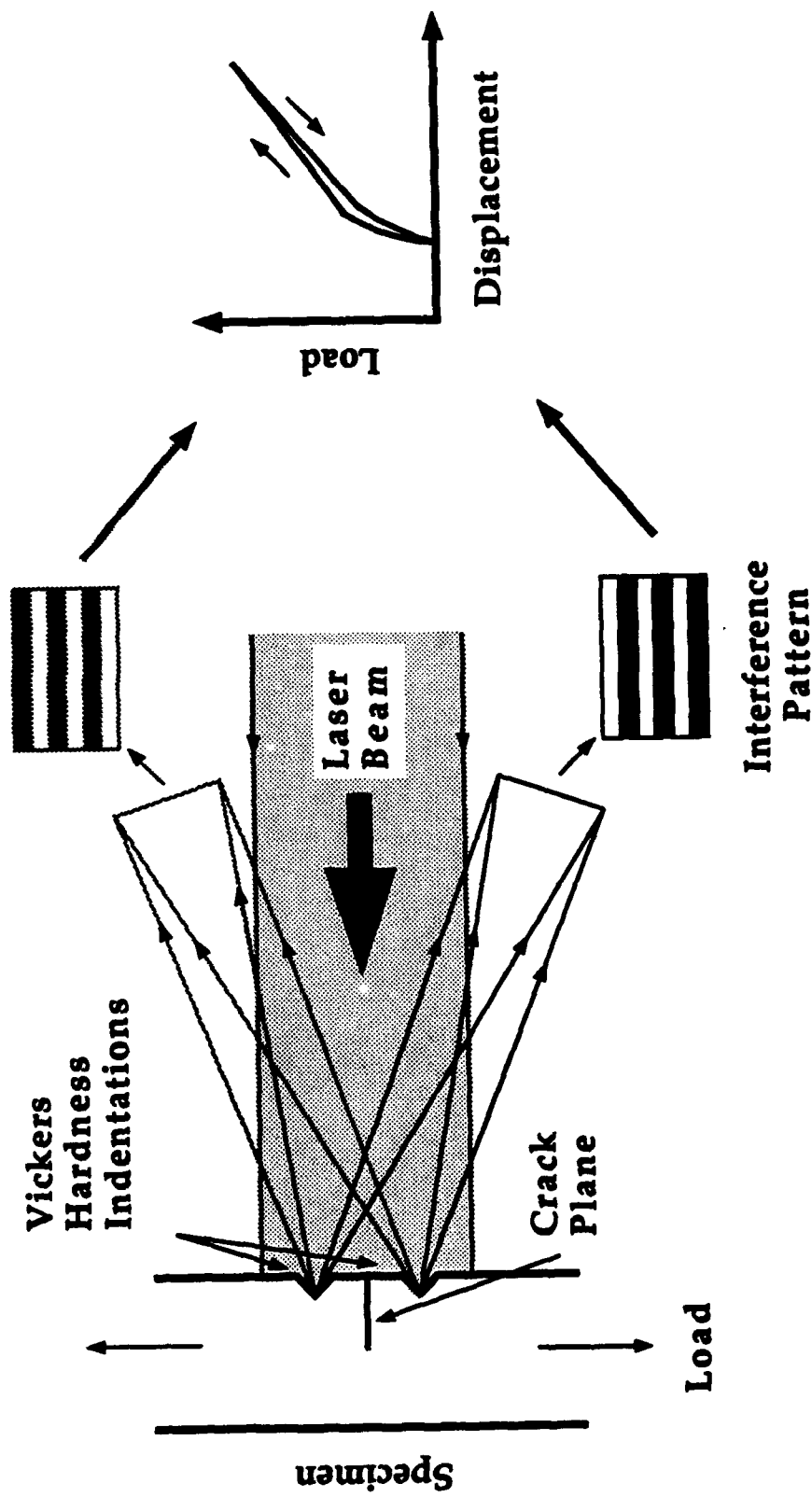


Fig. 1.6

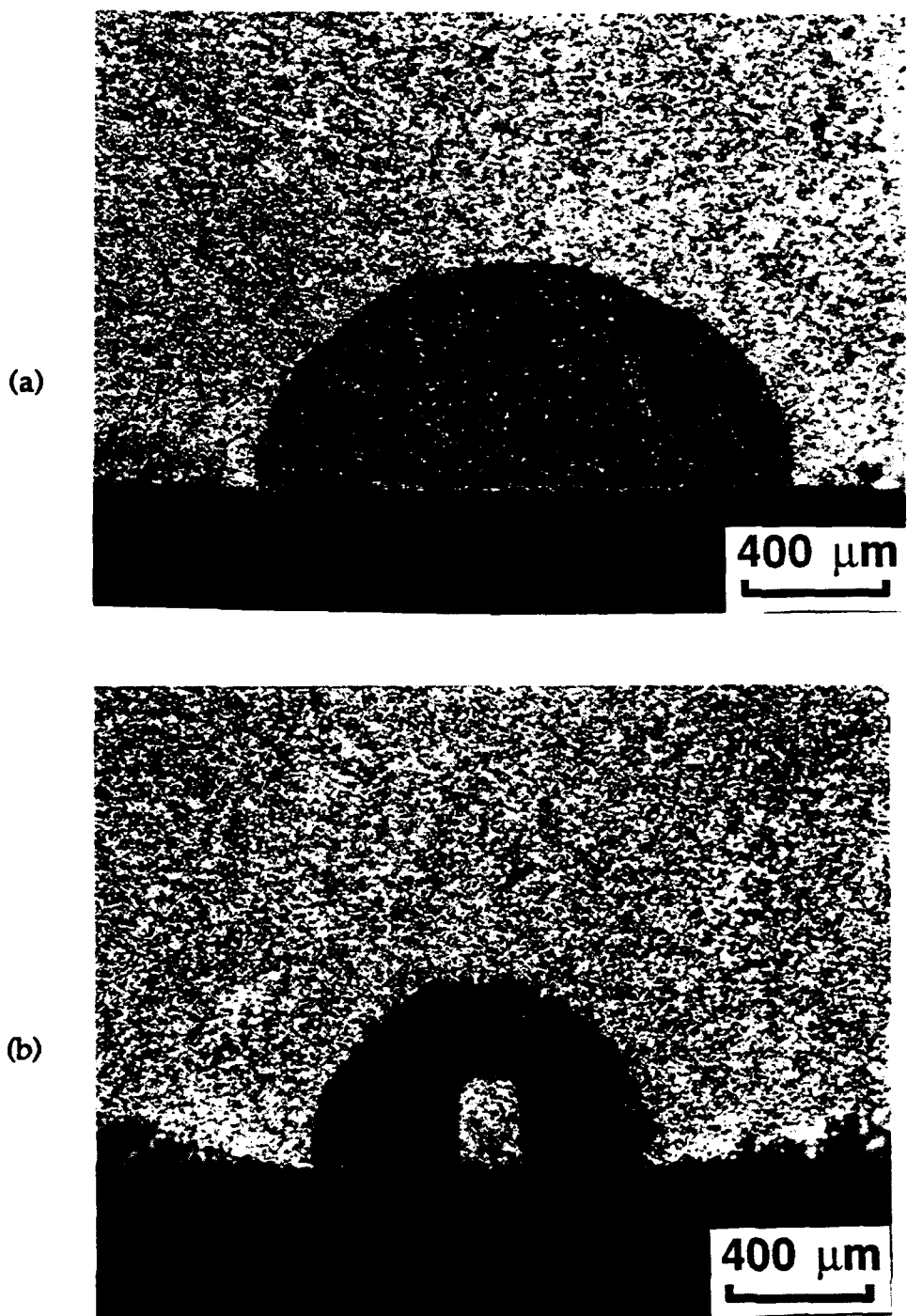


Figure 1.7. Crack shapes after heat tinting of cracks grown from (a) shallow and (b) deep notches

length can result in some error in the apparent aspect ratio. The likely errors in aspect ratio due to errors in surface crack length measurement are discussed in Appendix 1.1. It is likely that for some materials exhibiting large anisotropy in fatigue crack growth resistance, cracks can grow with aspect ratios larger than 2, in which case the stress intensity factor equation, and hence the compliance expression, may be inaccurate. In addition, due to the asymptotic behavior of crack compliance at large aspect ratios, small errors in surface crack length can cause large errors in aspect ratio. This aspect is further discussed in Appendix 1.2.

The determination of aspect ratio is also important for very small crack lengths at which the crack is likely to exhibit large fluctuations in crack shape due to the local non-continuum nature of crack growth influenced by microstructure. However, there are limits to the smallest crack size for which the aspect ratio can be estimated accurately. As the surface crack length decreases, the compliance of the crack approaches that of the crack-free specimen, reducing the sensitivity of the CMOD measurements. This problem is addressed in Appendix 1.3, and the limitations of the present approach are discussed.

#### 1.3.4 Calculation of crack growth rates

The crack growth rates at the specimen surface were calculated using a polynomial regression routine [1.24] to reduce the data of photo surface crack length and cycle count. In a fashion similar to that specified by ASTM Standard E-647, this involves performing a quadratic regression on all data points within a specified crack length interval and calculating crack growth rate from the slope at the midpoint of the interval. Simultaneously, the aspect ratio data within the same interval are regressed independently to calculate  $d(a/c)/dN$  at the midpoint of the interval. Crack growth rate at the crack depth was calculated using the expression:

$$\frac{da}{dN} = c \frac{d(a/c)}{dN} + (a/c) \frac{dc}{dN} \quad \text{.....(1.4)}$$

The corresponding stress intensity factors at the specimen surface and at the crack depth were calculated using the same values of  $c$  and  $a/c$  at the midpoints using the Newman-Raju equation for surface cracks [1.31].

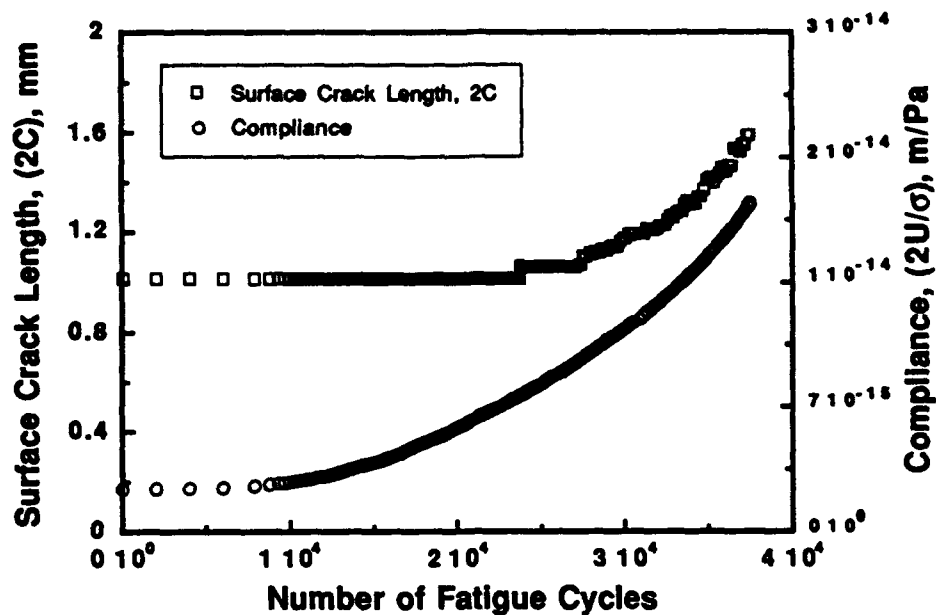
Crack closure loads were measured from the load versus crack-opening-displacement curves from which compliance was calculated. The crack closure load was determined as the load at which non-linearity starts in the unloading part of the curve. The closure loads were used for the calculation of  $\Delta K_{eff}$ , assuming that the closure occurs at the same load all around the crack front, irrespective of the crack aspect ratio.

#### 1.4. RESULTS AND DISCUSSION

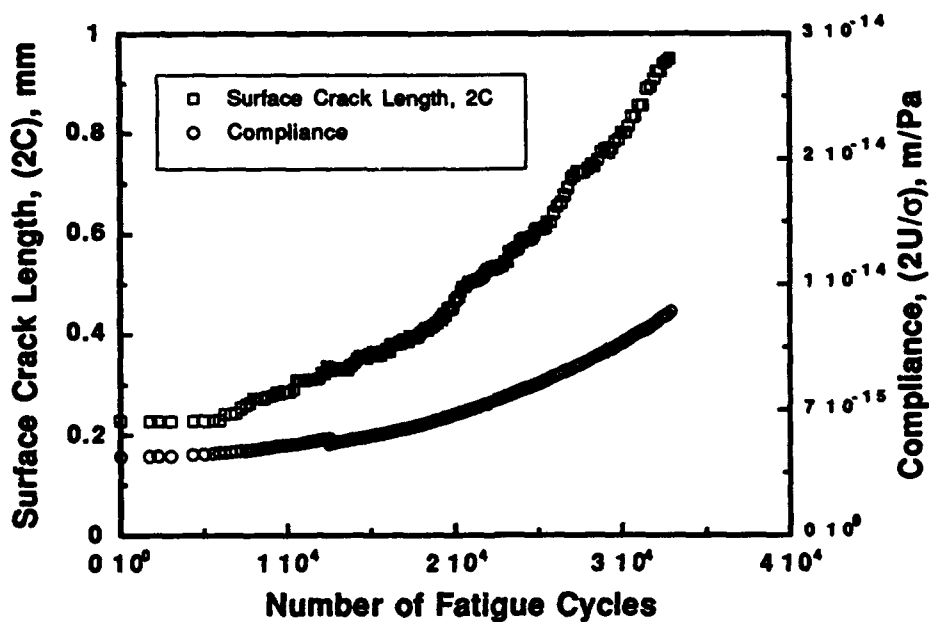
Examples of the test data, consisting of the compliance and surface crack length as a function of fatigue cycles, for the case of shallow and deep notches are presented in Figs. 1.8(a) and (b), respectively. While a smooth variation in compliance is seen, the increment in surface crack length, obtained from photomicrographs is discontinuous, exhibiting alternating arrest and growth stages on the microstructural scale. When the crack tip is arrested, either at the surface or at depth, crack growth respectively at the depth or at the surface would occur, producing a continuous change in compliance. However, when the crack tip at the depth is growing and the crack tip at surface is temporarily retarded at a microstructural barrier, a discontinuous change in surface crack length would be seen. This is because either the crack length increment at surface or at depth would cause a change in compliance, and hence the variation in compliance is smooth and continuous. The variations in aspect ratio calculated via Eqns. (1.2) and (1.3) as a function of surface crack length during crack growth from shallow and deep EDM notches are presented in Figs. 1.9(a) and (b), respectively. The solid lines represent the predicted variation in the aspect ratio from pre-existing hypothetical shallow and deep cracks. The predicted variation is calculated by assuming a deep crack with the same aspect ratio and surface crack length as the notch. The notch aspect ratios used in the calculations were measured from the broken specimens after heat tinting (Figs. 1.7(a) and (b)). From the crack growth law obtained by fitting data from several large crack growth tests to the equation

$$\log \left[ \frac{da}{dN} \right] = C_1 \sinh \left[ C_2 (\log (\Delta K) + C_3) \right] + C_4 \quad \text{.....(1.5)}$$

and using the stress intensity factor at the surface, the crack growth rates of the surface tips were calculated. The constants  $C_1$ ,  $C_2$ ,  $C_3$  and  $C_4$  in eqn. (1.5) are 1.1465,



1.8 (a)



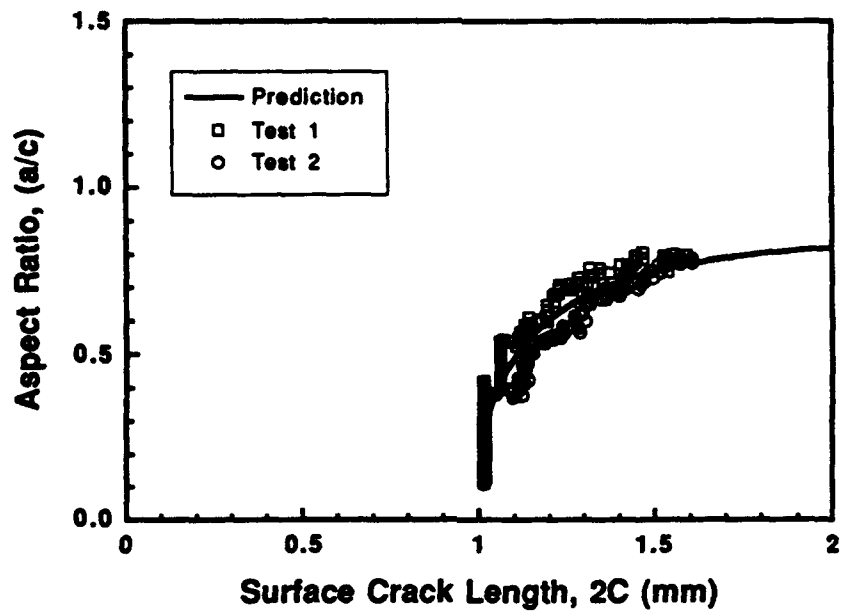
1.8 (b)

Fig. 1.8. The variation of surface crack length and crack compliance as a function of fatigue cycles in (a) shallow and (b) deep-notch specimens

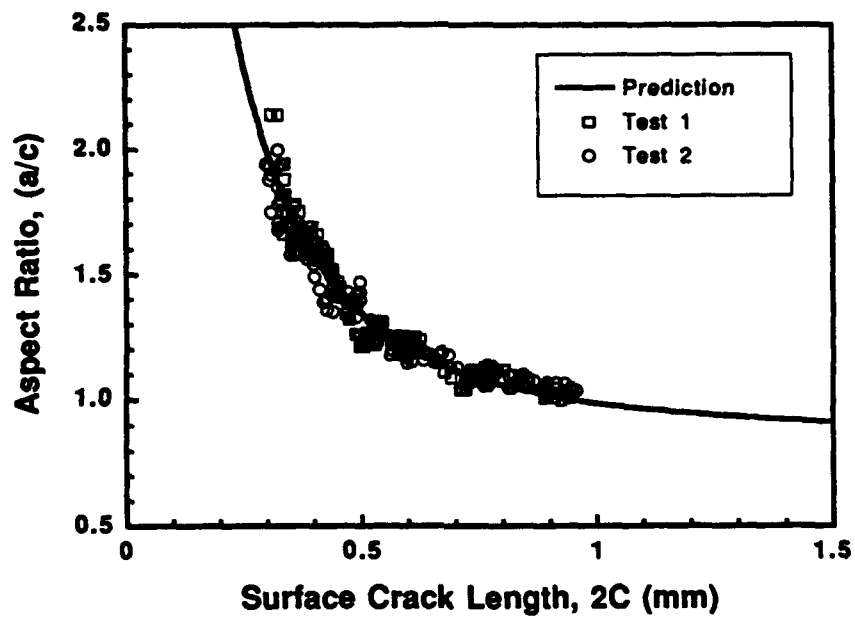


2.6235, -0.9638 and -7.6387, respectively. The number of fatigue cycles required for a small specified increment ( $2\text{ }\mu\text{m}$ ) in surface crack length is then calculated. Simultaneously, knowing the stress intensity factor, the crack length increment at the depth for the same number of cycles using the same crack growth law is calculated. The new aspect ratio is then taken as the ratio between the current crack length at the depth and the half-crack length at the surface. As the hypothetical shallow and deep cracks grow, the aspect ratios gradually reach that of the semicircular crack. This procedure is repeated until the crack grows large enough to make the stress intensity factor uniform all around the crack front.

The data generated from experiments, presented in Figs. 1.9(a) and (b), are from two tests in each case. As can be seen, very good agreement is found between the measured and predicted variation of aspect ratio. For the deep notch case, the experimental data in Fig. 1.9(b) are given only for crack lengths for which the aspect ratio is less than 2.0. As determined from heat tinting, a crack having an initial notch aspect ratio of 2.8 achieved an aspect ratio of 2.0 when the surface crack length was about  $300\text{ }\mu\text{m}$ . At crack lengths lower than this value, the crack has seldom grown out of the entire notch front, as confirmed by several experimental observations. An example of the heat tinted fracture surface when the crack was about  $270\text{ }\mu\text{m}$  is given in Fig. 1.10(a). The crack front is marked by dotted lines and the crack has initiated only from the part of the notch. Although the notch is deeper, it can be seen from Fig. A.1.2.1, that no significant change in the stress intensity factor at the crack depth occurs until the crack aspect ratio dropped below approximately 2.0. As a result, the crack has not initiated at the depth when  $a/c \geq 2.0$ . The calculated aspect ratio for this crack is 2.5, whereas the measured value is 2.1. At this stage the segment of the uncracked notch front, due to its finite root radius, would contribute to the measured compliance, and the compliance of this crack would be larger than the equivalent crack with a sharp tip all along the crack front. In addition, for  $a/c > 2$ , in the asymptotic region of the compliance curve, a small change in compliance can result in a large error in the calculated aspect ratio. Figure. 1.10(b) presents an example of the crack with a measured aspect ratio of about 2.1 and a surface crack length of  $320\text{ }\mu\text{m}$ . The crack has apparently initiated all along the periphery of the notch, including the depth. Upon further growth, the aspect ratios agree well with the predicted variation in aspect ratio (Fig. 1.9). In view of these observations, calculated aspect ratios  $> 2.0$  (for crack lengths  $< \text{about } 300\text{ }\mu\text{m}$ ) were considered to be in error and were discarded.



1.9 (a)



1.9 (b)

Fig. 1.9.A comparison of the experimentally and predicted crack aspect ratios for cracks growing from (a) shallow and (b) deep notches

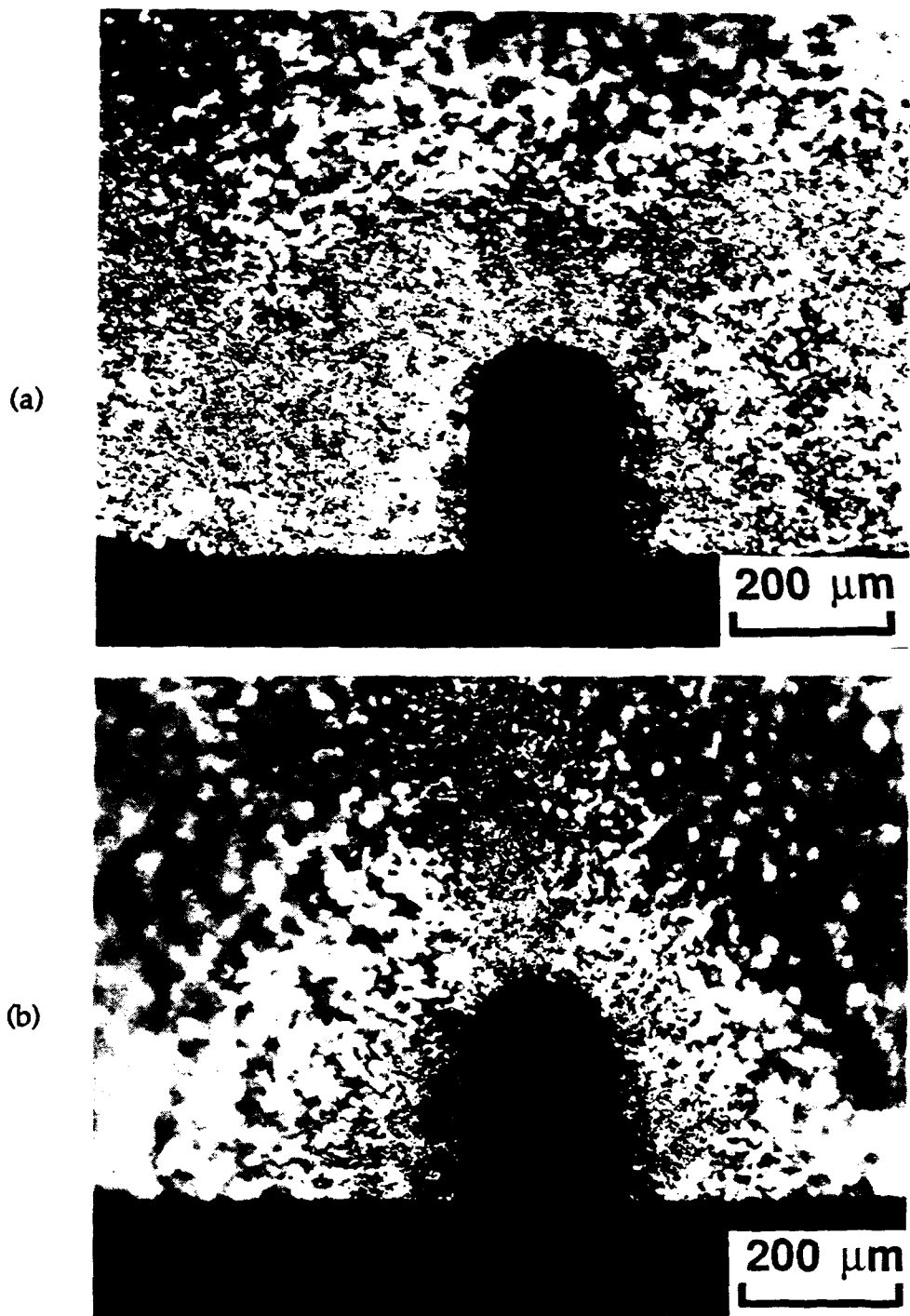
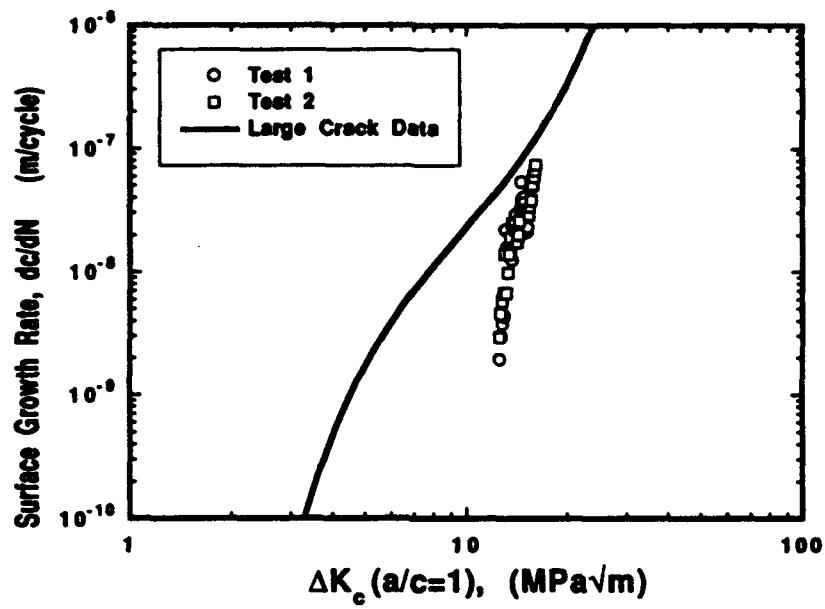


Figure 1.10. Optical micrographs illustrating crack shapes delineated by heat tinting at various stages of crack growth from the notch; (a)  $a/c=2.3$ ,  $2c=270\text{ }\mu\text{m}$  and (b)  $a/c=2.0$ ,  $2c=300\text{ }\mu\text{m}$

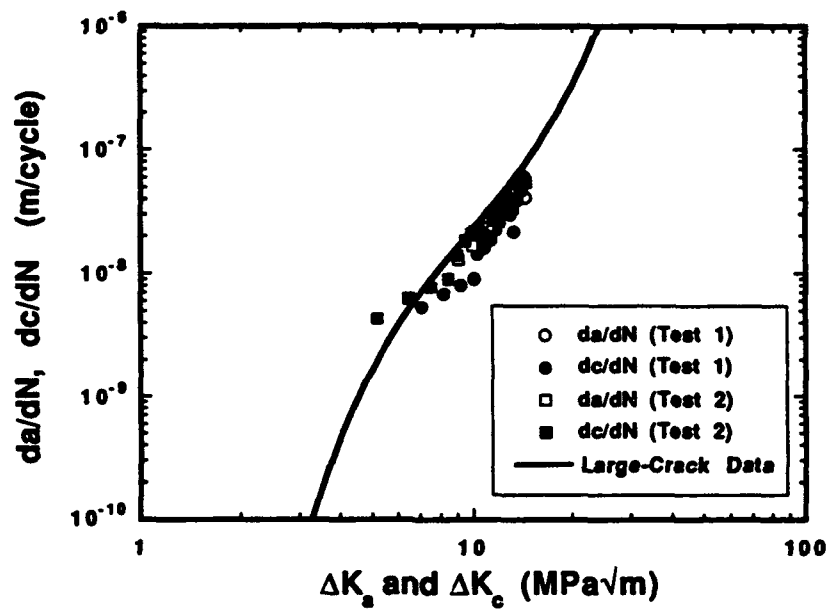
On the other hand, in the case of a shallow notch, the effect of the notch on the measured aspect ratios at the very early stages of crack growth was absent. As can be seen from Fig. 1.9(a), the predicted variations agree very well with the experimental data from the inception of crack growth from the notch.

The accuracy of crack aspect ratio measurements can be verified by comparing the fatigue crack growth rates of the cracks growing from the notches. After accounting for the variations in the aspect ratio in stress intensity factors and growth rates, the surface crack growth rates should agree with the large-crack data generated on two dimensional cracks. This is illustrated in Figs. 1.11(a-c) for the shallow crack configuration. Figures. 1.11(a) and (b) illustrate the crack growth data from several tests without and with the incorporation of aspect ratio into the calculations respectively. The data in Fig. 1.11 (a) were reduced by using only the surface crack length data obtained from photographic measurements and assuming  $a/c=1$  for the calculations. The solid line represents the large crack growth data generated from C(T) specimens (eqn. (1.5)). Since, for the shallow notch, the actual  $\Delta K$  at surface,  $\Delta K_C$ , is smaller than the apparent  $\Delta K$  of a semicircular crack,  $\Delta K_C(a/c=1)$ , the crack growth data in Fig. 1.11(a) are shifted to higher  $\Delta K$  levels relative to the large-crack data. After incorporating the aspect ratio variation into the calculations, the crack growth data at the surface and at the depth of the surface cracks agree with the large-crack trend (Fig. 1.11(b)). In these figures, crack growth at the surface,  $dc/dN$  is plotted against  $\Delta K_C$  (stress intensity range at surface) while the crack growth rates at depth are plotted in terms of  $\Delta K_a$  (stress intensity range at depth). Fig. 1.11(c) shows the crack growth data of surface cracks, both in terms of  $\Delta K_{eff}$  at the surface and at the depth. In the calculations, the same level of closure load measured from the load-displacement curve was used for the determination of the effective stress intensity ranges. This was found to be satisfactory for the surface crack data generated in the present study.

Similarly, Fig. 1.12 (a-c) illustrates the variations of crack growth for the deep notch configuration. When a constant aspect ratio,  $a/c=1$ , was assumed for the calculations, it can be seen from Fig. 1.12(a) that the surface crack growth rates initially were faster than those of the large cracks. After incorporating the aspect ratio variations into the calculations, crack growth rates both in terms of  $\Delta K$  and  $\Delta K_{eff}$  agree well with the large-crack trends.

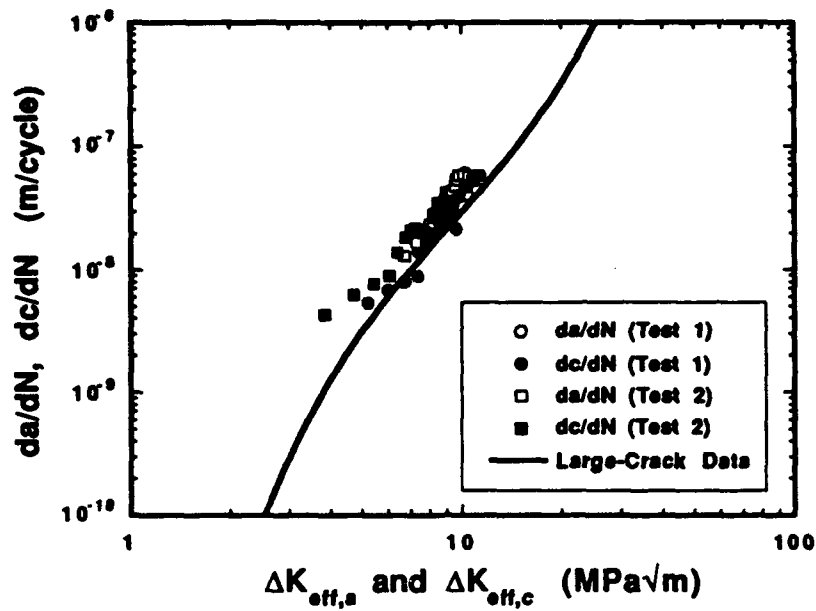


1.11(a)



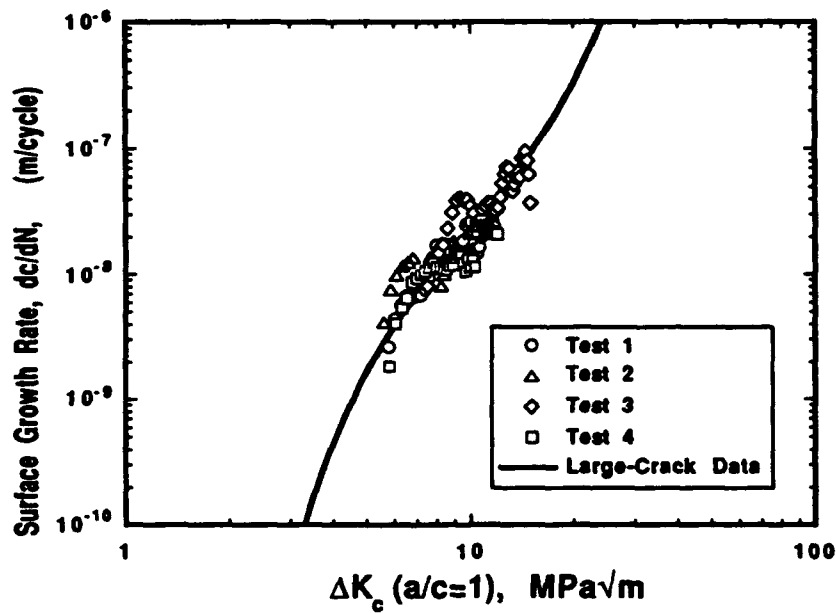
1.11(b)

(Figure caption overleaf)

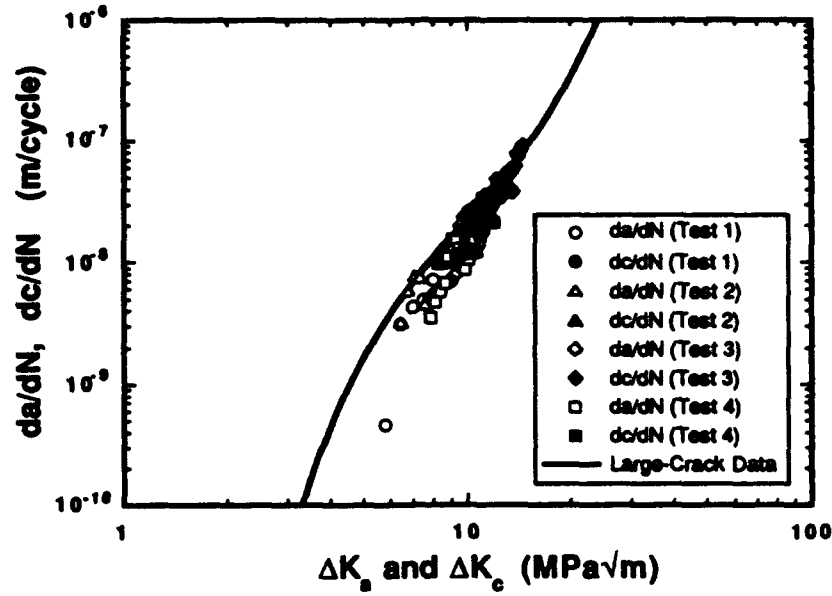


1.11(c)

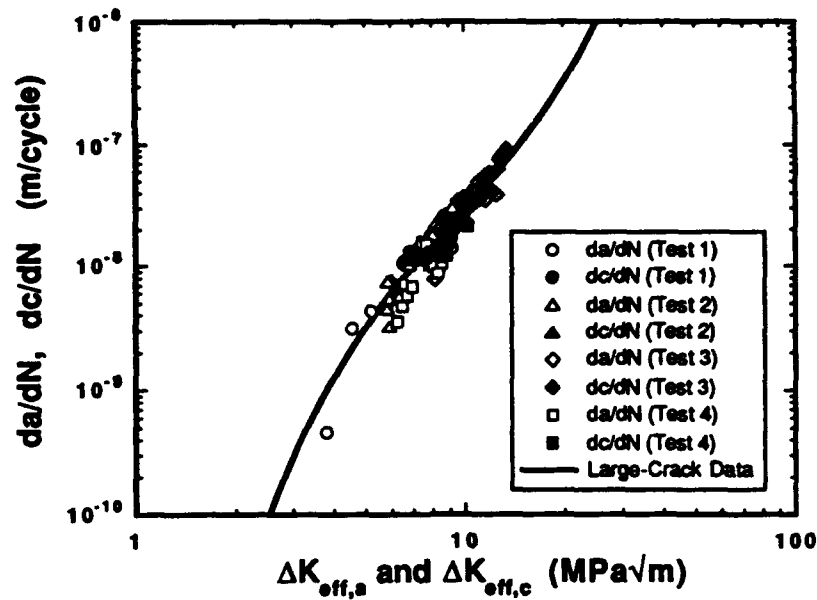
Fig. 1.11. A comparison of fatigue crack growth rates of cracks growing from a shallow notch as a function of  $\Delta K$ , without and with aspect ratio correction, (a) and (b) respectively and (c) with aspect ratio correction as a function of  $\Delta K_{eff}$  compared with the large crack growth data



1.12(a)



1.12(b)



1.12(c)

Fig. 1.12. A comparison of fatigue crack growth rates of cracks growing from deep notch as a function of  $\Delta K$ , without and with aspect ratio correction, (a) and (b) respectively, and (c) with aspect ratio correction as a function of  $\Delta K_{eff}$  compared with the large crack growth data

If the compliance measurements of a crack, asymmetrically growing with respect to its original location of initiation, are continuously made using the set of indentations placed at the center of the original crack, the measurements would underestimate the true compliance of the crack and thereby the aspect ratio. The correction of compliance through eqn. (1.3) is illustrated in the following experiment involving a surface crack grown from a semicircular notch. The crack was initiated from the notch under normal conditions of fatigue loading (stress level of  $0.4 \sigma_y$  and  $R=0.1$ ) and grown to about 1.5 mm in surface length. A first set of indentations was placed across the center of the crack and a second set of the indentations was placed across a location about 20  $\mu\text{m}$  from one of the crack tips. Compliance measurements were continuously made from both sets of indentations as the crack grew, and the crack was photographed at the same intervals. This produced independent data sets for the two compliance measurement locations. These measurements were made until the crack grew to about 2.5 mm in surface crack length. Figure 1.13 illustrates the crack with the two sets of indentations after the end of the test.

The measured compliance from both locations are presented as a function of surface crack length in Fig. 1.14. Also presented is the compliance corrected using Eqn. (1.3) for the asymmetry of measurement location, as well as the measure of asymmetry,  $(p/r)$  during the crack growth. It can be seen that when  $p/r$  varied from about 0.98 to 0.5, the compliance corrected for asymmetry agrees very well with the correct compliance measured at the center. As a further test of the accuracy of such corrections, crack aspect ratios were calculated from the compliance measurements at the center as well as from the corrected asymmetric compliance and are presented in Fig. 1.15. It is to be noted that the crack always grew in a semicircular shape in this specimen, and the aspect ratio measurements from both compliance measurements agreed well with  $a/c=1.0$ , as expected.

The above results confirm that precise measurements of crack aspect ratios can be made continuously during the growth of surface cracks. The present approach could be useful in the investigation of shapes of small surface cracks influenced by the interactions between crack tip and material microstructure. Further, the effects of changes in the mechanical as well as microstructural characteristics of surface layers, modified by treatments for fatigue strength improvement, on the behavior of surface cracks can also be assessed.



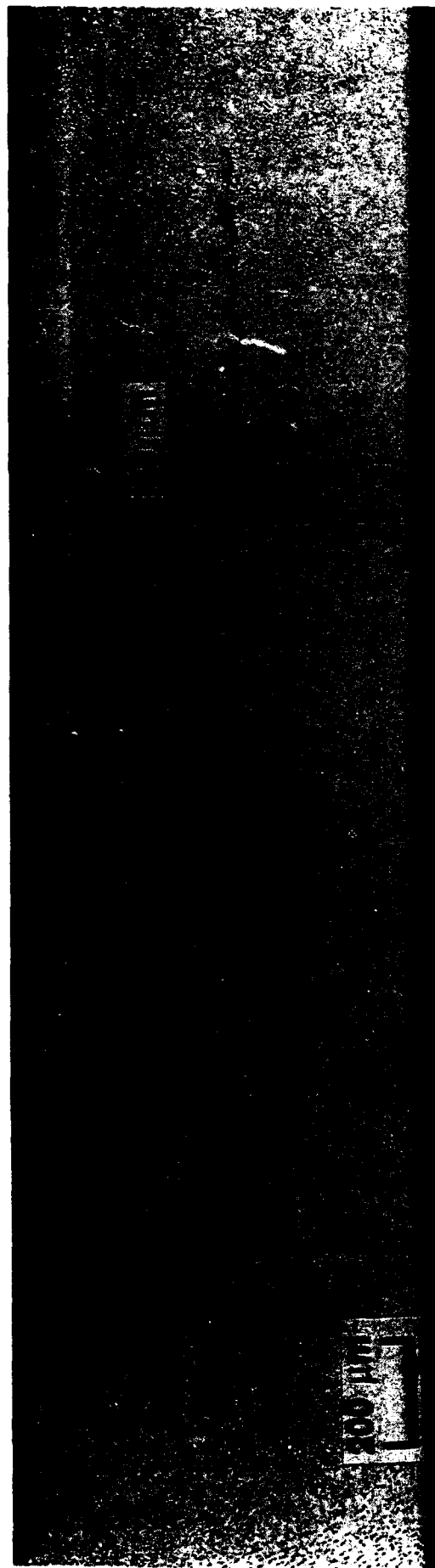


Figure 1.13. Optical micrograph of a crack grown from a semicircular notch illustrating the two locations of compliance measurement

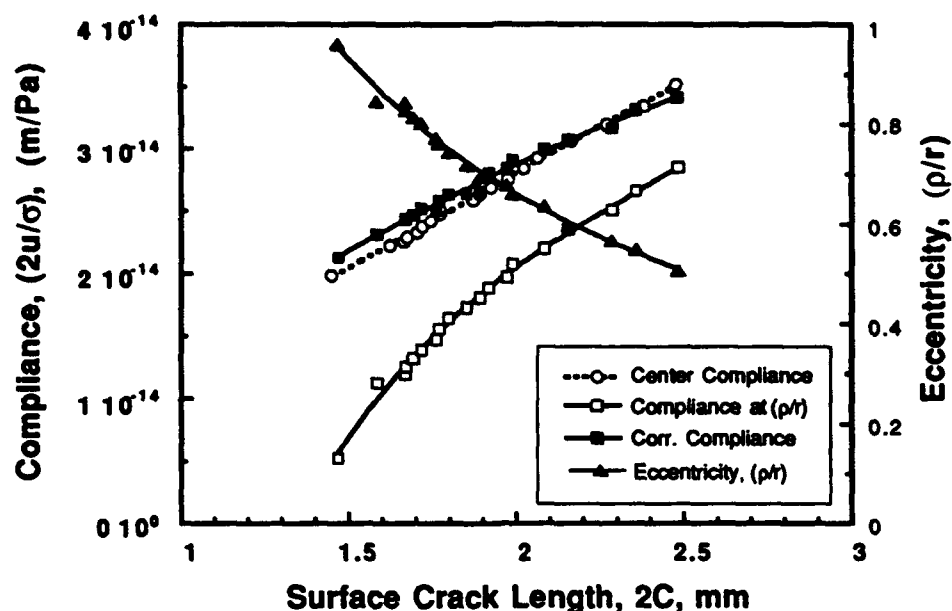


Fig. 1.14. Variation of crack compliance measured at two locations (Fig. 1.13) when the crack grew from 1.5 mm to 2.5 mm. Also shown are the compliance measurements corrected for the asymmetry in the measurement location as well as the eccentricity (a measure of asymmetry of the measurement location)

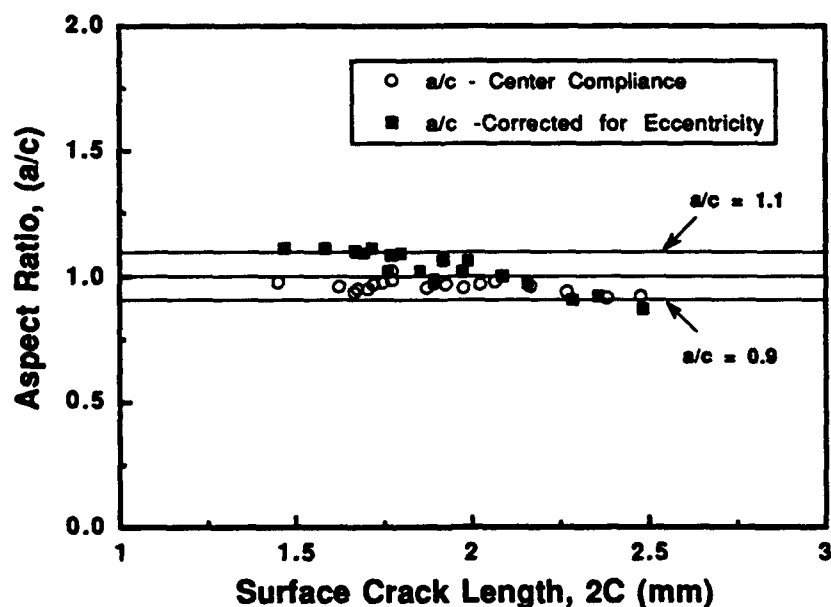


Fig. 1.15. A comparison of the aspect ratio calculated from the compliance measured at the center of the crack with that calculated from compliance measured from the asymmetric location after correction

## 1.5. CONCLUSIONS

An approach to measure the aspect ratios of three dimensional surface cracks continuously during growth from a small crack to a large crack in fatigue was developed. The technique uses a laser interferometric system for the measurement of crack compliance and a photomicroscopic system for the measurement of surface crack length. Aspect ratios were calculated from these measurements using a compliance expression valid for  $0.2 \leq a/c \leq 2.0$ . The calculated aspect ratios for cracks growing from EDM notches of different geometries (shallow or deep) were shown to be in good agreement with the expected variations in aspect ratio. Further, it was shown that effects on compliance measurement due to asymmetric growth of a surface crack are well taken into account by the expression for the correction of crack-asymmetry. The fatigue crack growth rates, after incorporating the variations in aspect ratio in the calculations, agreed with the large-crack trend.

## 1.6 RECOMMENDATIONS

Further research is required to study the effects of crack shape variations on the development of crack closure, in particular, to isolate the loads at which closure occurs at the surface crack tip as well as the crack tip at depth. This will be useful in accurately estimating the effective stress intensity ranges at these locations.

## APPENDIX 1.1

Errors in the measurement of surface crack length involving photographing and digitizing would be reflected as errors in the calculated aspect ratios. Since the resolution of displacement measurements by laser interferometry is of the order of  $0.1 \mu\text{m}$ , the influence of errors in displacement on the calculated aspect ratio is considered as negligible. An estimate of error in aspect ratio, due to error in surface crack length can be made as follows. It is assumed that a surface crack of length  $2c = 1.0 \text{ mm}$  exists in a specimen of thickness  $3.0 \text{ mm}$  and width  $7.0 \text{ mm}$ . By varying the aspect ratio of this crack from  $0.2$  to  $2.0$ , the values of compliance for this crack were calculated from Eqn. (2). Then introducing errors,  $+\Delta(2c)$  for overestimation and  $-\Delta(2c)$  for underestimation, into the surface crack length, using the previously calculated compliance for a range of aspect ratios, the new aspect ratios  $(a'/c')$  were estimated. The typical % errors (over estimation or under estimation) introduced in surface crack length were  $2, 5, 10$  and  $20\%$ . Then the error in the estimated aspect ratio,  $(a'/c')$ , was calculated as

$$\% \text{ Error in aspect ratio} = \frac{(a'/c') - (a/c)}{a/c} \times 100 \quad \dots(\text{A.1.1.1})$$

The percent error in aspect ratio is plotted as a function of actual aspect ratio  $(a/c)$  in Fig. A.1.1.1. It can be seen from the figure that the errors in  $a/c$  diverge at large values of aspect ratio. The error can be considered small as long as the measurement of surface crack length is made with errors less than  $2\%$ . Since the errors in the crack lengths measured from photomicrographs are usually of the order of  $1\%$  [1.24], the aspect ratios estimated are fairly accurate.

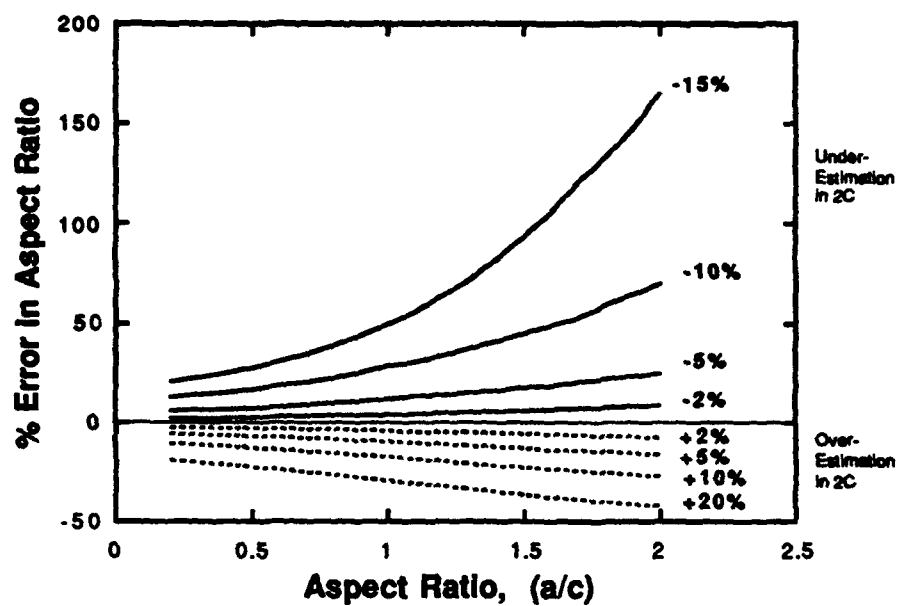


Fig. A.1.1.1. An estimation of % error in the calculated aspect ratio due to errors in surface crack length for a range of aspect ratios of crack of 1.0 mm in surface length

## APPENDIX 1.2

The stress intensity factor equation of Newman-Raju is plotted in terms of non-dimensional stress intensity factor calculated both at the surface and at depth as functions of  $(a/c)$  in Fig. A.1.2.1. It can be seen that at large  $a/c$  values, typically higher than about 2.5, the stress intensity factors are insensitive to aspect ratio, since the geometry of the crack approaches that of the center, through-crack in a tensile specimen. It is likely that the aspect ratio during calculation can increase unrealistically if the compliance of the crack is at the region of asymptotic behavior ( $a/c \geq 2.5$ ) due the crack growing deeper than  $a/c = 2$ , in which case, the iteration process on aspect ratio would diverge (see Fig. A.1.1.1). Hence, to circumvent the situation of the iterative process exceeding aspect ratio 2.5, the iteration was stopped when  $a/c$  exceeded 2.5 and the aspect ratio for these cases was taken as 2.5 for the stress intensity factor calculations. This is expected to cause only a small error in stress intensity factor calculation, because of the asymptotic nature of stress intensity factor at large  $a/c$  values.

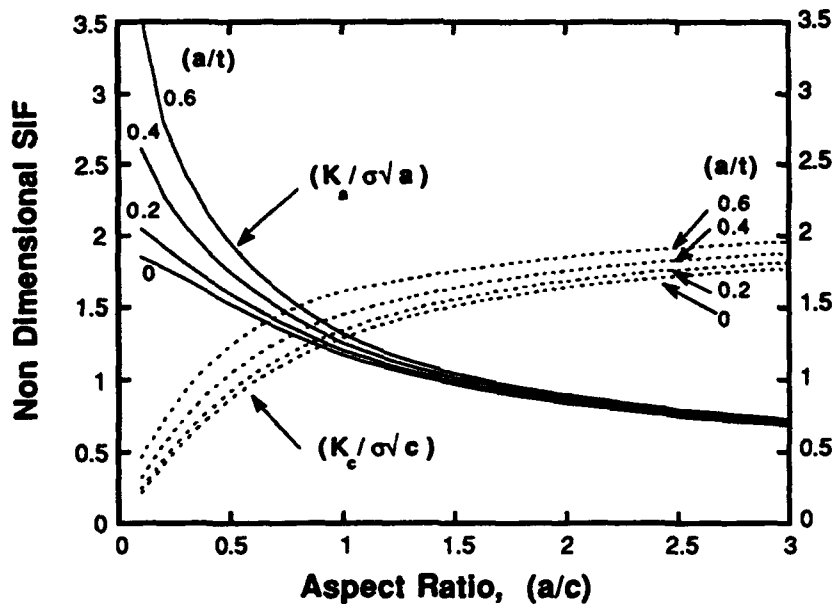


Fig. A.1.2.1. The variation of non-dimensional stress intensity factors at the surface and at the depth of a surface crack as a function of aspect ratio, as calculated using the Newman-Raju formula [1.25]

### APPENDIX 1.3

In the measurements of aspect ratios of small surface cracks, there is a limit to the smallest crack size for which the compliance can be reliably measured. If the spacing between the indentations used to measure displacements is fixed, the compliance approaches that of the uncracked specimen as the size of the crack approaches zero. As long as the compliance of the crack is larger than that of the compliance of the uncracked specimen measured with the same indent spacing, the compliance is little influenced by the elastic displacements of the bulk material enclosed between the indentations. Since there is a limit to the smallest indent spacing that can be chosen to measure displacements without affecting the crack tip stress fields, there is a limit to the crack size for which the compliance is larger than the uncracked case. This limit will also depend of the aspect ratio of the crack. The effect of the size of the crack relative to the indent spacing on compliance will be assessed in this section. The compliance of the uncracked specimen, subjected to stress ' $\sigma$ ' with indent spacing ' $d$ ' and modulus  $E$  can be written as

$$\frac{2U}{\sigma} = \frac{d}{E} \quad \dots(A.1.3.1)$$

where  $2U$  is the displacement measured across the indentations in the absence of the crack. For a semi-infinite specimen ( $a/t \rightarrow 0$ ), with a surface crack of length ' $2c$ ' the compliance can be written from Eqn. 2 as

$$\frac{2U}{\sigma} = 1.76 \frac{\sqrt{8}}{E} c (1-\nu^2) \lambda \frac{M_1}{\sqrt{Q}} \quad \dots(A.1.3.2)$$

Dividing A.1.3.2 by A.1.3.1 and denoting the compliances with and without a crack as  $\Phi_{\text{crack}}$  and  $\Phi_{\text{No crack}}$  respectively,

$$\frac{\Phi_{\text{crack}}}{\Phi_{\text{No crack}}} = 0.88 \sqrt{8} \left( \frac{2c}{d} \right) (1-\nu^2) \lambda \frac{M_1}{\sqrt{Q}} \quad \dots(A.1.3.3)$$

The variables  $\lambda$ ,  $M_1$  and  $Q$  are the same as in Eqn. 1.2. The normalized compliance in Eqn. A. 1.3.3 is plotted as a function of the normalized surface crack length ( $2c/d$ )

in Fig. A.1.3.1 for several crack aspect ratios. It can be seen that except for the shallow crack case,  $a/c=0.2$ , the compliance of the crack is larger than the elastic compliance of the specimen for  $2c/d \geq 1.0$ . Hence the compliance measurements for cracks  $2c/d \geq 1.0$ , can be considered to be little influenced by the elastic displacements of the specimen.

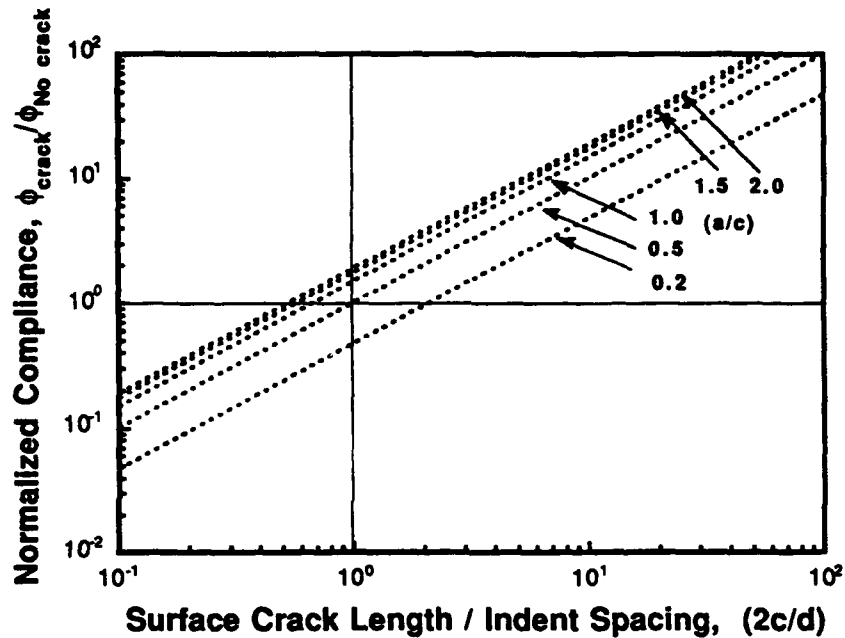


Fig. A.1.3.1. The variation of the ratio of compliance of a surface crack to that of the crack-free specimen as a function of normalized surface crack length



## CHAPTER 2

### THE GROWTH BEHAVIOR OF SMALL FATIGUE CRACKS IN TITANIUM ALUMINIDE ALLOYS

#### 2.1 INTRODUCTION

Understanding of growth behavior of small cracks in high strength materials is important, since the crack sizes at which unstable fracture might occur are much smaller relative to conventional materials. In particular, titanium aluminide alloys currently under development, have relatively low ductility and fracture toughness, often limiting the unstable crack size to a few mm. In this study, small crack growth behavior of two titanium aluminide alloys, viz., Ti-24Al-11Nb and Ti-25Al-17Nb-1Mo were investigated under nearly identical microstructural condition. Both alloys belong to  $\alpha_2$  (Ti<sub>3</sub>Al) class, and the later has been suggested [2.1] to possess a better combination of strength and fracture toughness than the former. Earlier work [2.2, 2.3] in the Materials Behavior Branch, Materials Directorate, Wright laboratory revealed that the development of shapes of three dimensional surface cracks in Ti-24Al-11Nb is influenced by microstructure, making it necessary to measure the continuous variations in crack shape to calculate crack growth data accurately in this material. The objective of the present study was to document the growth characteristics crack shape development of small cracks in Ti-25Al-17Nb-1Mo and compare them with small cracks in Ti-24Al-11Nb.

#### 2.2 EXPERIMENTAL PROCEDURE

The material used in this investigation was a vacuum arc melted and cast alloy of nominal composition Ti-24Al-11Nb. Cylindrical castings of approximate dimensions: 200 mm in diameter and 280 mm in height were isothermally forged down to a circular disk of about 50 mm in thickness and 400 mm in diameter (80% reduction) at 1065°C at a strain rate of 0.1 min<sup>-1</sup> and air cooled to room temperature. Sections of the disk were heat treated according to the schedule: 1150°C/30 min./air cool/815°C/30 min./air cool/593°C/8hr/air cool to produce basketweave microstructure. Similarly, the vacuum arc melted and hot rolled plates of Ti-25Al-17Nb-1Mo were heat treated following the schedule: 1175°C/30 min./direct salt bath quench to 815°C/30 min/air cool, giving a similar but finer microstructure as Ti-

## 24Al-11Nb.

Small-crack tests were performed on electropolished specimens of rectangular cross-section containing a mild notch ( $K_t = 1.037$ ). The specimen design is the same as the one used in chapter 1. For Ti-24Al-11Nb, fatigue cracks were initiated at a stress level of  $0.6\sigma_y$  ( $\sigma_y$  is yield strength) with a stress ratio,  $R = -1$ . After a crack of 150-200  $\mu\text{m}$  in surface length (2c) had been formed, two Vickers microhardness indentations were placed across the crack for the measurement of crack mouth opening displacement (CMOD) using a laser interferometric system. Fatigue tests were conducted at room temperature at a frequency of 10 Hz with  $R=0.1$ , at stress levels of  $0.6-0.8\sigma_y$ . Since small cracks could not be naturally initiated in Ti-25Al-17Nb-1Mo, electro-discharge-machined (EDM) notches of about 150  $\mu\text{m}$  in surface length and semicircular in shape were employed to initiate cracks, typically under stress levels of  $0.4-0.5 \sigma_y$  at  $R=0.1$ . Surface lengths of small cracks were recorded using an automated photomicroscopic system, and CMOD measurements were made using the laser interferometric displacement measurement system. Crack growth rates at the specimen surface, as well as at the crack depth, were calculated based on the estimated aspect ratio ( $a/c$ , where 'a' is crack depth) using an incremental polynomial regression technique. The details of the system and data reduction methods are described in detail elsewhere [2.4-2.6]. Crack growth data for large cracks were generated using compact tension (C(T)) specimens. Crack closure measurements for the small and large cracks were made from the unloading compliance data acquired by the laser interferometric system and the data from clip-on gages, respectively.

## 2.3 RESULTS

The microstructures are shown in Fig. 2.1(a&b) and microstructural and mechanical property data are presented in Table 2.1. The microstructure of Ti-24Al-11Nb consist of large prior beta grains of the order of 200 to 1000  $\mu\text{m}$  and  $\alpha_2$  platelets of size 1-3  $\mu\text{m}$ . The prior beta grains of Ti-25Al-17Nb-1Mo were of the order of 600 to 1500  $\mu\text{m}$  and  $\alpha_2$  platelets of size  $\leq 1 \mu\text{m}$ . The average prior beta grain size was larger and the thickness of  $\alpha_2$  platelets were lower for the Ti-25-17-1 alloy compared to Ti-24-11. The larger prior beta grain size could be due to the higher temperature for beta heat treatment in Ti-25-17-1. However, the finer platelet could be due to the isothermal transformation at 815°C employed for Ti-25-17-1. Small

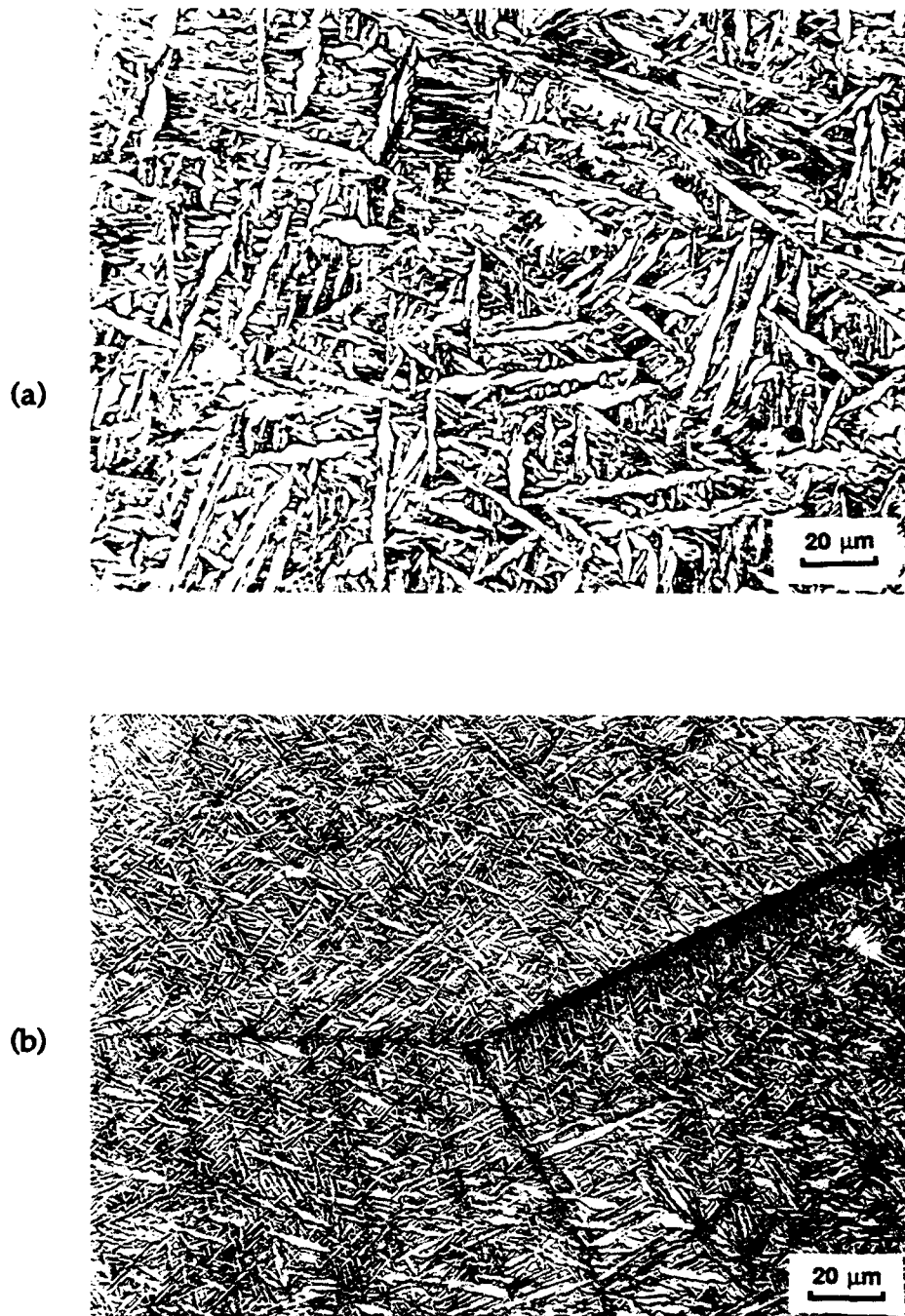


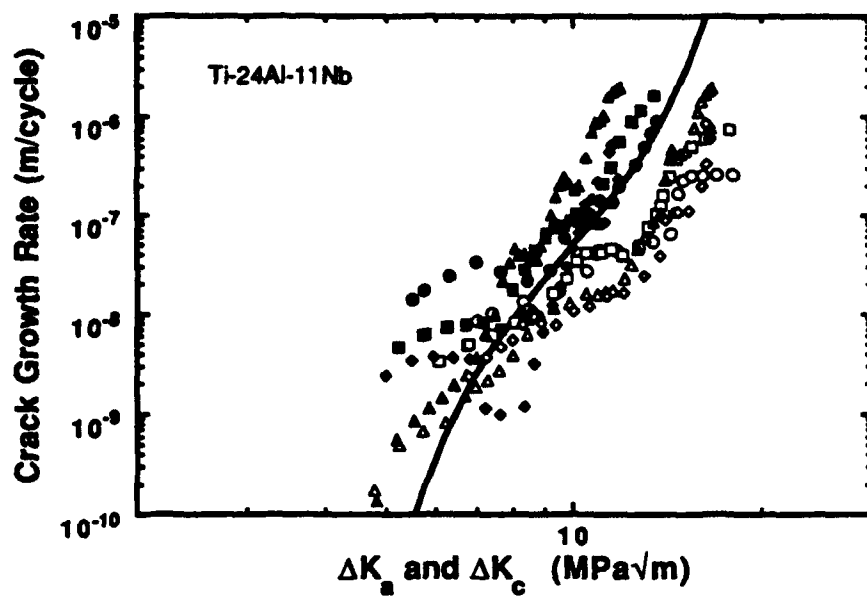
Figure 2.1 Microstructures of (a) Ti-24-11 and (b) Ti-25-17-1 alloys

cracks in Ti-24-11 generally initiated at prior beta grain boundaries, and the crack propagated into more than one grain at the final crack size of about  $\geq 2000 \mu\text{m}$ . In Ti-25-17-1, since the EDM notches were located in the interior of the grain, cracks generally propagated within one grain until the final unstable fracture intervened at about crack sizes of 400-800  $\mu\text{m}$ .

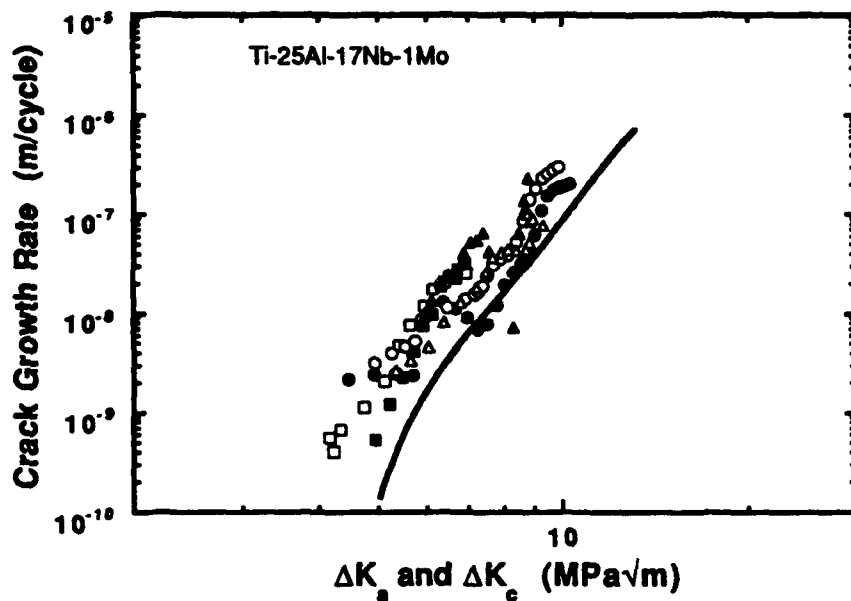
**Table 2.1 Microstructure and Mechanical Property Data for Ti-24-11 and Ti-25-17-1**

Material	Prior $\beta$ grain size ( $\mu\text{m}$ )	$\alpha_2$ platelet size ( $\mu\text{m}$ )	0.2% YS (MPa)	UTS (MPa)	% El	% RA	K <sub>c</sub> (MPa $\sqrt{\text{m}}$ )
Ti-24-11	600	1-3	639	758	2.4	3.8	14-16
Ti-25-17-1	900	0.4-1	998	1134	3.4	6.6	8-11

Fatigue crack growth data of small and large cracks are presented in Fig. 2.2(a & b) for Ti-24-11 and Ti-25-17-1 respectively, as a function of  $\Delta K$ . Crack growth data are also presented as a function on  $\Delta K_{\text{eff}}$  in Fig. 2.3 (a & b) for Ti-24-11 and Ti-25-17-1 respectively. The small-crack data consist of both  $da/dN$  and  $dc/dN$  as a function of stress intensity factor range at the crack depth ( $\Delta K_a$  or  $\Delta K_{\text{eff},a}$ ) and at the surface position ( $\Delta K_c$  or  $\Delta K_{\text{eff},c}$ ), respectively. The solid curve represents a fit to three large-crack tests under both decreasing and increasing  $\Delta K$  conditions. Although the crack growth behavior of the large cracks are nearly the same for both the materials, significant differences in crack growth behavior between Ti-24-11 and Ti-25-17-1 can be seen. In particular, crack growth rates at the depth are clearly greater than that at the surface position for Ti-24-11, indicating that cracks propagate with deep crack morphologies ( $a/c > 1$ ). The aspect ratio as a function of surface crack length for Ti-24-11, presented in Fig. 2.4, suggests that the small cracks maintained deep crack morphologies over most of their growth period in all tests. On the other hand, no significant differences between crack growth rates at the depth and surface position were seen for Ti-25-17-1. This is consistent with the data on  $a/c$  presented in Fig. 2.5, indicating that the cracks maintained a nearly semicircular shape, and the aspect ratios varied little during crack growth.

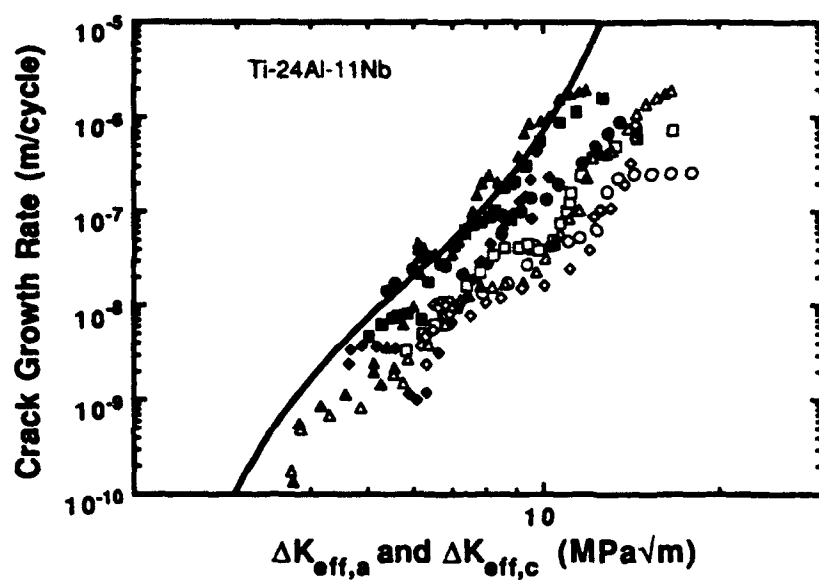


2.2 (a)

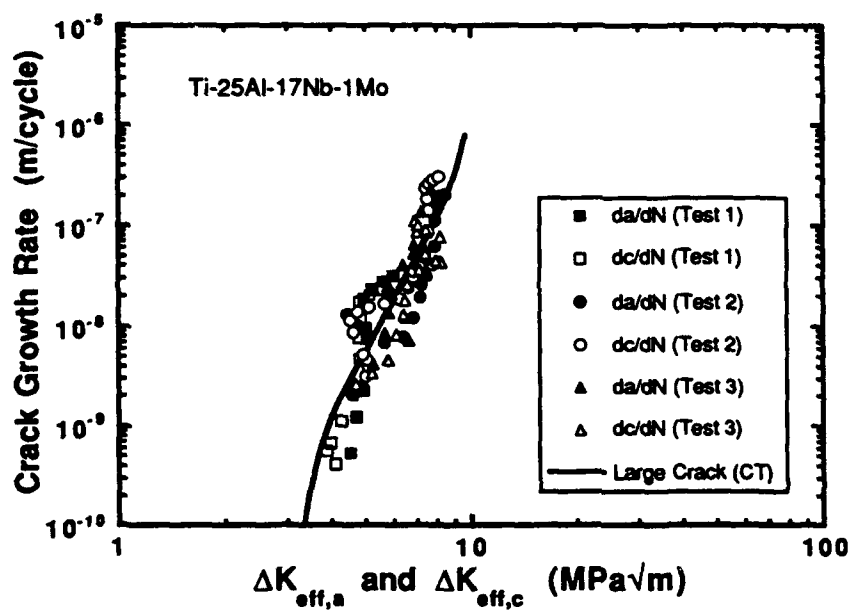


2.2 (b)

Fig. 2.2. Crack growth rates versus  $\Delta K$ ; (a) Ti-24-11 and (b) Ti-25-17-1  
(Solid symbols:  $da/dN$  vs.  $\Delta K_a$ ; Open symbols:  $dc/dN$  vs.  $\Delta K_c$ )



2.3 (a)



2.3 (b)

Fig. 2.3. Crack growth rates versus  $\Delta K_{\text{eff}}$ ; (a) Ti-24-11 and (b) Ti-25-17-1  
(Solid symbols: da/dN vs.  $\Delta K_{\text{eff},a}$ ; Open symbols: dc/dN vs.  $\Delta K_{\text{eff},c}$ )

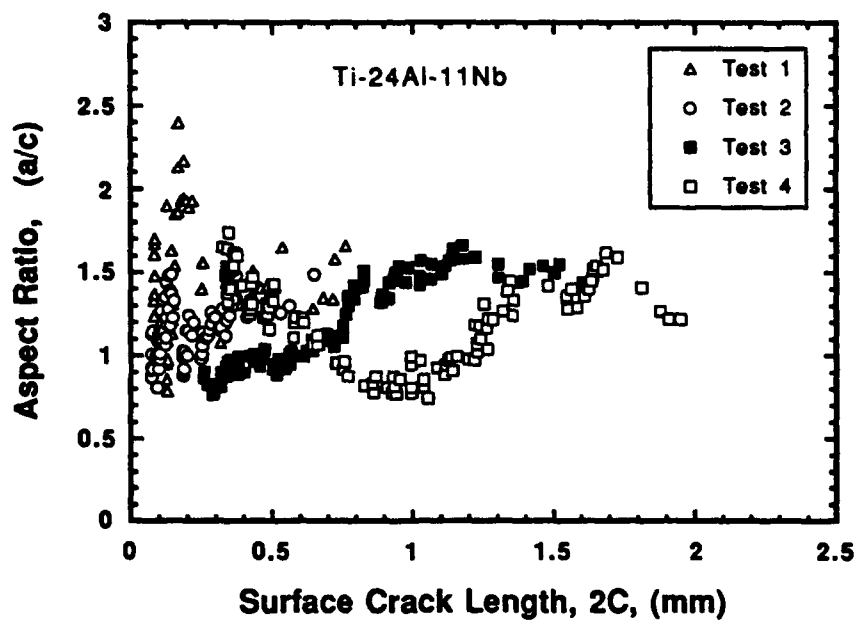


Fig. 2.4. Aspect ratio vs. surface crack length in Ti-24-11

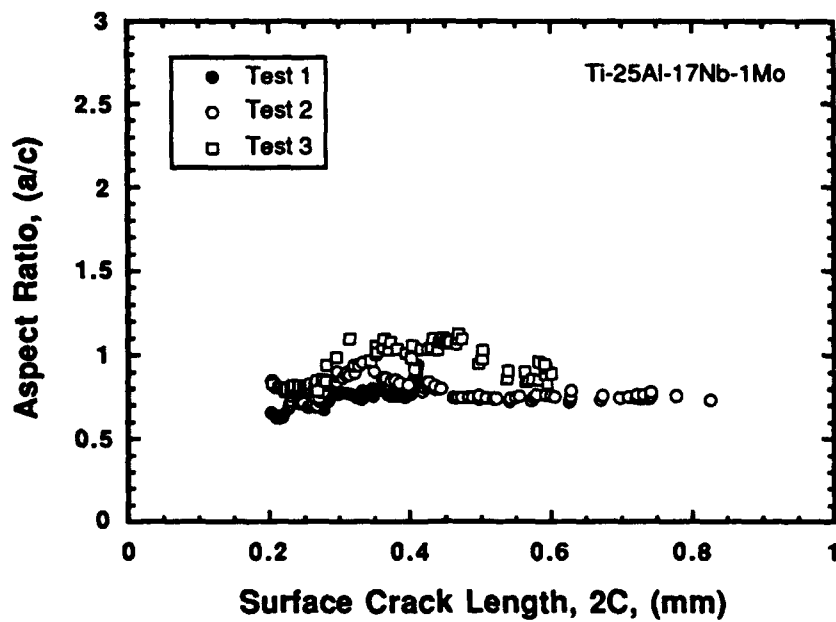


Fig. 2.5. Aspect ratio vs. surface crack length in Ti-25-17-1

## 2.4. DISCUSSION

The similarities in large-crack growth behavior between the morphologically similar microstructures of these two alloys is expected. This could be due to the nearly brittle fracture of less ductile  $\alpha_2$  phase during crack growth, irrespective of its morphology. Hence, the compositional difference of Ti-25-17-1 relative to Ti-24-11 appears to have no effect on crack growth characteristics. The difference in microstructure seems to arise mainly from the difference in heat treatment approach employed.

The variations in crack aspect ratio have been shown [2.3] to be important in the growth of small fatigue cracks in Ti-24-11 under different microstructural conditions. The measurement approach has also been demonstrated in chapter 1 to be accurate enough to track the continuous variations in crack aspect ratio in model experiments. In this respect, the variations in aspect ratio encountered in Ti-24-11 can be considered to be intrinsic to the microstructure and not due to any measurement error. On the other hand, a far lower degree of variation in aspect ratio was observed in Ti-25-17-1. A notable difference is the way in which the cracks were initiated. While cracks could be initiated naturally by fully reverse fatigue cycling in Ti-24-11, Ti-25-17-1 was almost immune to fatigue crack initiation under normal stress levels employed ( $\sigma/\sigma_y=0.8$ ). At stresses higher than this level, cracks could be initiated which soon were arrested followed by specimen failure either from an internally initiated crack or crack initiated elsewhere, for example, specimen corners. The use of EDM notches facilitated the initiation of cracks with no difficulty at low stress levels ( $\sigma/\sigma_y=0.4-0.5$ ). However, this is different from Ti-24-11, in terms of the environment in which the cracks initiated as well as the regions of microstructure through which the crack would eventually grow. Crack path profiles for Ti-24-11 material is shown in Fig. 2.6. Similarly, the profile of the crack grown from an EDM notch in Ti-25-17-1 specimen is shown in Fig. 2.7. The grain boundary cracks in Ti-24-11 after initiation, propagated in two grains of different orientations as well as along the part of the boundary extended from the surface into the depth. These different parts of the microstructure in Ti-24-11 apparently influenced the development of the shape of the cracks and hence the crack growth rates at the surface and at the depth. Since the portions of grain boundary had aligned regions of  $\alpha_2$  platelets, this could have been an easier path for the crack front at depth, while the crack front at the surface





CRACK PATH IN THE BASKETWEAVE MICROSTRUCTURE 200  $\mu$ m

Figure 2.6. Crack path profile of a small crack in Ti-24-11

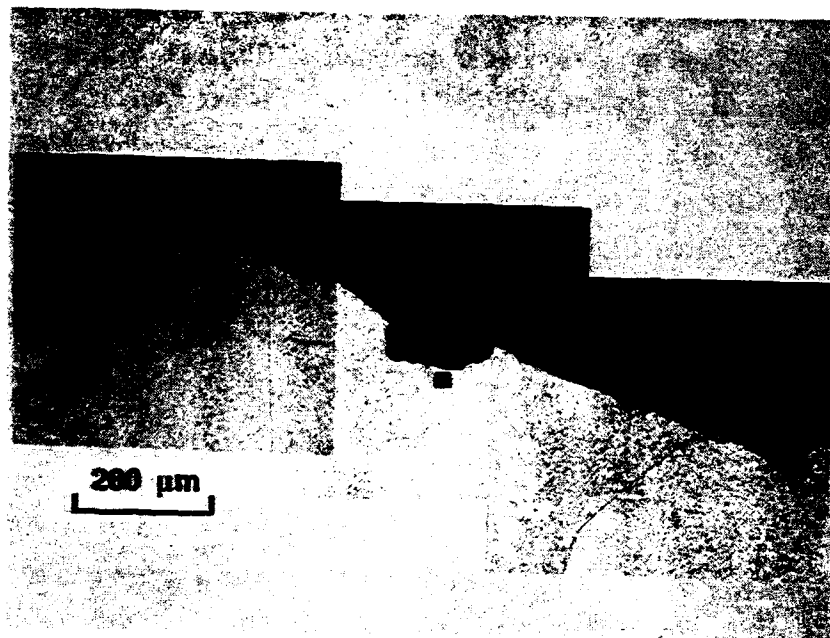


Figure 2.7. Crack path profile of a small crack in Ti-25-17-1

position encountered basketweave intragranular microstructure, possibly offering relatively high resistance. These conditions are absent for the cracks initiated from EDM notches in Ti-25-17-1 and except for a few instances, the cracks propagated within a single prior beta grain and less frequently into more than one grain. Hence it is likely that the crack front encountered a region of nearly uniform crack growth resistance, resulting in similar crack growth rates for crack tips at surface as well as at depth. Except for this difference, small crack behavior of Ti-25-17-1 is nearly the same as Ti-24-11.

## 2.5 CONCLUSIONS

Small cracks in Ti-24-11 initiated in regions along grain boundaries and grew with deep crack geometries, resulting in different crack growth rates at surface and at depth. In Ti-25-17-1, small cracks maintained nearly semicircular shape and growth rates were similar all along the crack front. This appears to be due to the growth of small cracks within a grain in the latter material. The large-crack data of both materials were also found to be similar. The lack of crack closure at small crack sizes was partly responsible for the apparent faster propagation of small cracks relative to large cracks in both materials.

## 2.6 RECOMMENDATIONS

Since the presence of grain boundary aligned platelet regions appear to influence the early growth of small cracks, it is likely that they have a significant effect on smooth specimen fatigue life, and this merits further investigation.

## CHAPTER 3

### SIMULATION OF CRACK SHAPE AND CRACK GROWTH RATES IN POLYCRYSTALLINE Ti-8Al TITANIUM ALLOY

#### 3.1 INTRODUCTION

Since the first work of Pearson [3.1], the growth behavior of naturally initiating small surface fatigue cracks have generated a great deal of interest [3.2]. Although the motivation is partly to understand the factors responsible for the rapid anomalous growth of such cracks compared to those commonly pursued using conventional fracture mechanics specimens, a general consensus on the possible use of small crack data in some form of life prediction methodology appears to be emerging.

It has been suggested that the anomalous growth effects are principally due to the lack of a fully developed crack wake to cause crack closure [3.3], plasticity effects at notch roots [3.4] and possibly a different form of stress singularity [3.5] unlike large cracks. While there is no doubt that these factors could be partly responsible for the anomalous behavior, there is also evidence of microstructural effects such as arrests of small cracks at grain boundaries [3.6-3.8]. However, there is no unified view on the relative importance of these factors, either singly or collectively, in rationalizing the anomalous behavior for engineering alloys of diverse mechanical behavior.

Relatively little attention has been paid to the effects of the shape of small surface cracks at the very early stages of their growth on crack growth behavior. It is clear that the crack aspect ratio ( $a/c$ ;  $a$ =crack depth and  $c$ = half surface length) enters the known solutions [3.9] of stress intensity factor ( $K$ ) calculations for a surface crack. In general, a semicircular shape ( $a/c=1.0$ ) is assumed because of the fact that at large crack sizes, the crack maintains approximately this shape and also because of the difficulties in measuring true crack shape at each crack length. However, the assumption of semicircular shape at early stages of crack growth, which is of prime interest, need not be always true. This is due to microstructurally induced perturbations which are significant in changing the shape of surface cracks and

thereby cause a change in  $\Delta K$  with location along the crack front.

By a simple simulation, the present study illustrates that fluctuations in crack shape due to grain boundary induced perturbations can result in the apparent anomalous behavior, which in fact is not anomalous when interpreted in terms of actual  $\Delta K$  incorporating the true instantaneous aspect ratio of the crack. This has been supported by experimental observations of changes in aspect ratio in small cracks tracked using a laser interferometric displacement measurement system [3.10] as well as by observations reported in literature [3.11]. Results of a detailed experimental program to experimentally verify these simulations are presented in chapter 4. It has been shown that any small surface crack is likely to behave as a large crack when the microstructure induced perturbations are no longer great enough to affect  $\Delta K$  distribution along the crack front significantly. The results also suggest that Taylor and Knott's [3.12, 3.13] projections of a small crack of size  $10d$  ( $d$ =grain size) behaving as a large crack are closely linked to the aspect ratio variations due to grain boundary induced perturbations.

### 3.2 CRACK GROWTH SIMULATION

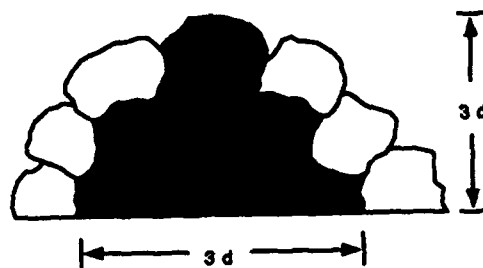
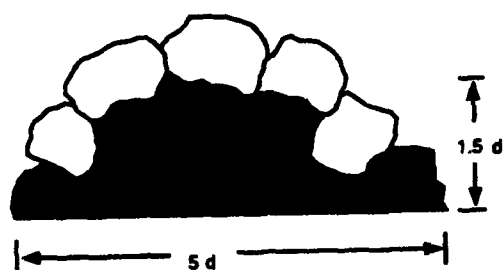
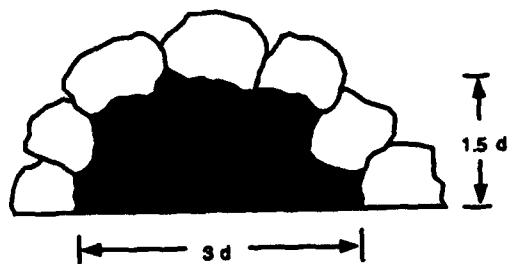
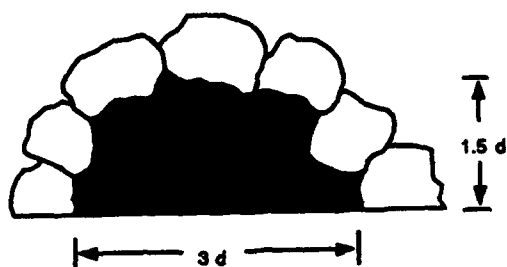
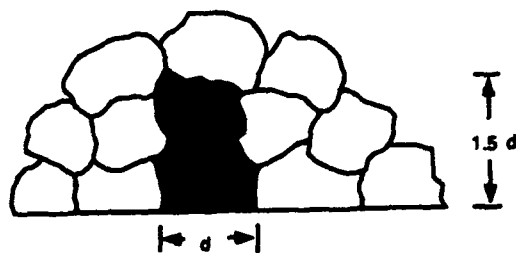
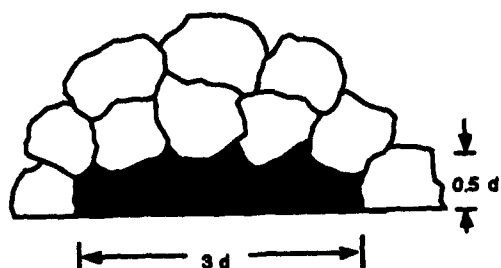
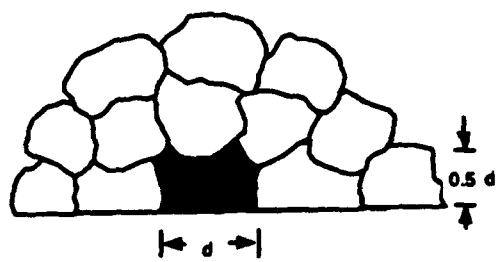
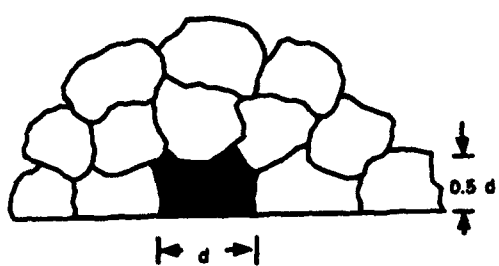
In the following, a crack growth process where the crack front is periodically arrested at a grain boundary alternatively at the surface and at depth is simulated. Considerable data [3.6-3.8] show the arrest of cracks at grain boundaries for over a magnitude of cycles corresponding to threshold condition. Wagner et al. [3.11] suggest that when a crack grows on the surface, its front at the depth is temporarily arrested. This deviation from equilibrium shape may be due to the differences in strengths of grains on the specimen surface and at the crack depth. As the crack grows shallower,  $\Delta K_a$  ( $\Delta K$  at depth) increases, and at a critical value, which is dependent on the strength of the blocking grain, the crack grows in depth direction until  $\Delta K$  becomes uniform all along the crack front. Crack growth at the depth could continue again, deviating from equilibrium shape to the extent determined by the strength of the grain blocking the surface tip. Once the required  $\Delta K_c$  ( $\Delta K$  at the surface tip) is reached, growth at the depth would stop and continue at the surface. It is unlikely that the two grains at both surface crack tips would have the same strength, and hence only uneven crack growth in the surface is realistic. However, for simplicity it will be assumed that crack extension occurs evenly at the surface. In brief, growth at any location of low resistance would ensue to the extent that the

crack shape deviates enough from equilibrium to the cause  $\Delta K$  value elsewhere along the crack front to increase sufficiently to overcome the resistance at those locations. The problem can be simulated including the statistical variations in grain size, shape and orientation and the strengths of the twist/tilt boundaries between the grains as well as the choice of a slip systems. However, for simplicity, this simulation considers the ideal growth in crack fronts at surface and depth alternatively.

For illustrative purposes, the two crack growth schemes A and B shown in Figs. 3.1(a&b) are employed. It is assumed that a semicircular crack of size  $2c=d$  exists or is nucleated in the preceding fatigue cycles. In Fig. 3.1(a) the surface crack tips are considered to propagate first. When  $2c=3d$ , crack growth at the depth is considered to occur. At  $a=1.5d$ , crack growth at the surface would occur and so on. In Fig. 3.1(b), the reverse case is considered. In both cases, crack tips are made to propagate by equal increments ( $\Delta(2c)$  or  $\Delta a = d/10$ ). For a given stress level, ( $\sigma_{\max}/\sigma_y=0.6$ ),  $\Delta K$  at the surface ( $\Delta K_c$ ) is calculated by incorporating both the actual aspect ratio at the instant of crack growth ( $\Delta K_{c,act}$  at surface or  $\Delta K_{c,act}$  at depth) and the assumed aspect ratio of 1.0 ( $\Delta K_{c,asp}=1$  at surface or  $\Delta K_{a,asp}=1$  at depth). Crack growth rates for these two cases are then calculated from a general Paris type expression

$$da/dN = 3.0 \times 10^{-12} (\Delta K)^{3.2} \quad \dots(3.1)$$

generated for Ti-4Al alloy [3.14]. Fig. 3.2(a&b) illustrate the variations in aspect ratio as the crack grows according to the sequences in Fig. 3.1(a&b) respectively. It is seen that there are large variations in aspect ratio until the crack is about ten times the grain size. Two experimental data sets presented in Fig. 3.3 (a) and (b) are strikingly similar to these variations. The data in Fig. 3.3 (a) are from Wagner et. al.[11] who determined aspect ratios of several cracks by electropolishing. The data in Fig. 3.3(b) is from the work of Larsen [3.14] on Ti-Al alloys. The aspect ratios were determined [3.15-3.17] from the measurements of compliance using a laser interferometric displacement measurement system as well as surface crack lengths from a photomicroscopic system. Considering the statistical nature of variations in grain size and the orientation relationships between grains which dictate the arrest, the trends closely resemble the predicted variations in aspect ratio. It should be noted that practically any trend between the bounds in Fig. 3.2 (a&b) is possible due to randomness in crack nucleation and propagation. When the crack growth rates as



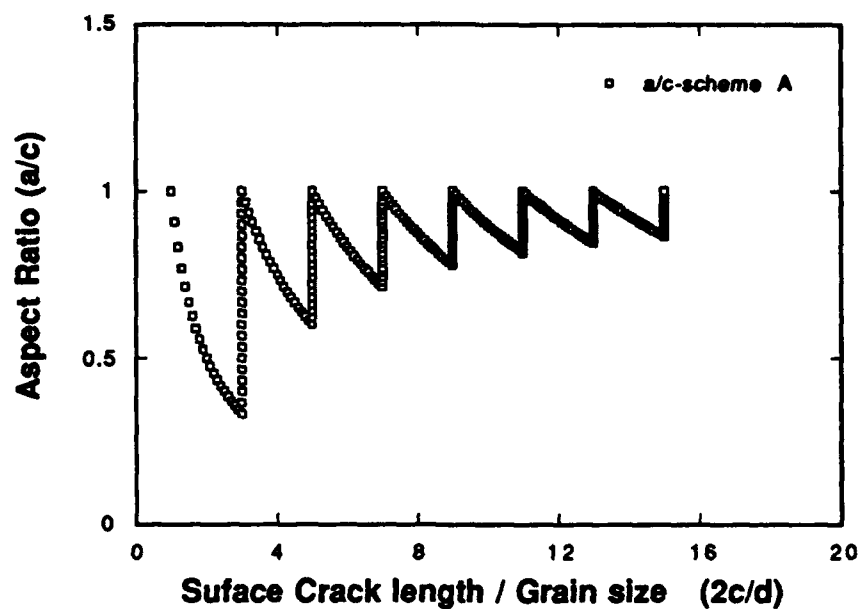
**SCHEME A**

**SCHEME B**

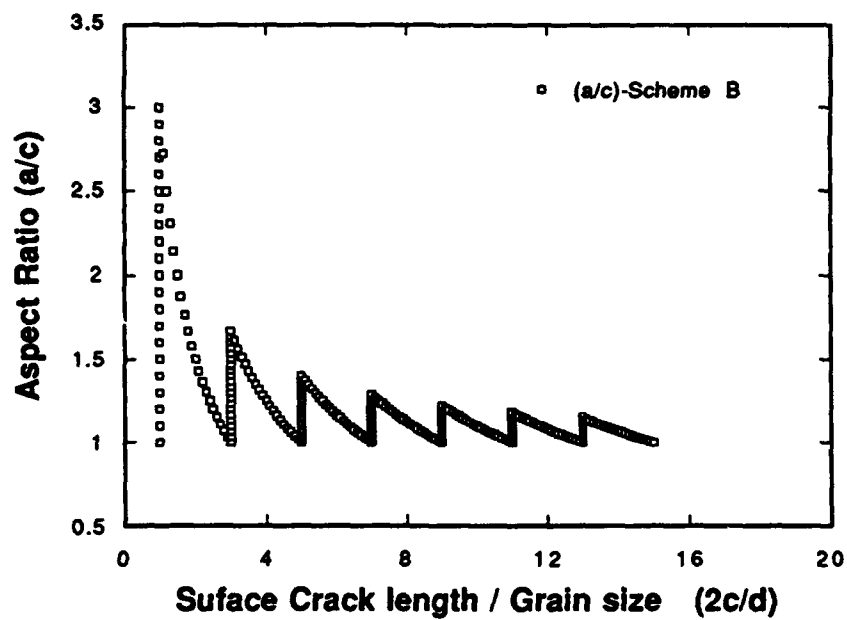
(a)

(b)

Fig. 3.1 (a) and (b): An illustration of crack growth schemes

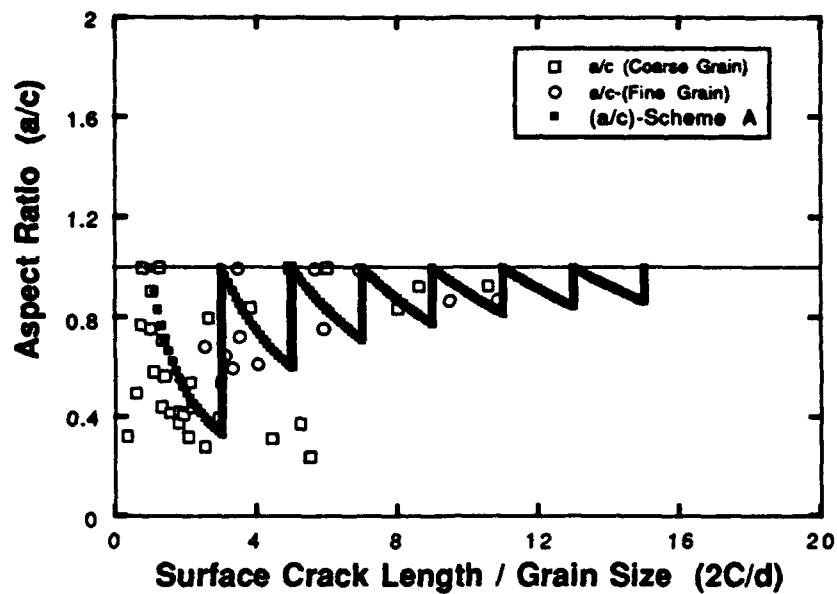


3.2 (a)

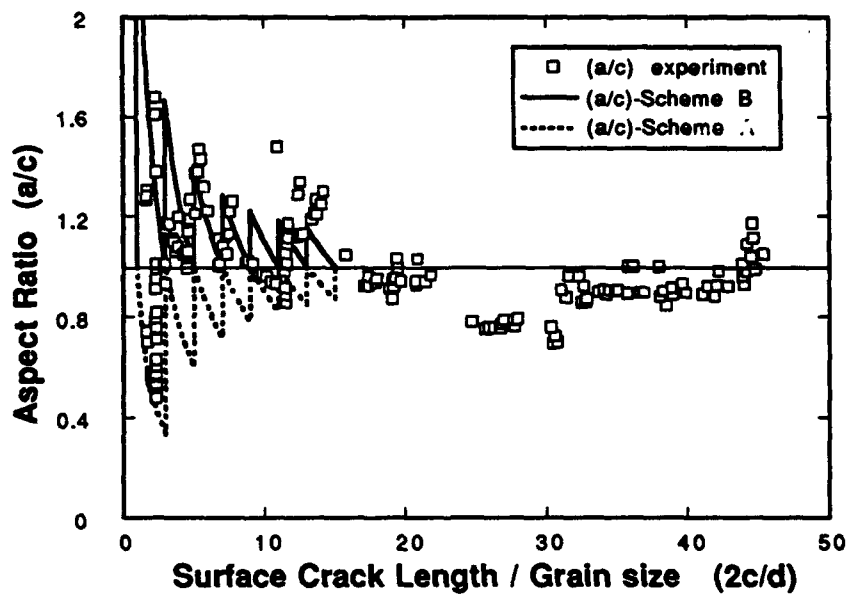


3.2 (b)

Fig. 3.2. The variation of aspect ratio from the simulation of crack growth according to (a) scheme A and (b) scheme B



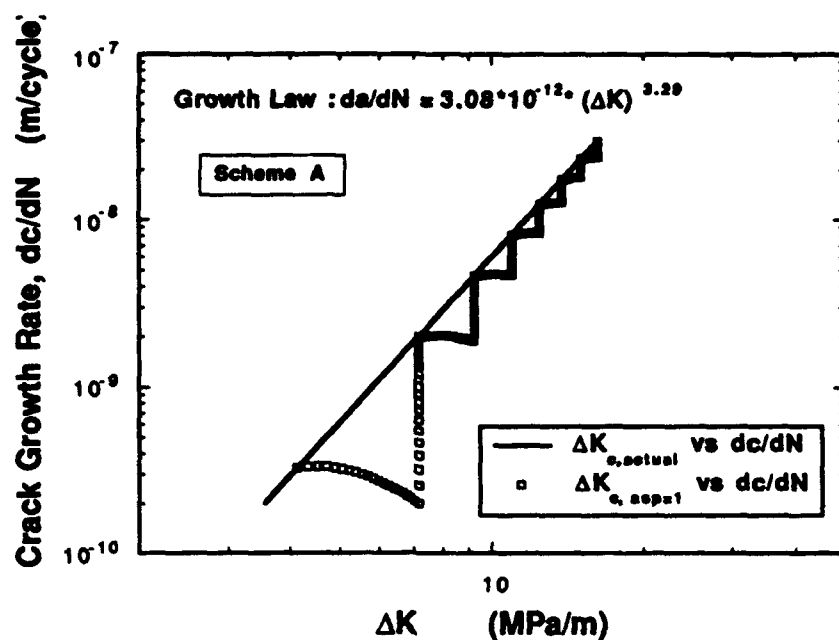
3.3 (a)



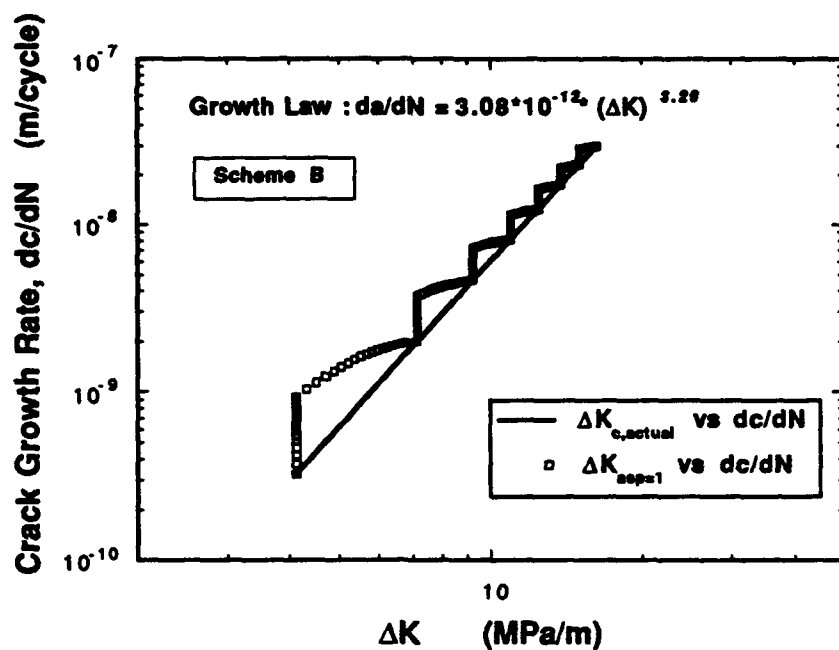
3.3 (b)

Fig. 3.3. A comparison of experimentally observed and theoretically simulated variations in aspect ratio, (a) scheme A compared with the data of Wagner et. al [3.11] and (b) scheme B compared with data from Larsen [3.14].





3.4 (a)



3.4 (b)

Fig. 3.4. Crack growth rates calculated with aspect ratio variations as well as with assuming  $a/c = 1$  for simulations (a) scheme A and (b) scheme B.

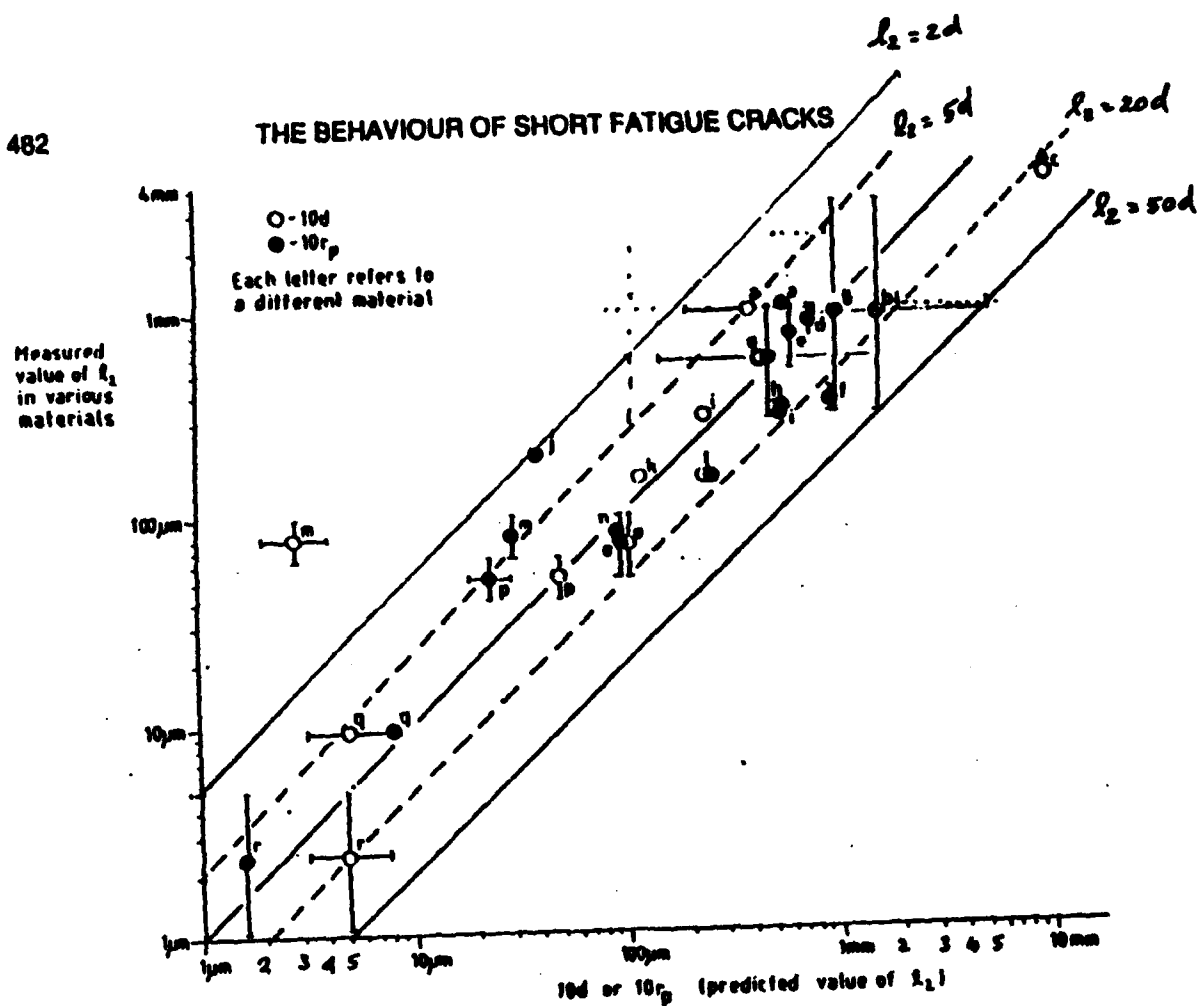
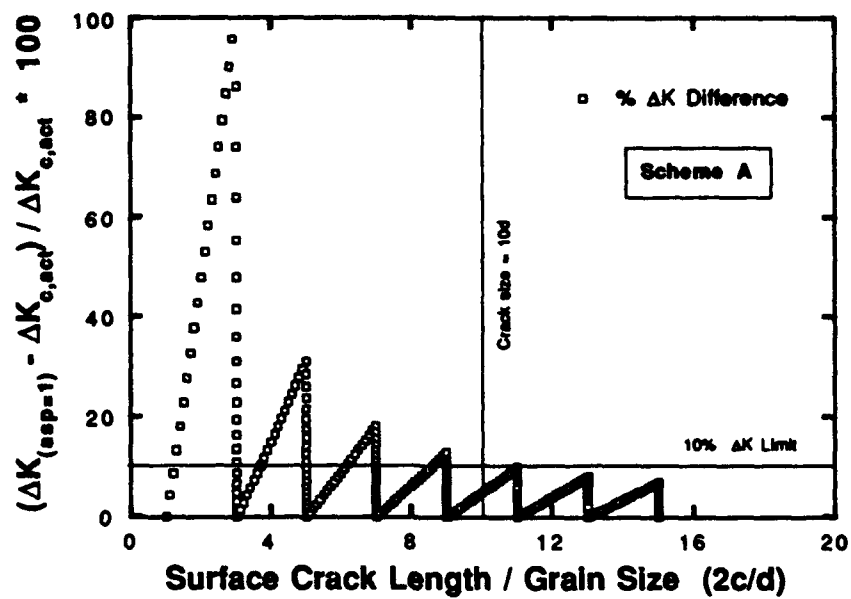
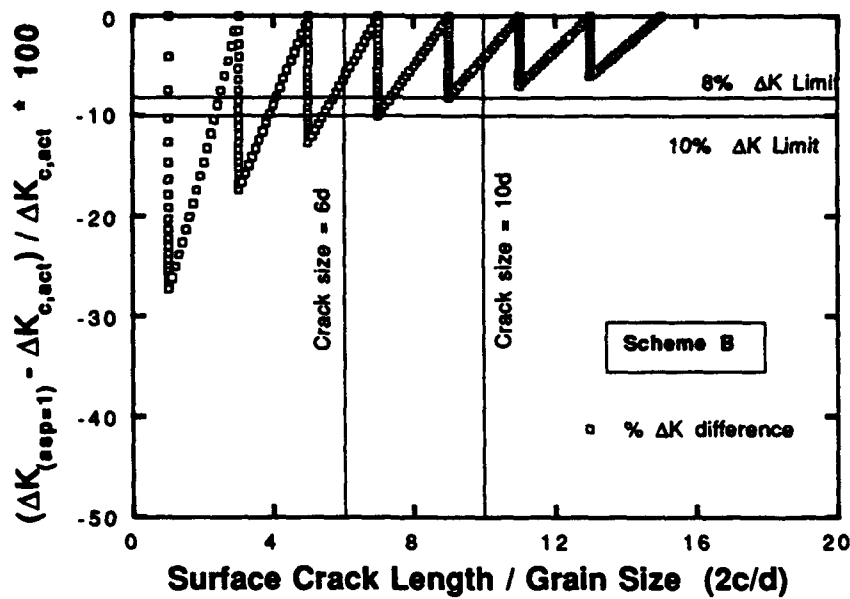


Fig. 3.5 The correlation between the grain size parameter and  $\Delta K_{th}$  proposed by Taylor and Knott [3.12, 3.13]



3.6 (a)



3.6 (b)

Fig. 3.6 Estimations of errors associated with the assumption of  $a/c=1$  in the crack growth simulations; (a) scheme A and (b) scheme B.

functions of  $\Delta K_{c,act}$  and  $\Delta K_{c,asp=1}$  for the two sequences are plotted (Fig. 3.4(a) and (b)), a dramatic effect of the assumption of semicircular crack shape on the apparently anomalous crack growth behavior is evident. The solid line is the plot resulting from calculations incorporating the actual aspect ratio. Therefore, part of the anomalous behavior of small surface cracks is due to the assumptions of semicircular shape during the initial stages of crack growth. However, at large crack sizes  $2c \geq 10d$ , the grain boundary induced perturbations are not large enough to cause fluctuations in  $\Delta K$ , and the anomalous growth behavior no longer exists.

It is now conventional to use Kitagawa type diagrams [3.18] to illustrate the crack size effects on fatigue. Taylor and Knott proposed a parameter ' $l_2$ ' above which  $\Delta K_{th}$  can be used to describe the threshold of a preexisting crack and further showed that it should approximately correspond to  $10d$  for a variety of alloys (Fig. 3.5). Below this crack size, factors such as crack closure,  $\Delta K$  estimation errors, constraint, crack deflection and plasticity effects either individually or collectively are likely to be responsible for the anomalous behavior. It is interesting to see that the  $\Delta K$  estimation errors involved in assumptions of semicircular shape for both sequences as shown in Fig. 3.6 (a&b) are large at small crack sizes. If an arbitrary choice of 10%  $K$  estimation error is permissible, this would approximately correspond to about  $10d$  for sequence A and  $5d$  for sequence B. Note that almost all of Taylor and Knott's data [3.12, 3.13] can be contained within bounds of  $5d$  and  $20d$  in Fig. 3.5. in which the range of the  $\Delta K$  estimation errors diminish (Fig. 3.6). If the statistical variations in grain size and grain boundary strength determining factors such as tilt or twist orientation relationships could be incorporated in the simulation, it is possible that the  $\Delta K$  errors would become negligible anywhere between  $3d$  and  $20d$  and the cracks would behave as large ones. It should be noted that the situations considered are two extreme cases, excluding random large grains in which fatigue cracks nucleate preferentially.

### 3.3 CONCLUSIONS

It can be concluded that part of the anomalous behavior of small surface cracks arises due to the assumptions of semicircular crack shape particularly at very early stages of crack growth. The anomalous nature, excluding that due to lack of fully developed closure levels, is shown to disappear when the actual crack shapes are considered for calculation. The effects of fluctuations in shape due to grain boundary

induced perturbations is negligible at the size of a crack when the crack shape perturbations are no longer great enough to influence  $\Delta K$  elsewhere along the crack front. Taylor and Knott's estimate of the parameter  $l_2=10d$  below which cracks behave anomalously appears to be associated with changes in crack shape. These results should have implications on the analysis and interpretations of growth behavior of small surface cracks in situations where crack shape deviations are possible.

### 3.4 RECOMMENDATIONS

Unlike the periodic arrangement of uniformly sized grains considered in this study, random grain size variations can be employed in the simulations. In addition, stress intensity factor solutions to accurately describe the  $K$  variation around the front of an arbitrarily shaped surface crack should be developed to better understand the driving force of a growing crack front. A study of the effects of perturbations in crack front induced by microstructure, analytically and through finite element methods would be helpful for further understanding in this area.

## **CHAPTER 4**

### **SMALL CRACK GROWTH IN TI-8Al MATERIAL WITH COARSE GRAIN SIZE.**

#### **4.1 INTRODUCTION**

An investigation was undertaken to study the small crack growth behavior in coarse grained Ti-8Al alloy. The primary objective was to measure the variations in crack shape and crack closure from crack sizes of about the size of a grain to crack sizes approaching the large-crack behavior. Earlier studies [4.1, 4.2] on a similar material indicate that a crack, after nucleating within a grain in fatigue, tends to propagate into adjacent grains. When the crack tip is close to the grain boundary, for example at the surface, it is temporarily retarded while the crack front at the depth continues to propagate. When the crack tip at the depth is retarded at a grain boundary, the surface crack tip resumes the growth. This alternate arrest and propagation at surface and depth has been suggested [4.2] to result in variations in crack growth rates which are much larger than observed for large cracks since large through cracks encompass several grains in a typical test. However, this alternate propagation mechanism should result in significant variations in crack shape at the early stages of crack growth, as illustrated by simulations conducted in chapter 3. Hence, in this investigation a coarse grained microstructure in Ti-8Al was chosen to track the variations in crack shape using the laser interferometric and photomicroscopic system. The measured variations in crack shape are compared with the theoretically simulated variations in crack shape for the same microstructure. It is to be noted that in the simulations an ideal microstructure is assumed with all grains of size equal to the average grain size determined experimentally from the material's microstructure.

#### **4.2 MATERIAL AND EXPERIMENTAL PROCEDURE**

Ti-8Al alloy vacuum induction melted and cast, was obtained in the form of rolled plates of size about 60cmX15cmx1.5cm. The as-rolled material contained some residual porosity when examined under an optical microscope. The pores were closed and a dense material was obtained by hot isotatic pressing of the plates at 927°C for 2 hrs under a pressure of 210 MPa. Specimen blanks were machined from the HIPed plates and heat treated at 975°C for 100hrs, followed by water quench.

During heat treatment the specimens were coated with glass powder to prevent oxidation. After heat treatment, microscopic examination of the specimens indicated oxidation only to about 0.2 mm below the surface. These layers were removed during the subsequent machining operation.

Small crack specimens and C(T) specimens for large-crack tests were machined from the specimen blanks according to the dimensions given in chapter 5. Specimen preparation procedures, such as mechanical and electropolishing, were identical to that described in chapter 1. It was found from trial experiments that small cracks which would subsequently grow could not be initiated naturally by fully reversed fatigue loading. Hence semicircular notches having dimensions of 150  $\mu\text{m}$  width and 70  $\mu\text{m}$  thickness at the surface and 75  $\mu\text{m}$  at depth were machined at the center of the electropolished cross section by electro-discharge machining. Cracks readily initiated from these notches under a nominal stress level of  $0.6\sigma_y$ . Generally the notches were located at the interior of the grains while occasionally the notch lay in two adjacent grains. All the small and large-crack tests were done at a stress ratio of  $R=0.1$ . At the end of the test, specimens were heat tinted following the procedure outlined in chapter 1. Table 4.1 illustrates the identifications of specimens tested for small cracks as well as the final crack length and aspect ratio determined from the heat tinting of fracture surfaces.

**Table 4.1 Specimen Identification with final crack length and Aspect Ratio Data**

<u>Specimen</u>	<u>Surface Crack Length</u> (mm)	<u>Crack Depth</u> (mm)	<u>a/c</u>
89481	1.416	0.685	0.97
89482	3.391	1.731	1.02
89483	3.231	1.84	1.14
89484	2.720	1.587	1.17
89486	4.272	Not Determined	
89487	3.751	1.607	0.86
89488	0.950	0.467	0.98
89491	1.754	0.798	0.91

## 4.3 RESULTS AND DISCUSSION

### 4.3.1 Large-Crack Data

The results of several tests on C(T) specimen to gather large crack growth data are presented in Fig. 4.1. The plot illustrates the variation of  $da/dN$  as a function of both  $\Delta K$  and  $\Delta K_{eff}$ . All the tests are for stress ratio of  $R=0.1$ . It can be seen that while the variation in crack growth rates in terms of  $\Delta K$  is minimal among the tests performed, crack growth rates in terms of  $\Delta K_{eff}$  showed a higher variability especially at low  $\Delta K$  levels. There could be two reasons for this behavior. First, at low  $\Delta K$  levels, crack growth is microstructurally sensitive in this coarse grained material. Secondly the variations in crack closure, because of this microstructure sensitivity, could be higher. The variation in closure levels, plotted in terms of  $K_{cl}$  as a function of  $K_{max}$  is illustrated in Fig. 4.2 for the tests in Fig. 4.1. As seen, there are significant variations in closure levels between the tests.

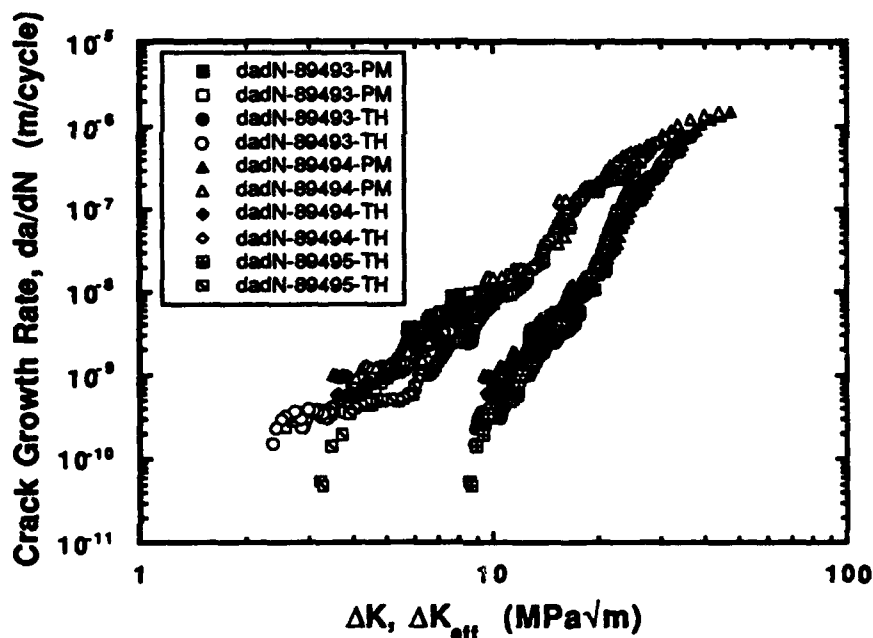


Fig. 4.1 Crack growth data of large cracks of Ti-8Al as a function of  $\Delta K$  and  $\Delta K_{eff}$ . PM-constant load, increasing  $\Delta K$  and TH-decreasing  $\Delta K$  tests.



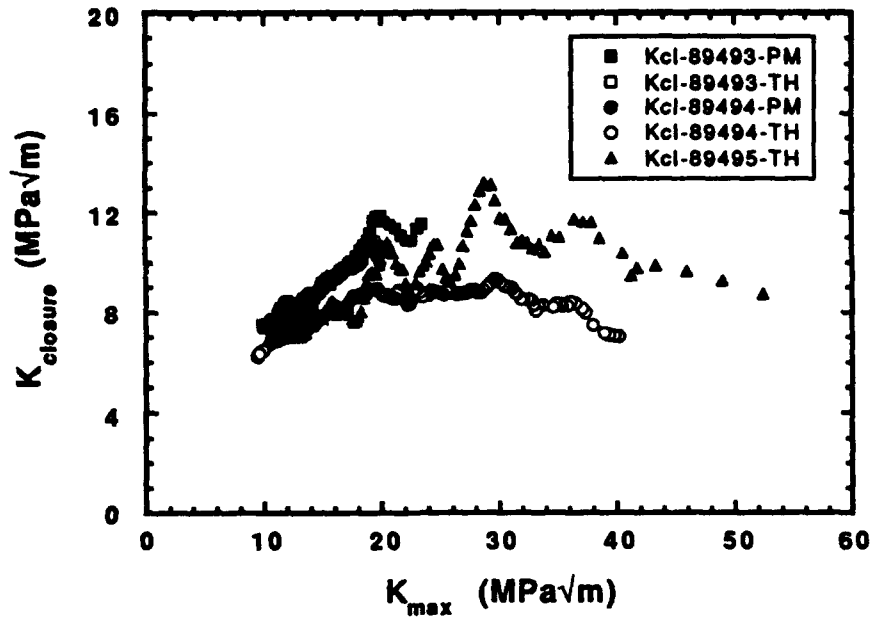


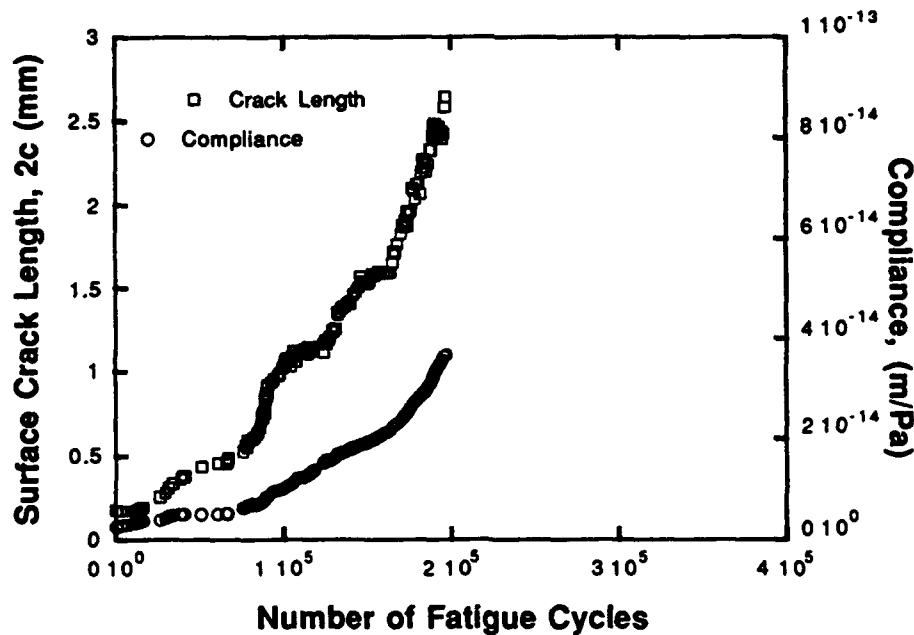
Fig. 4.2 Crack closure data of large cracks of Ti-8Al as a function of  $K_{max}$ . PM-constant load, increasing  $\Delta K$  and TH-decreasing  $\Delta K$  tests.

#### 4.3.2 Small Crack Growth Data

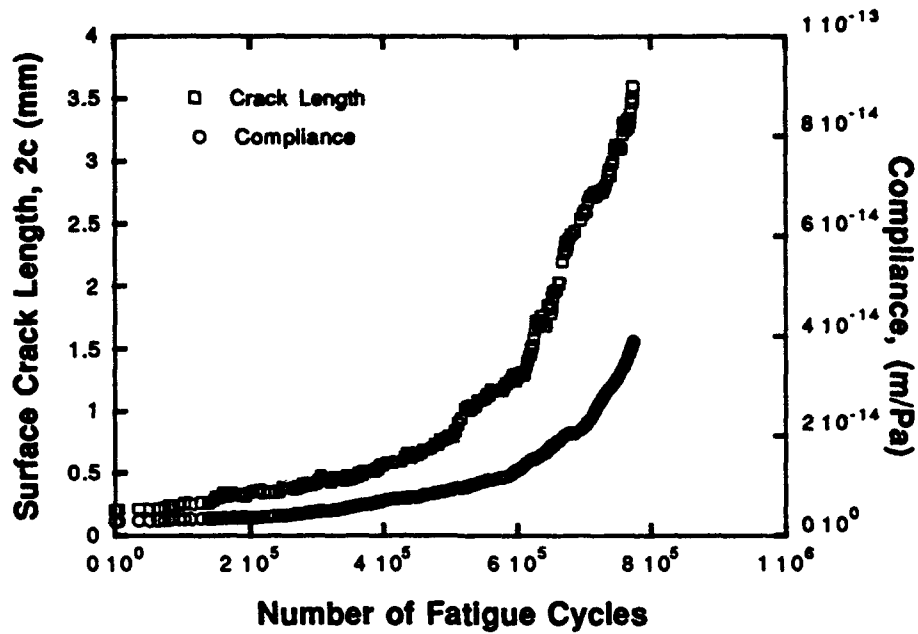
The use of a laser interferometric system and photomicroscopic system facilitated measurements of crack compliance and surface crack length continuously during fatigue at close intervals. Typically in a given test more than 200 sets of data of compliance and crack length were recorded as a function of fatigue cycles. The interval between any two measurements was typically 1% of the absolute crack length at which the measurement was made. This ensured data at close and uniform intervals convenient to give accurate variations in the trends of aspect ratio as a function of crack length.

Typical examples of compliance and crack length data are presented in Figs. 4.3 (a) and (b) for specimens 89483 and 89487, respectively. It can be seen that while the compliance increases continuously, the surface crack length is relatively more discontinuous as a function of fatigue cycles. This indicates that crack propagates discontinuously at surface. Since the increase in crack length either at the surface or at the depth would increase compliance, the compliance data appears smooth and continuous. Aspect ratios were determined through the procedure outlined in

chapter 1. Figs. 4.4-4.11 illustrate the variations in aspect ratio as a function of crack length for eight tests performed during this investigation. It is to be noted that the testing conditions were identical in all the tests and such a large number of tests were done mainly to reproduce results to give a greater confidence in data. The solid lines in the figures represent the predicted variations in aspect ratio according to the theoretical simulations illustrated in chapter. 3. The predictions for  $a/c \geq 1$  are for the crack growth sequence in which the crack propagates first into the grain at depth from a pre-existing crack of surface length equal to grain diameter and depth equal to half a grain diameter. The predictions for  $a/c \leq 1$  are for the sequence in which the crack propagate first from the surface tips. It is to be noted that the sequences employed in the simulations are arbitrary and cover only the two possibilities in crack growth from a preexisting cracks. It is possible that in actual experiments cracks can alternate between the two mechanisms, depending on whether the grain at the surface or the grain at depth is oriented suitably for crack propagation at any stage in crack growth. Nevertheless, the two sequences used in the predictions are more likely to occur if the grain size distribution is uniform. Deviations from the idealized variation are most likely to occur if the grain sizes are non-uniform, as seen in the microstructure.



4.3 (a) Specimen 89483



4.3 (b) specimen 89487

Fig. 4.3. The variation of surface crack length and compliance as observed in typical small crack tests in Ti-8Al; (a) for specimen 89483 and (b) for specimen 89487.

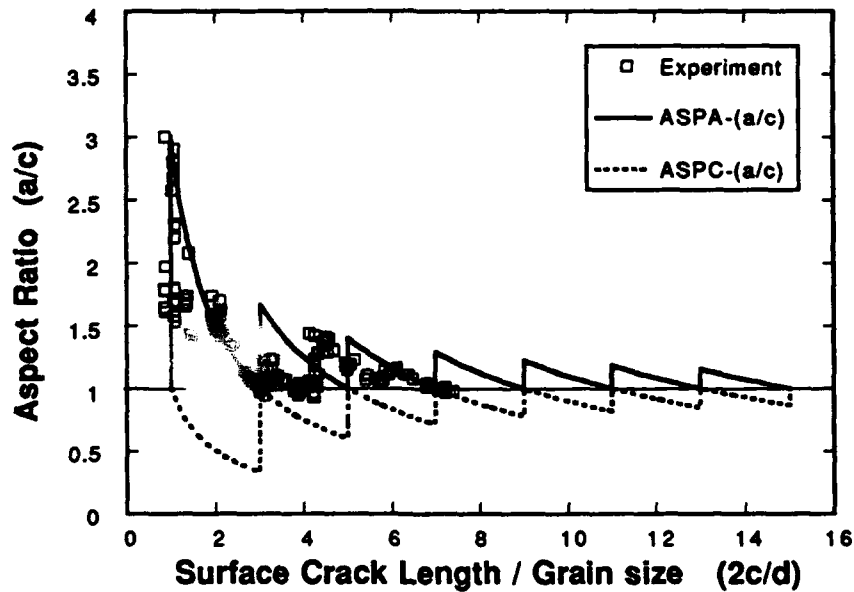


Fig. 4.4 specimen 89481

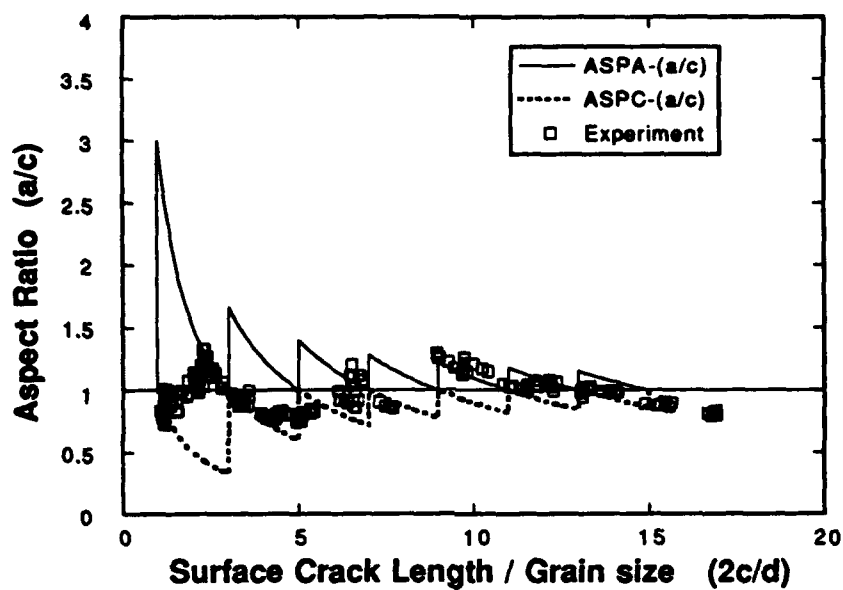


Fig. 4.5 Specimen 89482

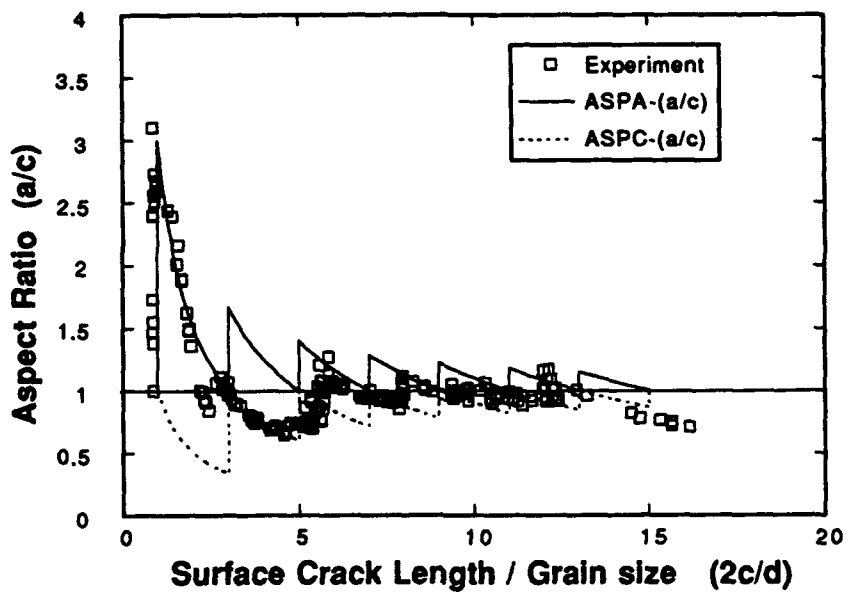


Fig. 4.6 Specimen 89483

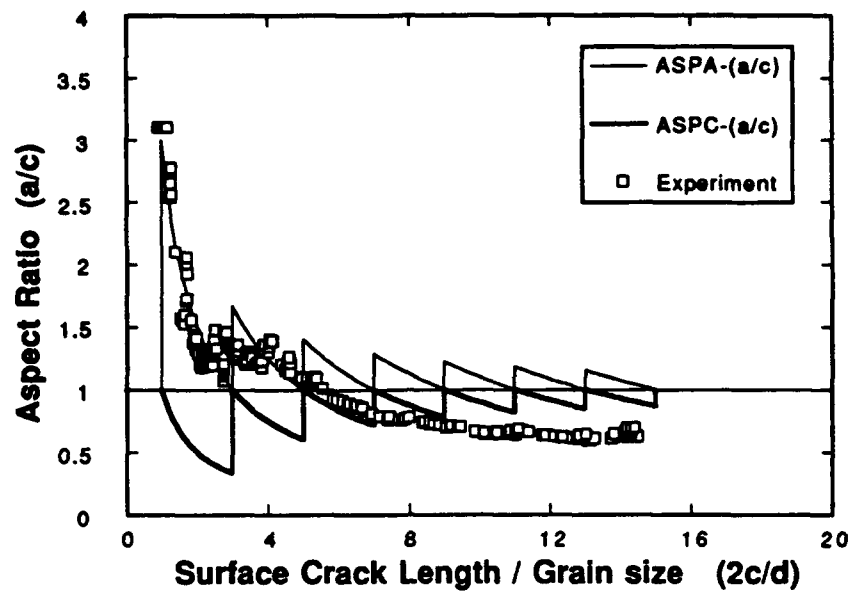


Fig. 4.7 Specimen 89484

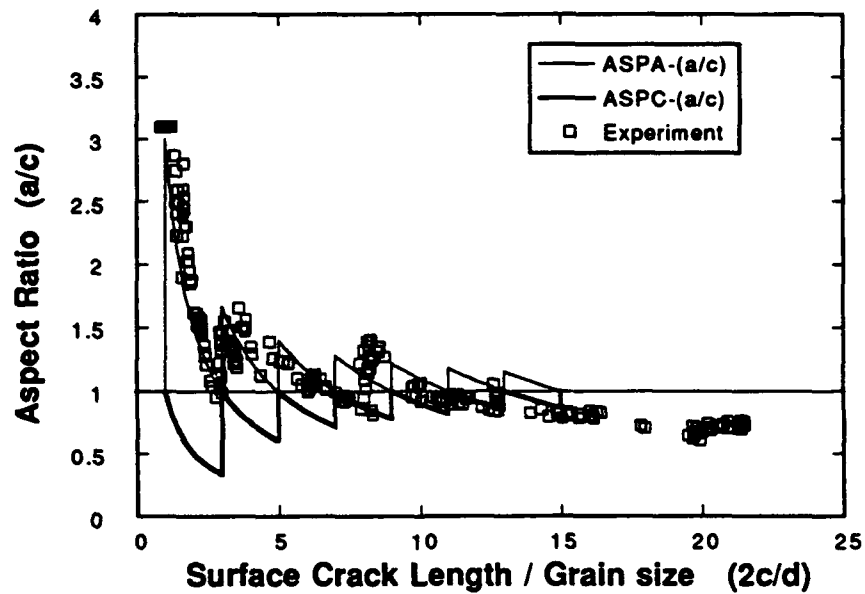


Fig. 4.8 Specimen 89486

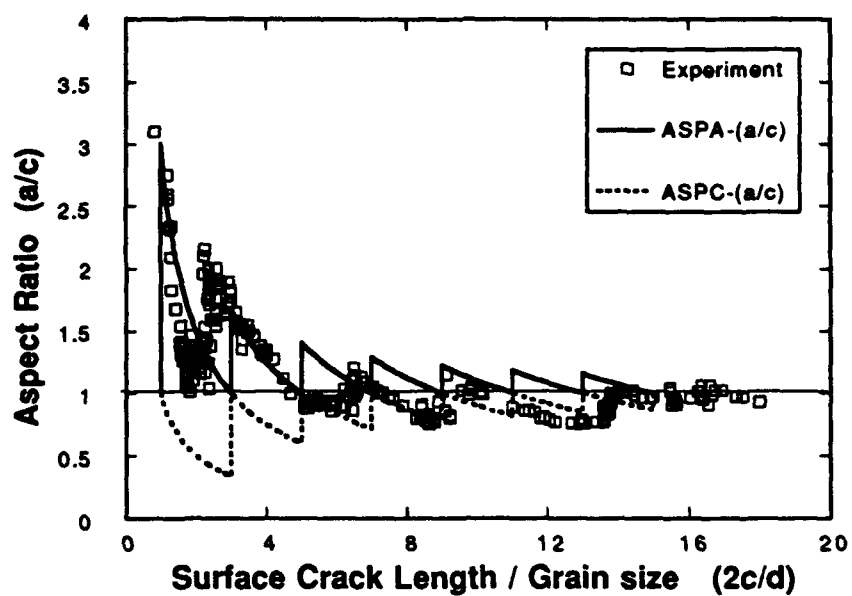


Fig. 4.9 Specimen 89487

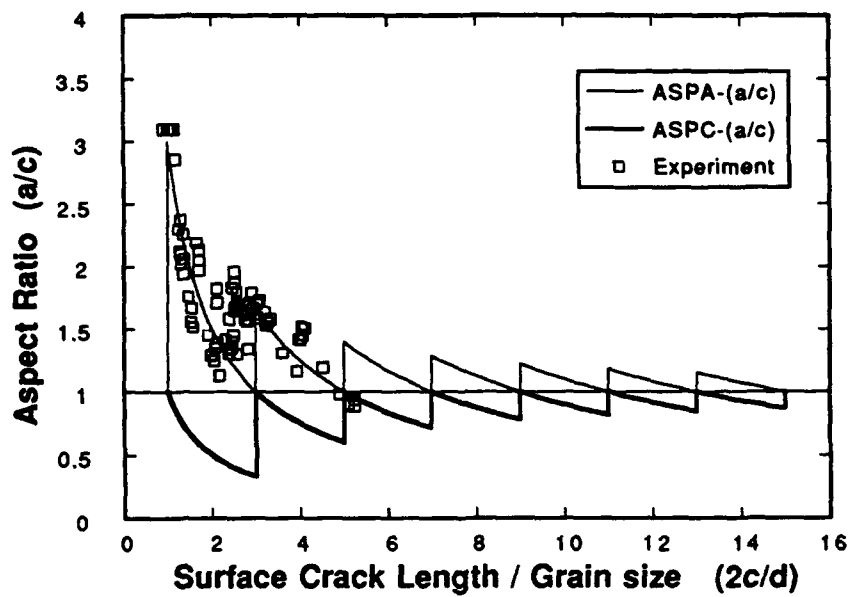


Fig. 4.10 Specimen 89488

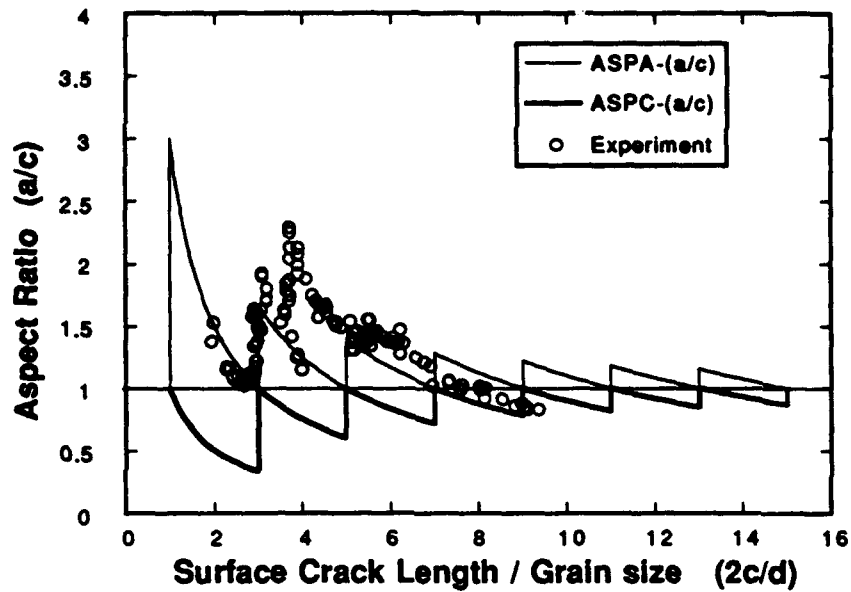


Fig. 4.11 Specimen 89491

Figs. 4.4-4.11: Comparisons of experimentally observed and theoretically simulated variations in aspect ratio.

Figs. 4.4-4.11 illustrate a good agreement of the experimentally measured variations in crack shape and the predicted behavior. This indicates that when small cracks are of the order of grain size, i.e., within a few times the grain size, large fluctuations in crack shape would occur. As can be seen in Figs. 4.12-4.15, crack paths in this material consisted of deflections at grain boundaries and crack branching, resulting in high tortuosity of crack path. Grain boundaries are known to provide temporary barriers to crack growth in a number of studies [4.3, 4.4]. These grain boundary retardations appear to correspond to large variations in crack shape when the crack sizes are of the order of few grain diameters. As the crack grows larger, the crack front encompasses more grains and the probability of finding a grain favorably oriented for crack growth increases, making the effects of retardation at a grain boundary less effective. In addition, at large crack sizes, the effect of perturbations of the crack front into a grain becomes less and less significant in altering the stress intensity elsewhere along the crack front. This appears to be the reason for less variations in aspect ratio at large crack sizes. According to the simulations in chapter 3, this size would be around 5-10 times the grain size. The

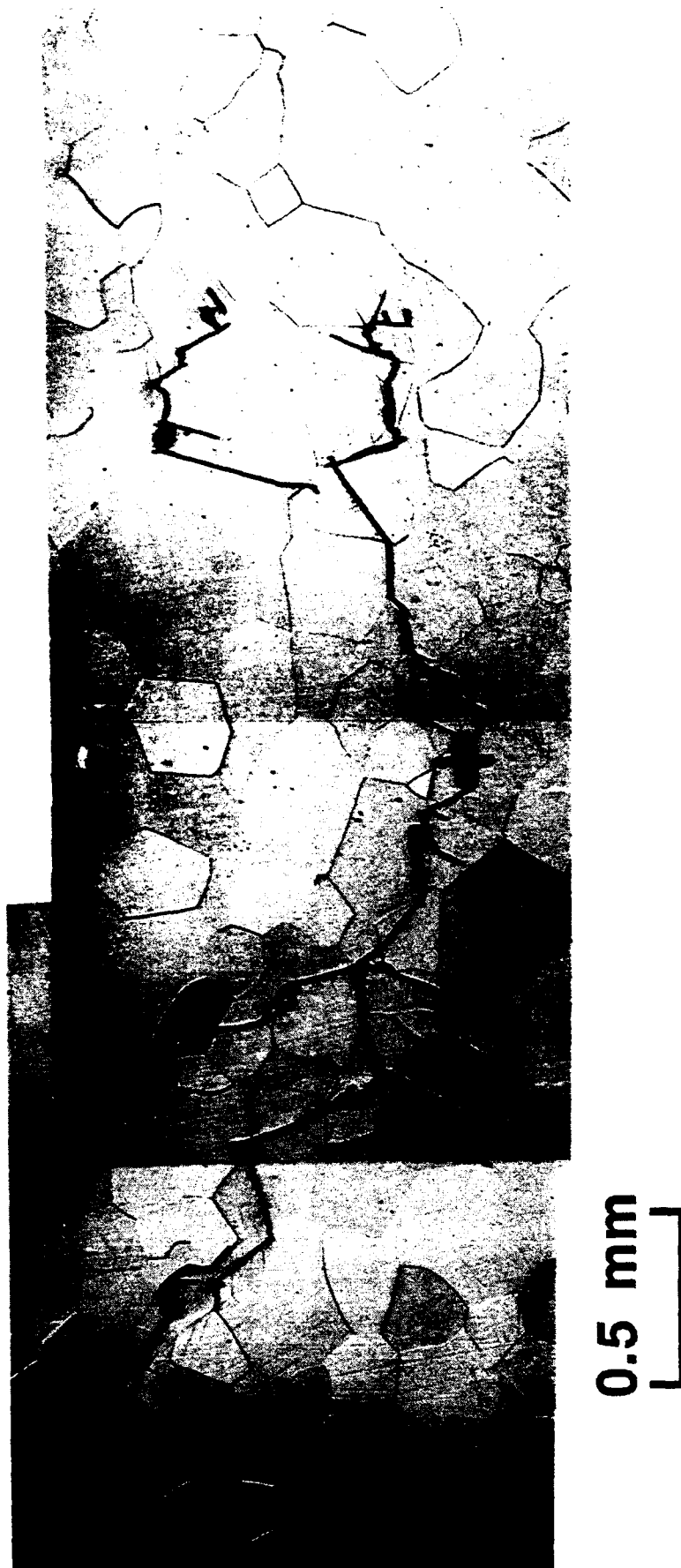


Figure 4.12 Small crack path profile at surface in specimen 89482



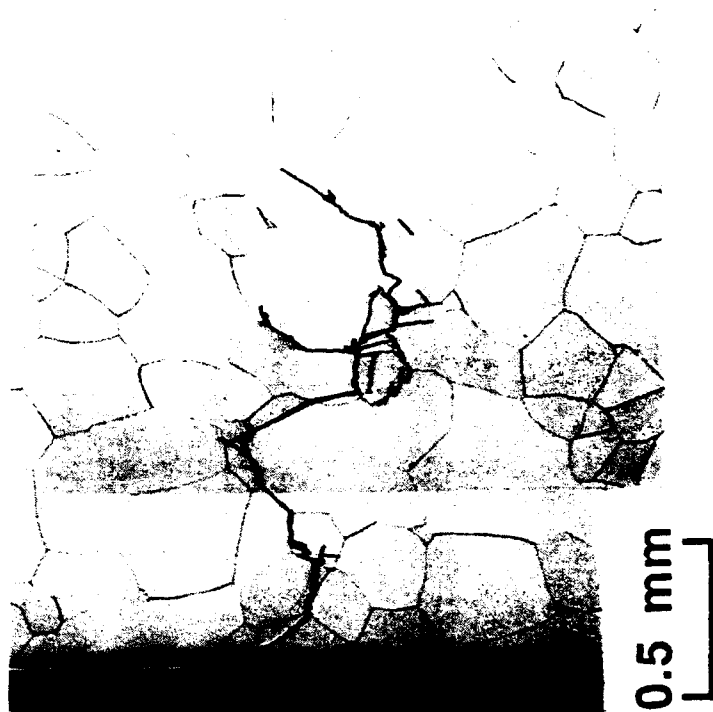


Figure 4.13 Small crack path profile at depth in specimen 89483



Figure 4.14 Small crack path profile at surface in specimen 89484

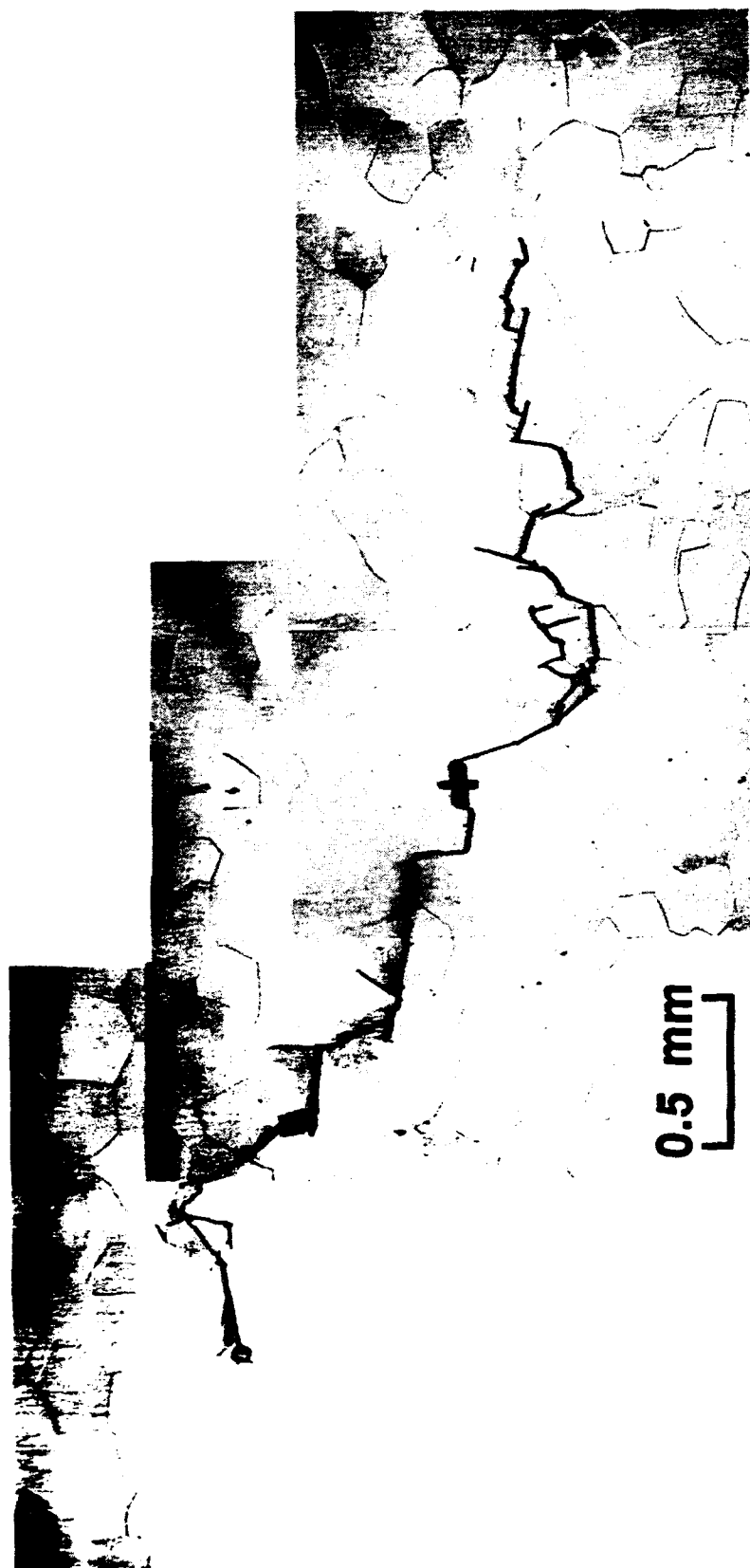


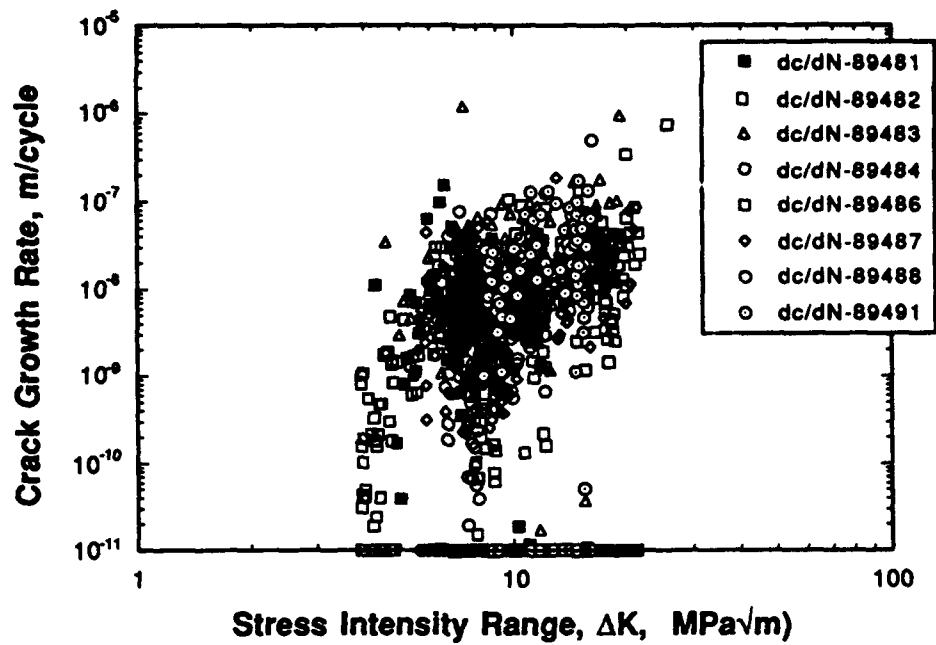
Figure 4.15 Small crack path profile at surface in specimen 89486

experimental data are consistent with this estimate, in general.

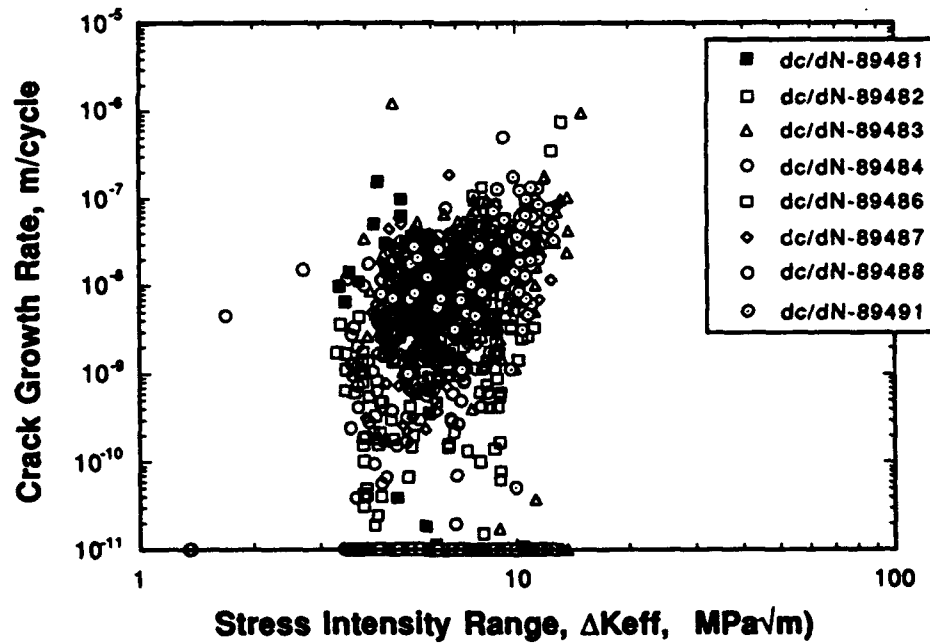
In conventional methods of data analysis of small cracks, this would cause significant errors in the  $\Delta K$  calculation if an assumption of  $a/c=1$  is used throughout the entire crack growth period. This aspect is further discussed in chapter 3. It is to be noted that in aspect ratio calculations, the value used for the elastic modulus in the compliance equation varied from 100 GPa to 150 GPa in order to assure the final aspect ratio at the end of the test agreed with the calculated data. A high value of modulus such as 150 MPa is high for a fully alpha Ti-8Al alloy. However, as the crack paths profiles indicate, that in addition to crack deflection at grain boundaries, the crack is highly tortuous that could arise due to periodic deflections at grain boundary alone. This could be the reason for the higher modulus values required to deduce consistent aspect ratio data.

#### 4.3.3 Crack Growth rates

Since the aspect ratios of a surface crack in this material vary significantly as a function of crack size, incorporation of this into the stress intensity range and growth rate calculations is necessary to accurately describe the crack growth behavior. Crack growth data for all the tests reported in this section were also reduced according to the procedure described in chapter 1. In tests on other materials, crack growth rates were calculated from an incremental polynomial regression of crack length data. Simultaneously, the aspect ratios were also regressed over the same interval, and then the crack growth rates at depth were calculated using the derivatives of surface crack length and aspect ratio with respect to fatigue cycles. Although for smooth variations in aspect ratio this procedure was found to be accurate, large and abrupt variations in aspect ratio such as those seen in this material required a slightly different method of calculation. From the set of data on surface crack length and aspect ratio, the crack length at the depth as a function of fatigue cycles is first calculated. Then these data were regressed independently to obtain crack growth rates at the depth, with regression interval being the same as that for the surface crack length. The stress intensity factor at the depth was calculated from the original regressed data on surface crack length and aspect ratio, having an identical regression interval. As will be shown later, this procedure was found to effectively take into account the sharp variations in aspect ratio.

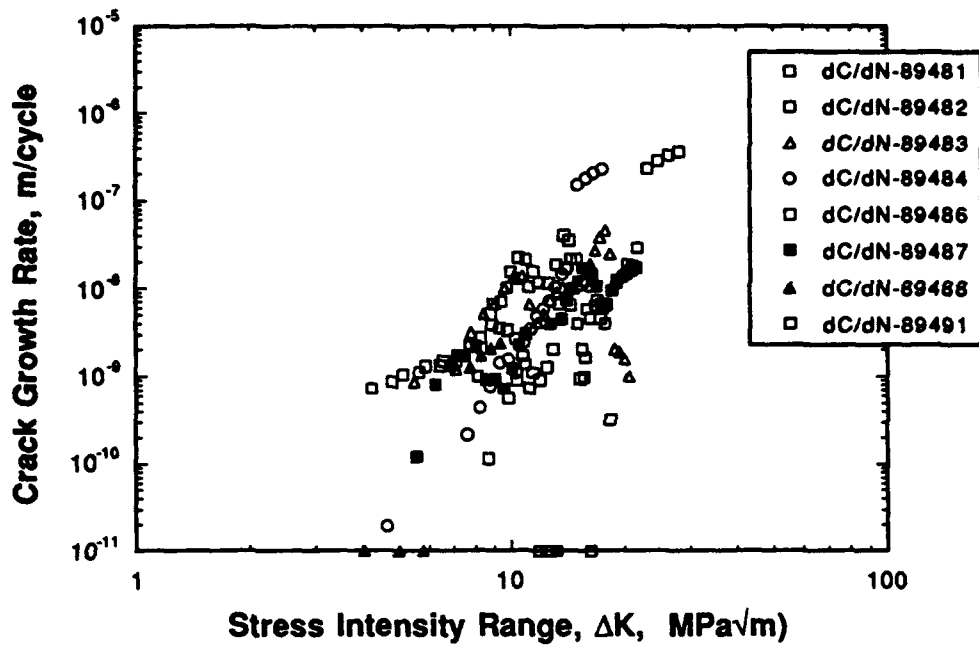


4.16(a)

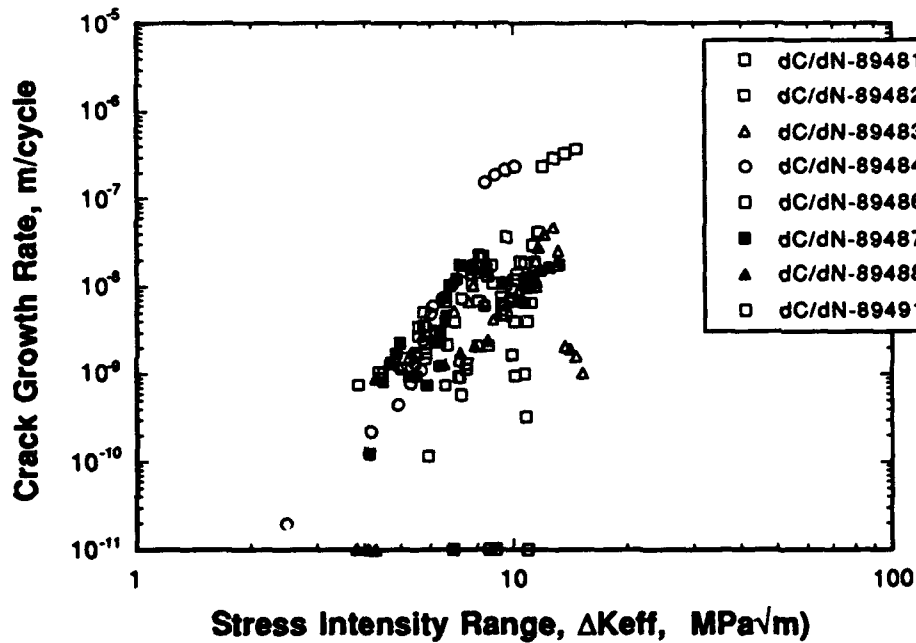


16(b)

Fig. 4.16. Fatigue crack growth rates of small cracks, deduced by secant method and assuming an aspect ratio of 1.0; as a function of (a)  $\Delta K$  and (b)  $\Delta K_{eff}$

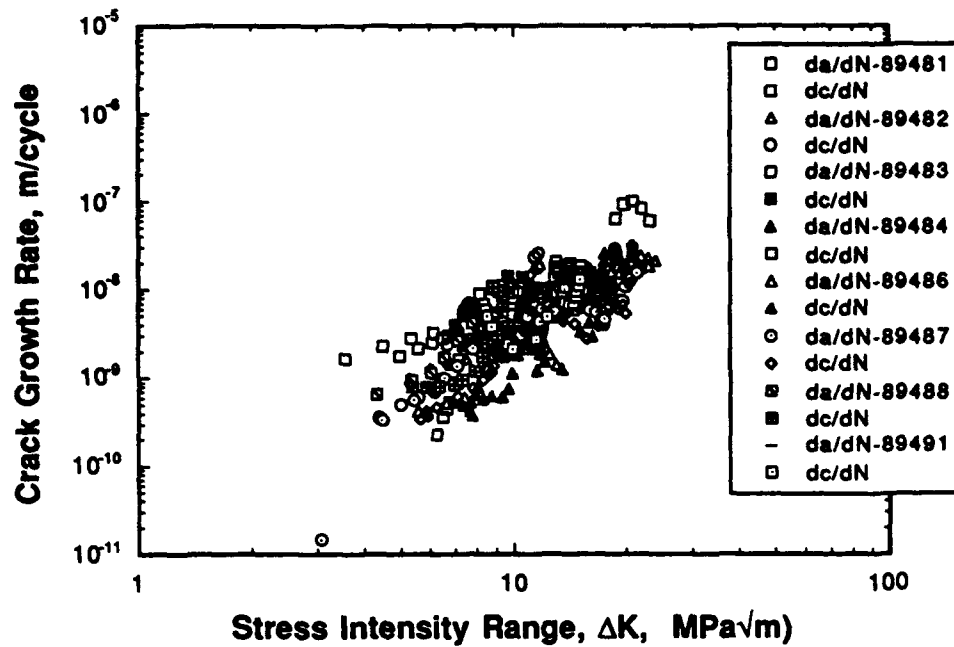


4.17(a)

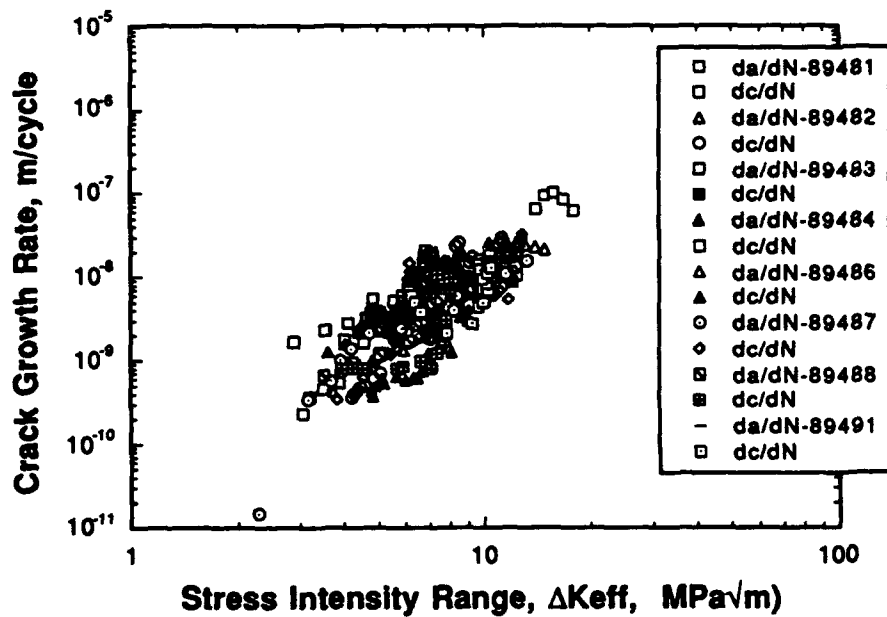


4.17(b)

Fig. 4.17. Fatigue crack growth rates of small cracks, deduced by incremental polynomial method and assuming an aspect ratio of 1.0; as a function of (a)  $\Delta K$  and (b)  $\Delta K_{eff}$



4.18(a)



4.18 (b)

Fig. 4.18. Fatigue crack growth rates of small cracks, after incorporating the variations in aspect ratio and reduced by incremental polynomial regression; as a function of (a)  $\Delta K$  and (b)  $\Delta K_{eff}$

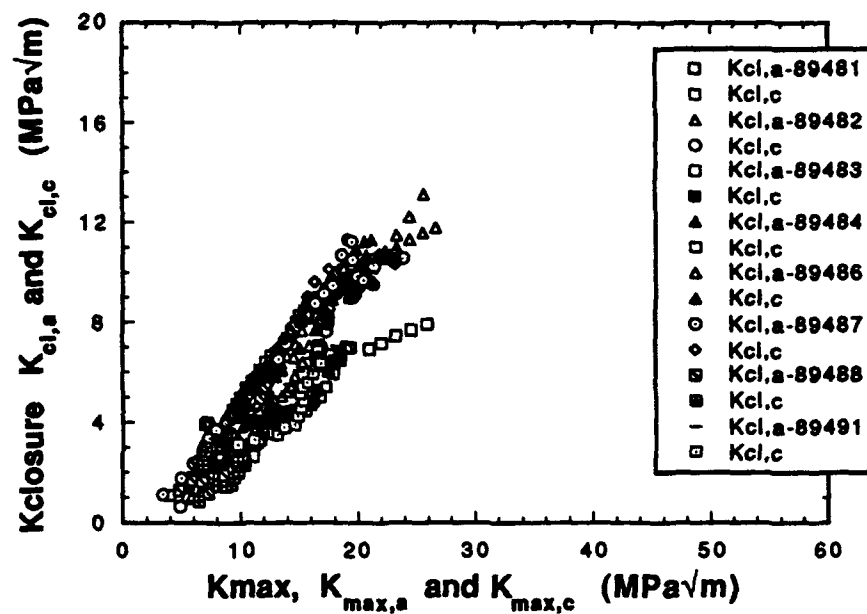


Fig. 4.19 The variation of fatigue crack closure levels at the surface  $K_{cl,c}$  and at the depth,  $K_{cl,a}$  in terms of respective  $K_{max}$  levels for all the small crack specimens tested in this study.



Fatigue crack growth data deduced using the secant method and assuming an aspect ratio of 1.0 through out the crack growth is presented in figs. 4.16 (a) and (b) as a function of  $\Delta K$  and  $\Delta K_{eff}$  respectively. It can be seen that the data exhibit scatter over several orders of magnitude in crack growth rates. This is a result of estimating growth rates between two successive crack length measurements, during which either the crack may be temporarily arrested or the crack length measurement may contain some error. As a result, anomalously high growth rates immediately after the crack has crossed a grain boundary or a zero crack growth rate when the crack is held at a grain boundary or even a negative crack growth rate due a measurement error in which a crack length is lower than the value at the last measurement, could occur. Hence it is necessary to suitably average the crack length over a period of cycles during which the crack length has increased by a specific amount. The objective of the polynomial regression is to ensure such an average is employed in the growth rate calculations. The crack growth data thus calculated, again assuming  $a/c=1$ , are presented in Figs. 4.17 (a) and (b) as a function of  $\Delta K$  and  $\Delta K_{eff}$ , respectively. It can be seen that the scatter in the crack growth data is considerably reduced. However, this procedure again employs an average aspect ratio,  $a/c=1.0$ . Crack growth data reduced after incorporating the variations in aspect ratio are presented in Figs. 4.18 (a) and (b) as a function of  $\Delta K$  and  $\Delta K_{eff}$  respectively. Both the data on surface crack growth rates,  $dc/dN$  and crack growth rates at the depth,  $da/dN$  are presented as functions of the respective stress intensity ranges at the surface,  $\Delta K_{eff,c}$  and  $\Delta K_{eff,a}$  and  $\Delta K_c$  and  $\Delta K_a$ . It can be seen that the scatter in the crack growth data has been significantly reduced after incorporating the aspect ratio variations. The small-crack data  $dc/dN$  and  $da/dN$  can be seen to agree well with the large through-crack data (compare Figs. 4.1 and 4.18) after correcting for crack closure. It should be noted that the improvement in crack growth rate correlation with large-crack data is dramatic, even when the aspect ratio was assumed to be 1.0. Further improvement after incorporating the aspect ratio variations are less dramatic since the former data is a result of averaging in crack length over a growth period and hence events of crack tip retardation and acceleration at the grain boundary are smoothed in the growth rate calculations. When compared with secant data in Fig. 4.16 (a) and (b), the crack growth data incorporating aspect ratio variations result in significant improvement in correlation with large crack data.

The variation in crack closure levels for all the small cracks tested in this study are presented in Fig. 4.19. A comparison of Figs. 4.19 and 4.2 suggests that crack closure levels were low when the crack sizes were small, but increased with crack extension to reach the level of closure occurring in large cracks. This is in good agreement with the observations made earlier [4.5] in a similar material having a finer grain size.

#### 4.4 CONCLUSIONS

The experimentally measured crack shapes of surface cracks in coarse grained Ti-8Al were found to generally agree with the theoretically simulated crack growth pattern involving alternate growth at surface and at depth. Fatigue crack growth rates of small cracks were found to correlate well with the large crack data after accounting for the variations in crack aspect ratio and crack closure. Crack closure developed as the small cracks grew and reached the level of large cracks.

## CHAPTER 5

### EFFECTS OF MICROSTRUCTURE ON LARGE CRACK GROWTH BEHAVIOR OF Ti-24Al-11Nb

#### 5.1 INTRODUCTION

Microstructure has been known [5.1] to affect the fatigue crack growth response in several advanced materials used in aerospace applications. An investigation was undertaken to study the fatigue crack growth behavior in the large crack regime as a function of microstructure in Ti-24Al-11Nb titanium aluminide alloy. It is known [5.2, 5.3] that microstructure and stress ratio influence fatigue crack growth behavior in conventional titanium alloys. However, with the exception of some preliminary investigations [5.4, 5.5], there has been no systematic study available on the effects of microstructural condition on crack growth resistance under cyclic loading. Hence, it is of interest to study the fatigue crack growth behavior in a new class of intermetallic alloy, exemplified by Ti-24Al-11Nb, under different stress ratios and microstructural conditions.

#### 5.2 EXPERIMENTAL PROCEDURE

The titanium aluminide alloy Ti-24Al-11Nb, of specific composition (at.%) 61.4% Ti, 27.3% Al, 10.8% Nb, 0.08% Fe, <0.03% Cu, <0.04% Ni, <0.04%Cr, 0.030% O, 0.032% N and 0.005% H, was heat treated to produce three different microstructural conditions. The material used in this investigation was a vacuum arc melted and cast alloy of nominal composition Ti-24Al-11Nb. Cylindrical castings of approximate dimensions: 200 mm in diameter and 280 mm in height were isothermally forged down to a circular disk of about 50 mm in thickness and 400 mm in diameter (80% reduction) at 1065°C at a strain rate of 0.1 min<sup>-1</sup> and air cooled to room temperature. Sections of the disk were heat treated according to the scheme in Table 5.1. The quantitative microstructural parameters are given in Table 5.1. The microstructures were selected on the basis of physical metallurgy of titanium alloys. While the basketweave structure possesses good strength and fatigue crack initiation resistance, the aligned colony structure possesses better

resistance to creep and fatigue crack growth and exhibits high fracture toughness. The  $\alpha_2 + \beta$  microstructure, as in the case of conventional titanium alloys, is likely to exhibit a balance of the above properties, while the  $\alpha_2$  microstructure is expected to possess good ductility and resistance to low-cycle fatigue.

The microstructures after heat treatment are shown in Figure 5.1(a-c). The beta heat treated microstructure consists of very large prior beta grains of the order of 200 to 1000  $\mu\text{m}$ , with the constituents being aligned  $\alpha_2$  platelets separated by a small amount of ordered beta ( $\beta_O$ ) with a compositional stoichiometry of  $\text{Ti}_2\text{AlNb}$  [5.6]. The  $\alpha_2$  phase is  $\text{Ti}_3\text{Al}$  and has an ordered hexagonal close packed structure (DO<sub>19</sub>). In this microstructure, due to the crystallography of  $\alpha_2$  phase and the large grain size, plastic deformation is inhomogeneous, leading to crack nucleation in fatigue at prior beta grain boundaries. The  $\alpha_2 + \beta$  microstructure consists of primary- $\alpha_2$  in a matrix of  $\alpha_2$  and ordered beta in the Widmanstatten form. Fatigue cracks in this microstructure often initiated at the primary- $\alpha_2/\beta$  interfaces. Microstructure D consists of fine equiaxed grains with discontinuous beta at the boundaries. Fatigue cracks mainly initiated along slip bands across the  $\alpha_2$  grains.

C(T) specimens were used for large-crack growth tests (Fig. 5.2). The specimens were machined from heat treated forgings with the choice of specimen location and direction of the notch being arbitrary. Stress ratios of  $R=0.1$ ,  $0.5$  and  $0.8$  were used for crack growth tests for each microstructure. In each stress ratio, typically two specimens were tested and in each specimen both the decreasing  $\Delta K$  threshold test, as well as increasing  $\Delta K$  constant load tests were performed to ensure consistent data. Hence for each stress ratio for a given microstructure, four data sets were generated. Precracking was done following the procedure recommended by ASTM test standard E-647 [5.7]. While tests at stress ratios  $0.1$  and  $0.5$  could be done without much difficulty, precracking and the subsequent threshold testing at  $R=0.8$  was difficult. A typical procedure adopted was first to precrack at a lower stress ratio and then gradually increase the  $K_{\text{min}}$  while keeping  $K_{\text{max}}$  constant to attain the desired stress ratio of  $0.8$  at the end of the precrack period. Following precracking only limited or no threshold crack growth data could be generated since the  $\Delta K$  was so low such that the crack growth rates were very slow ( $\leq 10^{-9}$  m/cycle). Hence, in majority of the  $R=0.8$  tests only the increasing- $\Delta K$ , constant-load test could be done successfully.

Table 5.1. Heat Treatment and Microstructural Parameters

Microstructure		Heat Treatment	Microstructural Parameters		
Identification	Type		Prior Beta Grain Size ( $\mu\text{m}$ )	Widmanstätten Colony Size ( $\mu\text{m}$ )	$\alpha_2$ Phase Size ( $\mu\text{m}$ )
A	Basketweave	1150°C / 30 min. / Air Cool 815°C / 30 min. / Air Cool 593°C / 8 hrs. / Air Cool	600		1-3
B	$\beta$	1150°C / 30 min. / Furnace Cool 815°C / 30 min. / Air Cool 593°C / 8 hrs. / Air Cool	1460	284	4-6
C	Primary- $\alpha_2$ + $\beta$	1080°C / 2 hrs. / Air Cool 593°C / 8 hrs. / Air Cool			15-25 (28 %)*
D	Equiaxed- $\alpha_2$	954°C / 8 hrs. / Furnace Cool to 593°C / 8 hrs. / Air Cool			27

\*  $\alpha_2$  Volume Percentage

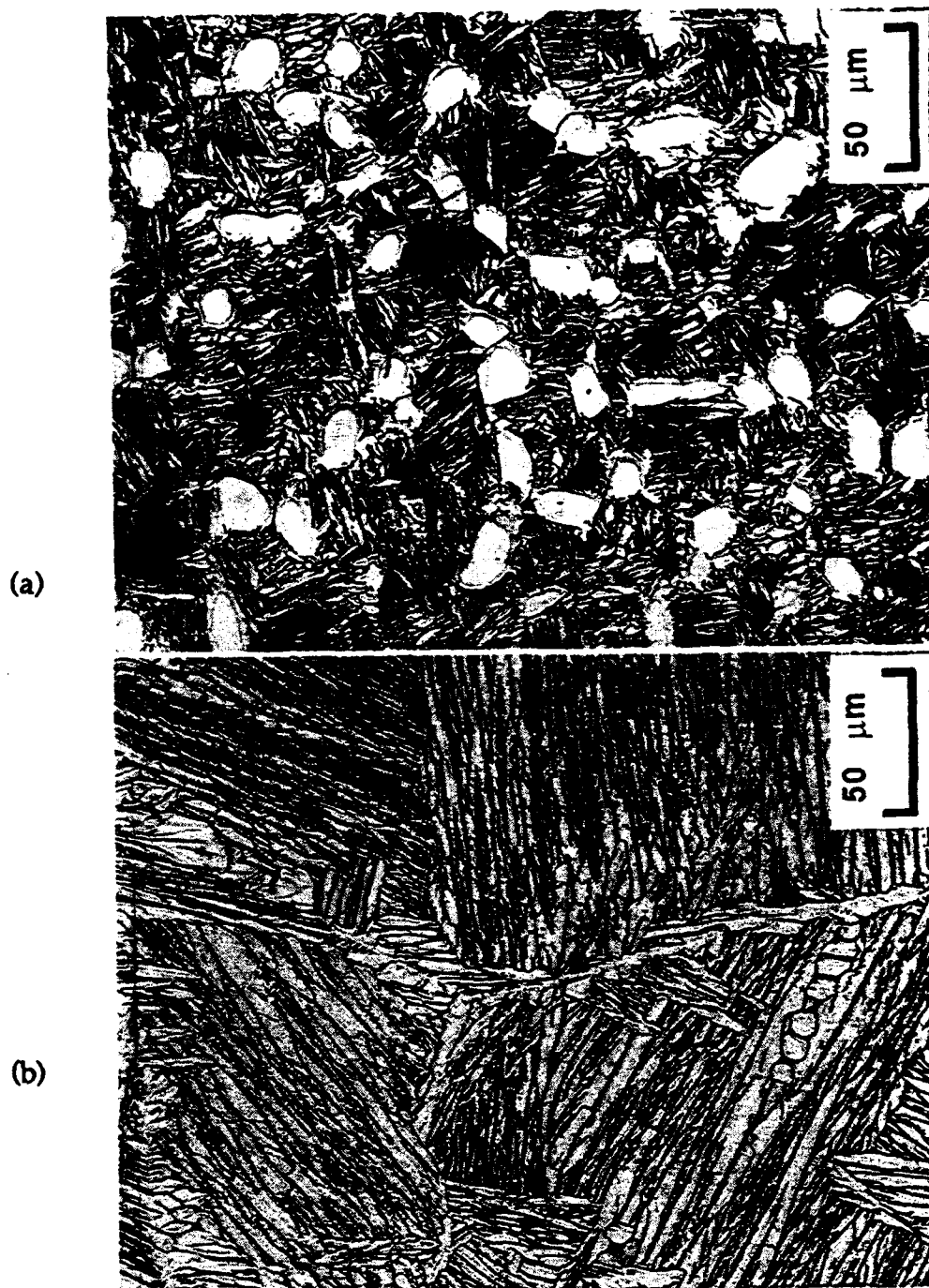
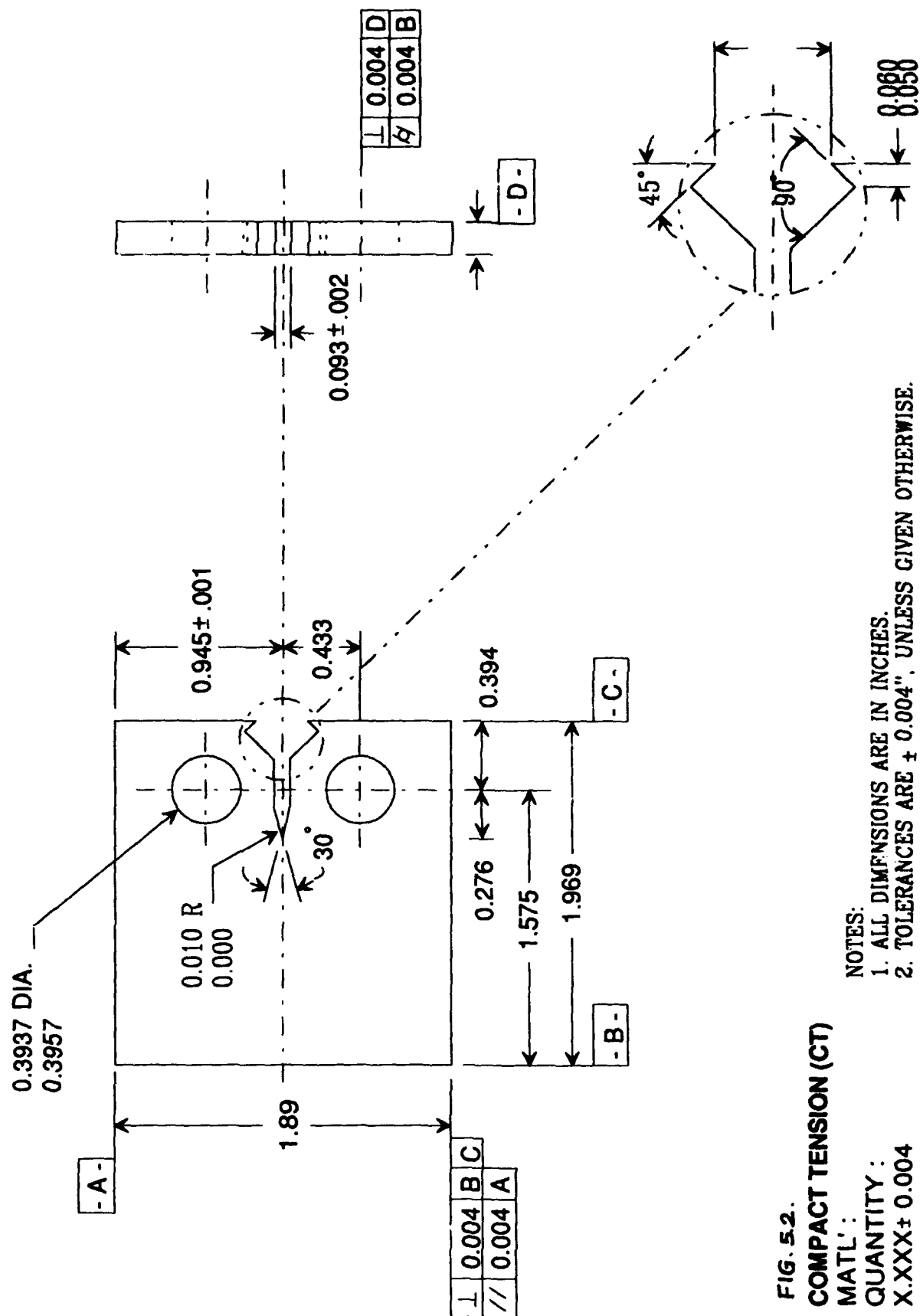


Figure 5.1 Microstructures after heat treatment (a)  $\alpha_2$ + $\beta$ , (b) fully  $\beta$  and (c) equiaxed  $\alpha_2$  microstructures



Figure 5.1 (c)





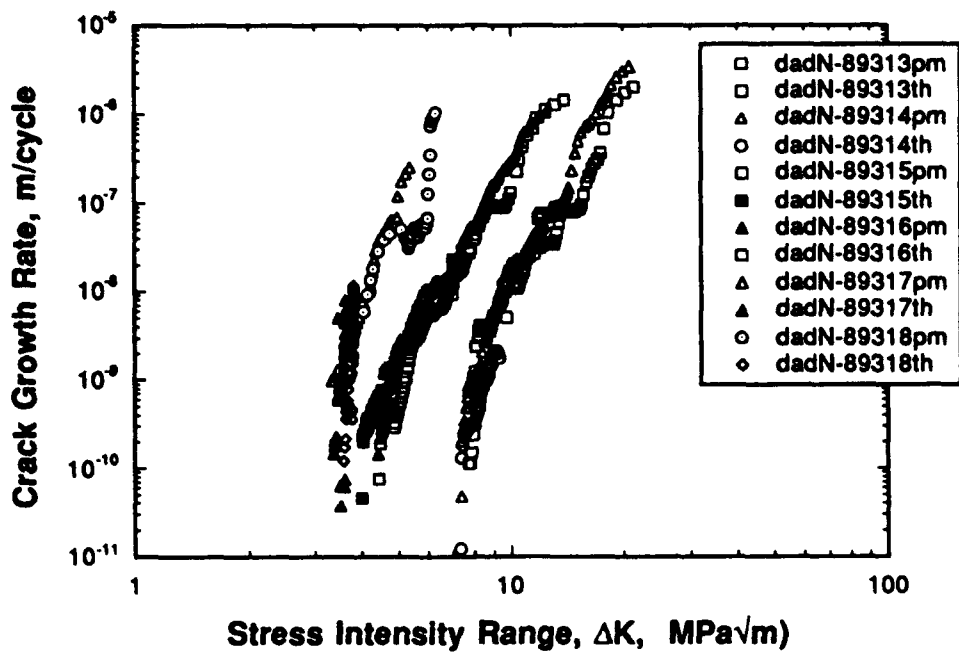
### 5.3 RESULTS AND DISCUSSION

Table 5.2 gives details on the tests at different stress ratios and the corresponding specimen numbers used for identification. In the following, the crack growth data will be presented and discussed for each microstructure in sequence. First, the crack growth data as a function of  $\Delta K$  for stress ratios of  $R=0.1$ ,  $0.5$  and  $0.8$  are presented in Fig. 5.3(a) for the  $\alpha_2+\beta$  microstructure. Fig. 5.3(b) shows the same data plotted as a function of  $\Delta K_{eff}$  for all the stress ratios. It can be seen that at each stress ratio, the crack growth data exhibit considerable scatter but not large enough to obscure the effects of stress ratio. While the effect of stress ratio on crack growth rate is more pronounced in terms of  $\Delta K$ , plotting in terms of  $\Delta K_{eff}$ , consolidated the  $R=0.1$  and  $0.5$  data. However, the  $R=0.8$  crack growth rates still show higher values compared to those for  $R=0.1$  and  $0.5$ . This could be due to a higher mean stress for the  $R=0.8$  data, which could induce static modes ( $K_{max}$  influenced) of crack extension in addition to cyclic crack extension. Crack closure was significant in only  $R=0.1$  tests. For  $R=0.5$  and  $0.8$  tests,  $K_{cl}$  values were lower than  $K_{min}$  throughout the tests. Hence crack closure influenced crack growth rates only at  $R=0.1$  tests. The variation of  $K_{cl}$  with  $K_{max}$  is presented in Fig. 4 for all the tests with  $R=0.1$ . It can be seen that closure levels remain constant around  $4 \text{ MPa}\sqrt{\text{m}}$  for the range of tests employed in the study.

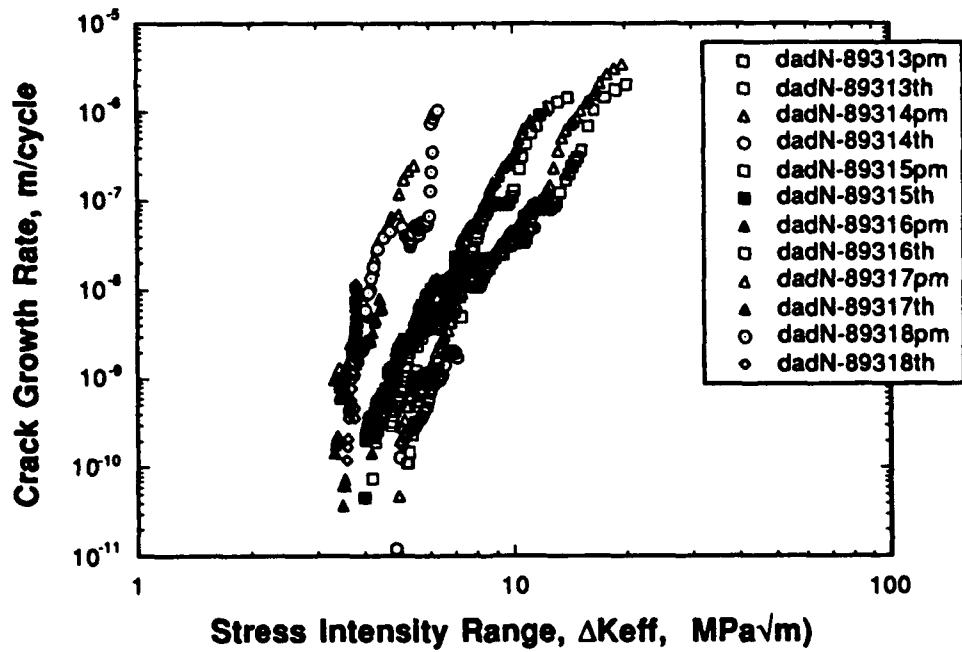
Crack growth data as a function of  $\Delta K$  and  $\Delta K_{eff}$  are presented for various stress ratios for the microstructure in the beta processed condition ( $\beta$  microstructure) in Figs. 5.5 (a) and (b) respectively. Similar to the  $\alpha_2+\beta$  microstructure, the  $\beta$  microstructure also exhibit the stress ratio effect on crack growth, particularly at high stress ratios. It can be seen that after plotting in terms of  $\Delta K_{eff}$ , the crack growth data for  $R=0.1$  and  $0.5$  agree well, while the data for  $R=0.8$  show significantly higher growth rates. This could again be due to the presence of  $K_{max}$  induced static fracture modes superimposed on the cyclic crack extension. Although the crack growth rates in terms of  $\Delta K_{eff}$  for  $R=0.1$  could be well reproduced after several tests, the crack closure variations for this microstructure were found to be non-unique. It can be seen in Fig. 5.6 that the variations in  $K_{cl}$  as a function of  $K_{max}$  are not reproducible between the tests conducted at  $R=0.1$ . This microstructure consisted of coarse lamellar colonies, which result in large deflections in crack path during crack growth. This is partly due to the inhomogeneous deformation arising from easy slip or shear parallel and across the lamellar structure due to slip compatibility

**Table 5.2 Specimen Identification and Stress Ratio for Large Crack Tests**

<u>Microstructure</u>	<u>Specimen</u>	<u>Type of Test</u>	<u>Stress Ratio</u>
$\alpha_2 + \beta$	89313pm	Increasing $\Delta K$	0.1
$\alpha_2 + \beta$	89313th	Decreasing $\Delta K$	0.1
$\alpha_2 + \beta$	89314pm	Increasing $\Delta K$	0.1
$\alpha_2 + \beta$	89314th	Decreasing $\Delta K$	0.1
$\alpha_2 + \beta$	89315pm	Increasing $\Delta K$	0.5
$\alpha_2 + \beta$	89315th	Decreasing $\Delta K$	0.5
$\alpha_2 + \beta$	89316pm	Increasing $\Delta K$	0.5
$\alpha_2 + \beta$	89316th	Decreasing $\Delta K$	0.5
$\alpha_2 + \beta$	89317pm	Increasing $\Delta K$	0.8
$\alpha_2 + \beta$	89317th	Decreasing $\Delta K$	0.8
$\alpha_2 + \beta$	89318pm	Increasing $\Delta K$	0.8
$\alpha_2 + \beta$	89318th	Decreasing $\Delta K$	0.8
$\beta$	89419pm	Increasing $\Delta K$	0.1
$\beta$	89419th	Decreasing $\Delta K$	0.1
$\beta$	89421pm	Increasing $\Delta K$	0.1
$\beta$	89421th	Decreasing $\Delta K$	0.1
$\beta$	89415pm	Increasing $\Delta K$	0.5
$\beta$	89415th	Decreasing $\Delta K$	0.5
$\beta$	89422pm	Increasing $\Delta K$	0.5
$\beta$	89422th	Decreasing $\Delta K$	0.5
$\beta$	89416pm	Increasing $\Delta K$	0.8
$\beta$	89420pm	Increasing $\Delta K$	0.8
Equiaxed $\alpha_2$	89444pm	Increasing $\Delta K$	0.1
Equiaxed $\alpha_2$	89444th	Decreasing $\Delta K$	0.1
Equiaxed $\alpha_2$	89445pm	Increasing $\Delta K$	0.1
Equiaxed $\alpha_2$	89445th	Decreasing $\Delta K$	0.1
Equiaxed $\alpha_2$	89447pm	Increasing $\Delta K$	0.1
Equiaxed $\alpha_2$	89447th	Decreasing $\Delta K$	0.1
Equiaxed $\alpha_2$	89448pm	Increasing $\Delta K$	0.5
Equiaxed $\alpha_2$	89448th	Decreasing $\Delta K$	0.5
Equiaxed $\alpha_2$	89451pm	Increasing $\Delta K$	0.5
Equiaxed $\alpha_2$	89451th	Decreasing $\Delta K$	0.5
Equiaxed $\alpha_2$	89446pm	Increasing $\Delta K$	0.8



5.3(a)



5.3(b)

Fig. 5.3. Fatigue crack growth rates of large cracks in  $\alpha_2+\beta$  microstructure at different stress ratios; (a) in terms of  $\Delta K$  and (b) in terms of  $\Delta K_{eff}$

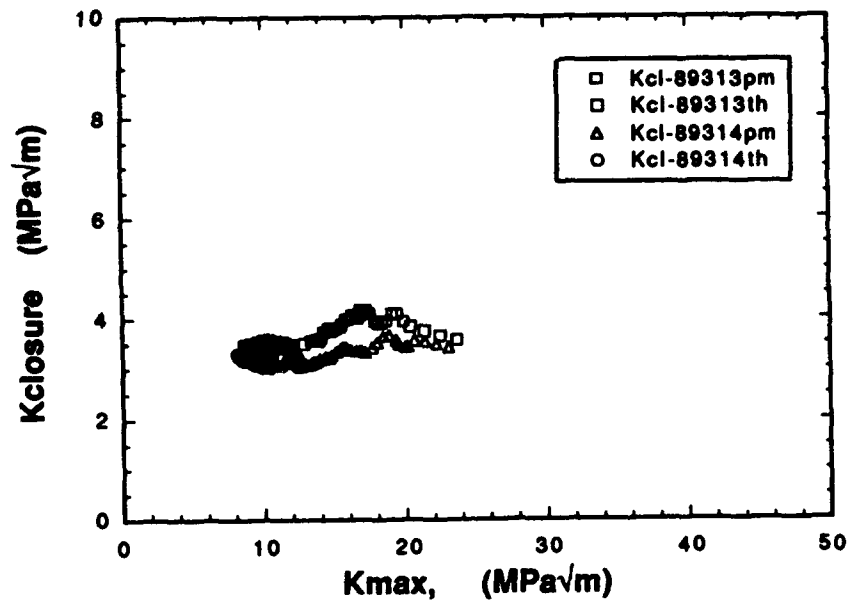
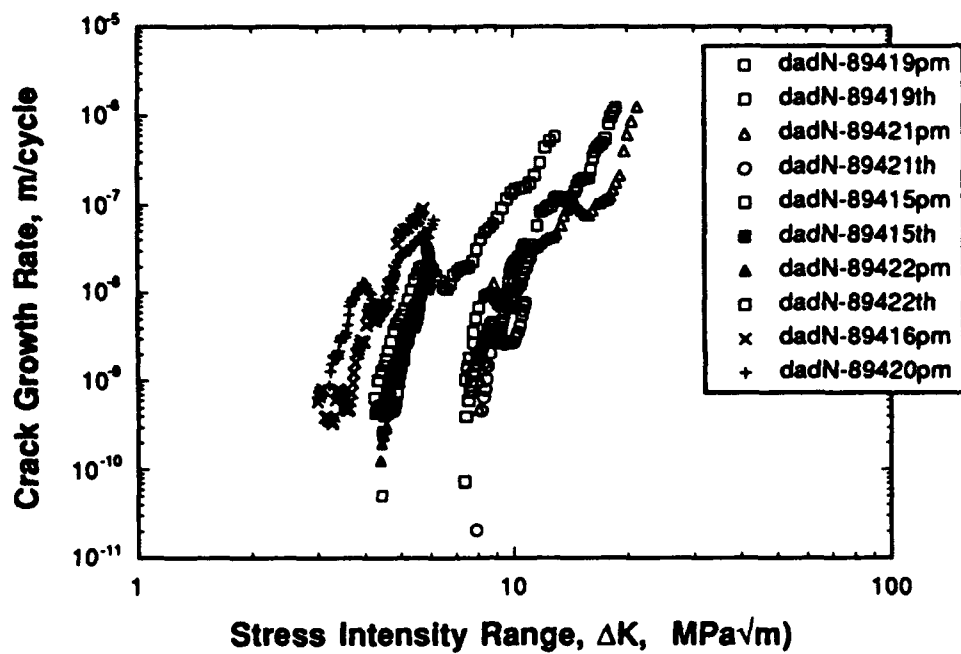
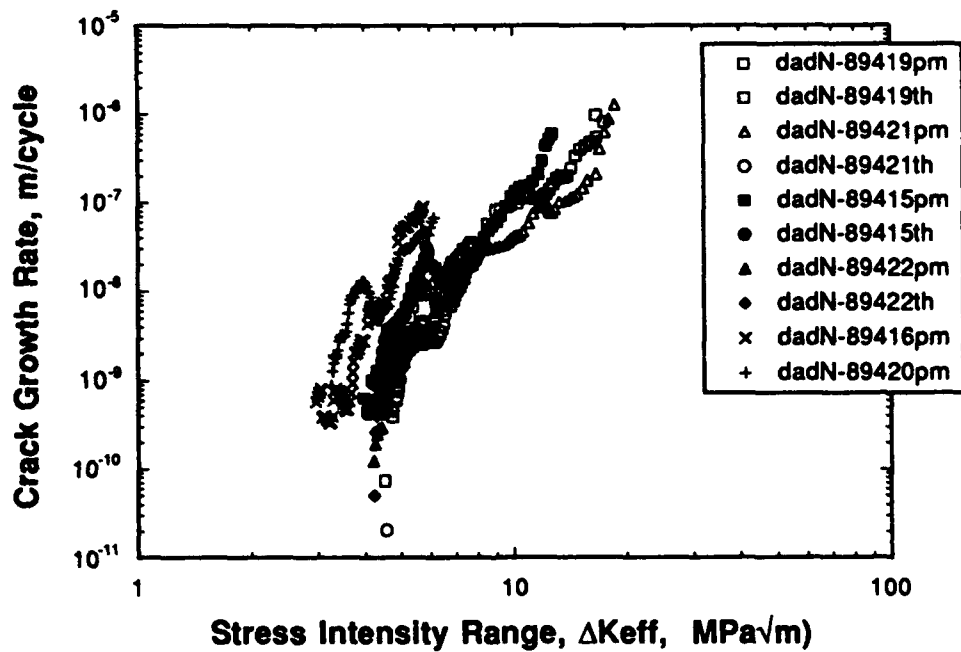


Fig. 5.4 The variation of  $K_{cl}$  as a function of  $K_{max}$  for  $R=0.1$  tests for the  $\alpha_2+\beta$  microstructure



5.5 (a)



5.5 (b)

Fig. 5.5. Fatigue crack growth rates of large cracks in  $\beta$  microstructure at different stress ratios; (a) in terms of  $\Delta K$  and (b) in terms of  $\Delta K_{eff}$

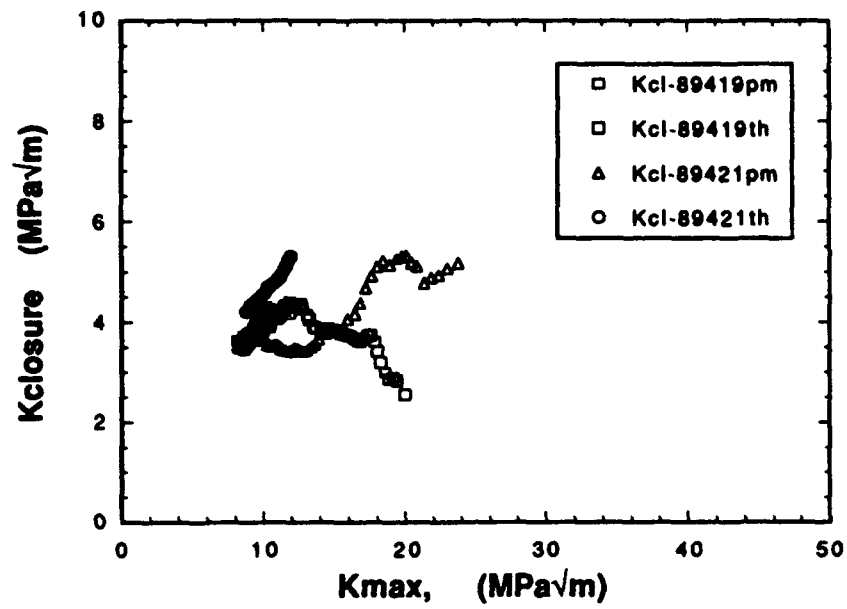
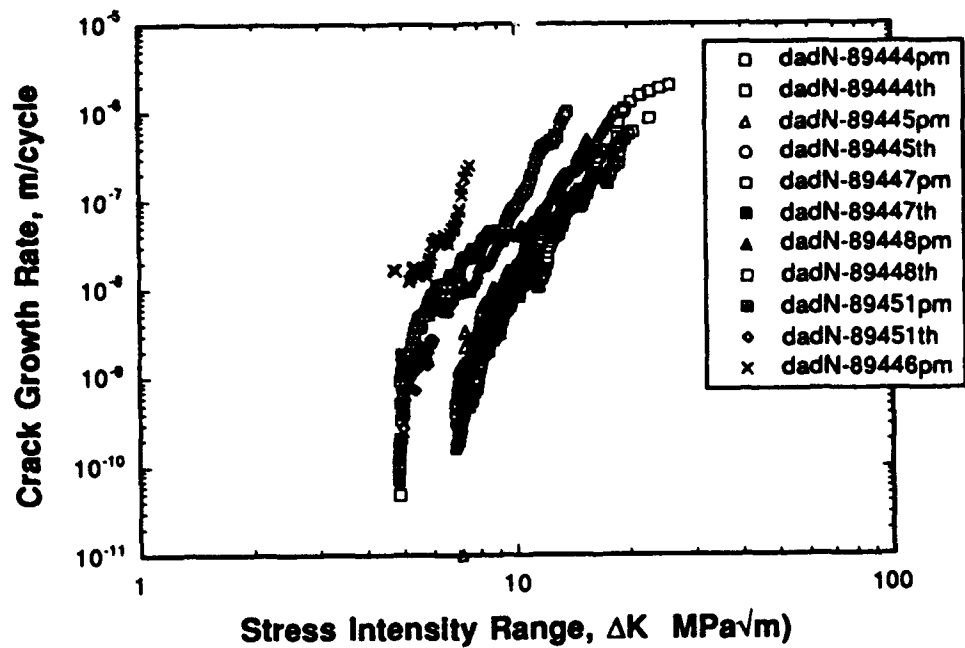
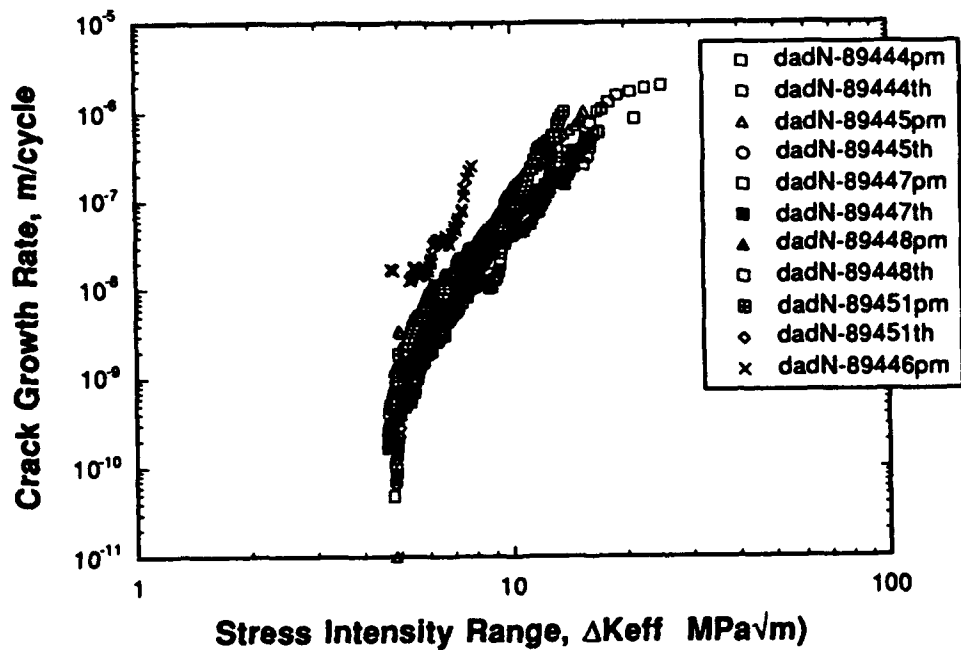


Fig. 5.6 The variation of  $K_{cl}$  as a function of  $K_{max}$  for  $R=0.1$  tests for the  $\beta$  microstructure



5.7(a)



5.7(b)

Fig. 5.7. Fatigue crack growth rates of large cracks in the equiaxed  $\alpha_2$  microstructure at different stress ratios; (a) in terms of  $\Delta K$  and (b) in terms of  $\Delta K_{\text{eff}}$

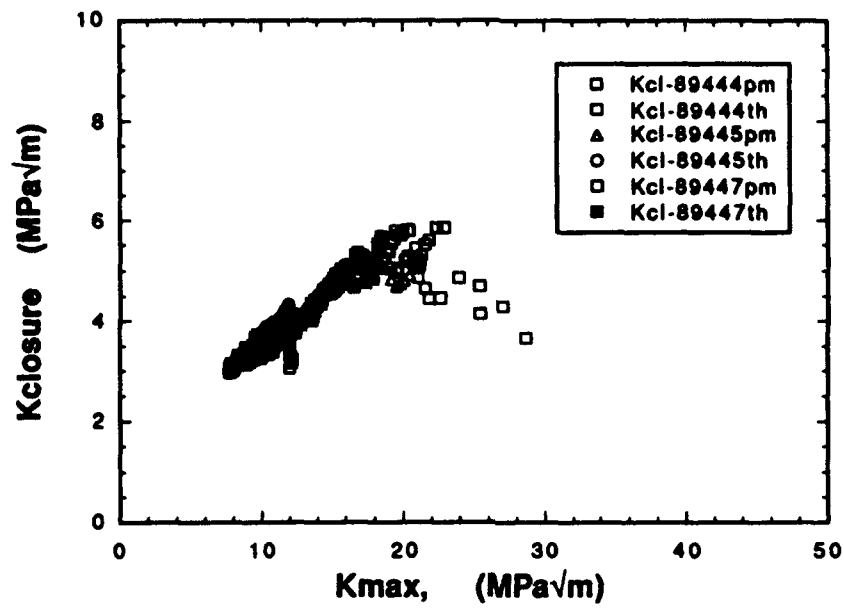


Fig. 5.8 The variation of  $K_{cl}$  as a function of  $K_{max}$  for  $R=0.1$  tests for the equiaxed  $\alpha_2$  microstructure



between the  $\alpha_2$  and  $\beta$  phases in the microstructure.

The results of crack growth tests for the completely equiaxed  $\alpha_2$  microstructure is very similar to that described above in the other two microstructures, viz., the  $\alpha_2+\beta$  microstructure and the  $\beta$  microstructure. The crack growth data as a function of  $\Delta K$  are given in Fig. 5.7(a), while the data as a function of  $\Delta K_{eff}$  are given in Fig. 5.7(b) for the different stress ratios employed in this study. Crack closure,  $K_{cl}$ , variation as a function of  $K_{max}$  is presented in Fig. 5.8. The crack closure variation in  $R=0.1$  tests is completely different in this microstructure, compared to the  $\alpha_2+\beta$  microstructure and the  $\beta$  microstructure. It can be seen in Fig. 8 that the  $K_{cl}$  first increases monotonically and then decreases with respect to  $K_{max}$  for all the tests in this microstructure, unlike the constant  $K_{cl}$  in  $\alpha_2+\beta$  microstructure and arbitrary  $K_{cl}$  variation in the  $\beta$  microstructure. The equiaxed  $\alpha_2$  microstructure consists of relatively fine equiaxed  $\alpha_2$  phases surrounded by discontinuous  $\beta$  phase. It is not clear whether this microstructural difference could have resulted in the closure behavior different from the other microstructures. Further investigation of crack closure behavior is required.

## 5.4 CONCLUSIONS

Fatigue crack growth behavior in all the microstructures, viz.,  $\alpha_2+\beta$  microstructure, the  $\beta$  microstructure and the equiaxed  $\alpha_2$  microstructure in Ti-24Al-11Nb alloy shows a strong sensitivity to stress ratio. The reproducibility of crack growth rates in a given test condition was good. The crack growth rates could not be consolidated even after accounting for the differences in crack closure. While the data at stress ratios  $R=0.1$  and  $R=0.5$  agree after correcting for crack closure,  $R=0.8$  data show significantly higher crack growth rates. This appears to result from the presence of static modes of crack extension at high stress ratios. Crack closure variations were different between the microstructures. Crack closure levels were constant for the  $\alpha_2+\beta$  microstructure, vary randomly in the  $\beta$  microstructure, while for the equiaxed  $\alpha_2$  microstructure, an increasing and then decreasing trend in crack closure, as a function of  $K_{max}$  was seen.

## REFERENCES

### Chapter 1

- (1.1) Surface-Crack Growth: Models, Experiments and Structures, ASTM STP 1060, W. G. Reuter, J. H. Underwood and J. C. Newman Jr., editors, ASTM, Philadelphia, PA 1990.
- (1.2) J. F. Yau, Fracture Mechanics: Seventeenth Volume, ASTM STP 905, J. H. Underwood, R. Chait, C. W. Smith, D. P. Wilhem, W. A. Andrews and J. C. Newman, Jr., editors, ASTM, Philadelphia, PA, 1986, pp. 601-624.
- (1.3) H. M. Muller, S. Muller, D. Munz and J. Neumann, Fracture Mechanics: Seventeenth Volume, ASTM STP 905, J. H. Underwood, R. Chait, C. W. Smith, D. P. Wilhem, W. A. Andrews and J. C. Newman, Jr., editors, ASTM, Philadelphia, PA, 1986, pp. 625-643.
- (1.4) T. A. Beer, Crack Shapes during Bi-axial Fatigue, Report No. 106, Materials Engineering - Mechanical Behavior, College of Engineering, University of Illinois at Urbana - Champaign, 1984.
- (1.5) I. F. C. Smith and R. A. Smith, Fatigue Fract. Engng. Mater. Struct., Vol. 5, No. 2, 1982, pp. 151-165.
- (1.6) J. L. Otegui, U. H. Mohaupt and D. J. Burns, Engng. Fract. Mech., Vol. 40, No. 3, 1991, pp. 549-569.
- (1.7) Y. Mutoh, G. H. Fair, B. Noble and R. B. Waterhouse, Fatigue Fract. Engng. Mater. Struct., Vol. 10, No. 4, 1987, pp. 261-272.
- (1.8) B. N. Cox and W. L. Morris, Fatigue'87, Proc. 3rd Int. Conf. Fatigue and Fatigue Thresholds, Vol. 1, EMAS Publishers Ltd., West Midlands, U. K., 1987, pp. 241-250.
- (1.9) P. K. Bolingbroke and J. E. King, Fatigue'87, Proc. 3rd Int. Conf. Fatigue and Fatigue Thresholds, Vol. 1, EMAS Publishers Ltd., West Midlands, U. K., 1987, pp. 281-290.
- (1.10) Y. Jingjun, P. Hongxun and K. Wei, Fatigue Fract. Engng. Mater. Struct., Vol. 13, No. 3, 1990, pp. 241-252.
- (1.11) K. Kishimoto, W. O. Soboyejo, R. A. Smith and J. F. Knott, Int. J. Fatigue, Vol. 11, No. 2, 1989, pp. 91-96.
- (1.12) C. W. Smith, Exp. Mech., Vol. , 1988, pp. 194-200.
- (1.13) E. Sommer, L. Hodulak and H. Kordisch, Trans. ASME, J. Pressure Vessels

Technology, Vol. , 1977, pp. 106-111.

- (1.14) H. Kitagawa and S. Takahashi, Proc. 2nd Int. Conf. Mechanical Behavior of Materials, 1976, pp. 627-631.
- (1.15) H. Kitagawa and S. Takahashi, Trans. Japan Soc. Mech. Engrs., Vol. 45, 1979, pp. 1289-1297.
- (1.16) L. Wagner, J. K. Gregory, A. Gysler and G. Lutjering, Small Fatigue Cracks, Proc. of International Workshop on Small Fatigue Cracks, R. O. Ritchie and J. Lankford, Eds., TMS-AIME, Warrendale, PA, 1986, pp. 117-124.
- (1.17) K. Tokaji, T. Ogawa, Y. Harada and Z. Ando, Fat. Fract. Engng. Mater. Struct., Vol. 9, No. 1, 1986, pp. 1-14.
- (1.18) A. W. Thompson, Proc. Int. Conf. Mechanical Behavior of Materials, Beijing, China, pp. 781-786.
- (1.19) P. Clement, J. P. Angeli and A. Pineau, Fat. Fract. Engng. Mater. Struct., Vol. 7, No. 4, 1990, pp. 251-265.
- (1.20) L. Farcy and M. Clavel, Proc. Conf. Advances in Aluminum and Magnesium Alloys, ASM International, Metals Park, OH, 1990, pp. 173-180.
- (1.21) K. S. Ravichandran and J. M. Larsen, Fracture Mechanics: 22nd Symposium, ASTM STP 1130, (Vol. 1), A. Saxena, H. A. Ernst and D. L. McDowell, Eds., ASTM, Philadelphia, PA, 1992, pp. 727-748.
- (1.22) K. S. Ravichandran and J. M. Larsen, Mater. Sci. Eng., Proc. Int. Conf. High Temperature Aluminides and Intermetallics, Vol. A153, 1992, pp. 499-507.
- (1.23) S. J. Hudak, Jr., D. L. Davidson and K. S. Chan, A. C. Howland and M. J. Walsch, Growth of Small Cracks in Aero-Engine Disk Materials, U. S. Air Force Report: AFWAL-TR-88-4090, Wright Patterson Air Force Base, OH, 1988.
- (1.24) J. M. Larsen, J. R. Jira and K. S. Ravichandran, Small-Crack Test Methods, ASTM STP 1149, J. M. Larsen and J. E. Allison, Eds., ASTM, Philadelphia, PA, 1992, pp. 57-80.
- (1.25) W. O. Soboyejo, K. Kishimoto, R. A. Smith and J. F. Knott, Fat. Fract. Engng. Mater. Struct., Vol. 12, 1989, pp. 167-174.
- (1.26) R. P. Gangloff, Fat. Fract. Engng. Mater. Struct., Vol. 4, 1981, pp. 15-23.
- (1.27) D. W. Carter, W. R. Canda and J. A. Blind, Surface Flaw Growth in Plates of Finite Thickness, U. S. Air Force Report: AFWAL-TR-86-4034, Wright Patterson Air Force Base, OH, 1986.
- (1.28) S. J. Holbrook and W. D. Dover, Engng. Fract. Mech., Vol. 12, 1979, pp. 347-364.
- (1.29) Y. Murakami and M. Endo, Engng. Fract. Mech., Vol. 17, 1983, pp. 1-15.

- (1.30) T. Fett, *Int. J. Fracture*, Vol. 36, 1988, pp. 55-69.
- (1.31) J. C. Newman, Jr., I. S. and Raju, *Fracture Mechanics: 14th Symposium, Vol.I: Theory and Analysis*, ASTM STP 791, J. C. Lewis and G. Sines, Eds., ASTM, Philadelphia, 1983, pp. I-238-I-265.
- (1.32) H. Tada, P. C. Paris and G. R. Irwin, *The Stress Analysis of Cracks Handbook*, 2nd Edition, 1985, Paris Productions Inc., St. Louis, Mo.
- (1.33) W. N. Sharpe, Jr., J. R. Jira and J. M. Larsen, *Small-Crack Test Methods*, ASTM STP 1149, J. M. Larsen and J. E. Allison, Eds., ASTM, Philadelphia, PA, 1992, pp. 92-115.

## **Chapter 2**

- (2.1) M. J. Blackburn and M. P. Smith, *Improved Toughness Alloys Based on Titanium Aluminides*, WRDC-TR-89-4095, Materials Directorate, Wright Laboratory, Wright Patterson Air Force Base, OH 45433, 1989.
- (2.2) K. S. Ravichandran and J. M. Larsen, *Fracture Mechanics: 22nd Symposium*, ASTM STP 1130, (Vol. 1), A. Saxena, H. A. Ernst and D. L. McDowell, Eds., ASTM, Philadelphia, PA, 1992, pp. 727-748.
- (2.3) K. S. Ravichandran and J. M. Larsen, *Mater. Sci. Eng.*, Vol. A153, 1992, pp. 499-507.
- (2.4) W. N. Sharpe, Jr., J. R. Jira and J. M. Larsen, *Small-Crack Test Methods*, ASTM STP 1149, J. M. Larsen and J. E. Allison, Eds., ASTM, Philadelphia, PA, 1992, pp. 92-115.
- (2.5) J. M. Larsen, J. R. Jira and K. S. Ravichandran, *Small-Crack Test Methods*, ASTM STP 1149, J. M. Larsen and J. E. Allison, Eds., ASTM, Philadelphia, PA, 1992, pp. 57-80.

## **Chapter 3**

- (3.1) S.Pearson, *Engg. Fract. Mech.*, 7(1975)235
- (3.2) *Small Fatigue Cracks*, Proc. 2nd Engg. Foundation Int. Conf./Workshop, Santa Barbara, edited R.O.Ritchie and J.Langford, 1986.
- (3.3) J.M.Larsen, T.Nicholas, A.W.Thompson and J.C.Williams in Ref.[2], p.499
- (3.4) P.Lalor, H.Sehitoglu and R.C.McClung, *The behavior of short fatigue cracks*. edited by K.J.Miller and E.R.de los Rios, EGF Publication, 1986, p.369
- (3.5) D.Taylor, *The behavior of short fatigue cracks*. edited by K.J.Miller and E.R.de

los Rios, EGF Publication, 1986, p.479

- (3.6) J.Langford and D.L.Davidson, in Ref.[2], p.51
- (3.7) K.Tokaji, T.Ogawa and Y.Harada, *Fat. Engg. Mat. Struct.*, 10(1987) 281
- (3.8) K.Tokaji, T.Ogawa Y.Harada and Z.Ando, *Fat. Engg. Mat. Struct.*, 9(1986) 1
- (3.9) J.C.Newman and I.S.Raju, *Fracture Mechanics, 14th Symposium, Vol.I: Theory and Analysis*, ASTM STP 791, edited by J.C.Lewis and G.Sines, ASTM, 1983, p.I-238
- (3.10) W. N. Sharpe, Jr., J. R. Jira and J. M. Larsen, *Small-Crack Test Methods*, ASTM STP 1149, J. M. Larsen and J. E. Allison, Eds., ASTM, Philadelphia, PA, 1992, pp. 92-115.
- (3.11) L.Wagner, J.K.Gregory, A.Gysler and G.Lutjering in Ref.[2], p.117
- (3.12) D.Taylor, *The behavior of short fatigue cracks*. edited by K.J.Miller and E.R.de los Rios, EGF Publication, 1986, p.479
- (3.13) D.Taylor and J.F.Knott, *Fat. Engg. Mat. Struct.*, 4(1981) 147
- (3.14) J.M.Larsen, PhD Thesis, Department of Metallurgy and Materials Science, Carnegie-Mellon University, Pittsburgh, 1987
- (3.15) K. S. Ravichandran and J. M. Larsen, *Fracture Mechanics: 22nd Symposium*, ASTM STP 1130, (Vol. 1), A. Saxena, H. A. Ernst and D. L. McDowell, Eds., ASTM, Philadelphia, PA, 1992, pp. 727-748.
- (3.16) K. S. Ravichandran and J. M. Larsen, *Mater. Sci. Eng.*, Vol. A153, 1992, pp. 499-507.
- (3.17) K.S. Ravichandran and J. M. Larsen, *An approach to measure the aspect ratios of three-dimensional surface cracks using a laser interferometric and photomicroscopic system*. *Fat. and Fract. Engg. Mat. Struct.*, (in press).
- (3.18) H. Kitagawa and S. Takahashi, *Proc. 2nd International Conference on Mechanical Behavior of Materials*, 1976, Boston, pp.627-631

#### **Chapter 4**

- (4.1) J.M.Larsen, PhD Thesis, Department of Metallurgy and Materials Science, Carnegie-Mellon University, Pittsburgh, 1987
- (4.2) L.Wagner, J.K.Gregory, A.Gysler and G.Lutjering in *Small Fatigue Cracks*, *Proc. 2nd Engg. Foundation Int. Conf./Workshop*, Santa Barbara, edited R.O.Ritchie and J.Langford, 1986, p.117
- (4.3) K.Tokaji, T.Ogawa and Y.Harada, *Fat. Engg. Mat. Struct.*, 10(1987) 281
- (4.4) K.Tokaji, T.Ogawa Y.Harada and Z.Ando, *Fat. Engg. Mat. Struct.*, 9(1986) 1

- (4.5) W. N. Sharpe, Jr., J. R. Jira and J. M. Larsen, Small-Crack Test Methods, ASTM STP 1149, J. M. Larsen and J. E. Allison, Eds., ASTM, Philadelphia, PA, 1992, pp. 92-115.

## **Chapter 5**

- (5.1) Fatigue Crack Growth Threshold Concepts, Edited by D. L. Davidson and S. Suresh, TMS-AIME, 1986.
- (5.2) Microstructure and Fatigue Crack Growth in Titanium Alloys, edited by J. C. Chesnutt, A. K. Chakraborty, TMS-AIME, 1989.
- (5.3) M. A. Hicks, R. H. Jeal and C. J. Beevers, Fat. Engng. Mater. Struct., 6 (1983) 51.
- (5.4) P. B. Aswath and S. Suresh, Metall. Trans., 22A (1991) p.817.
- (5.5) J. M. Larsen, in High Temperature Aluminides and Intermetallics, edited by S. H. Wang, C. T. Liu and D. Pope, TMS-AIME, Warrendale, 1991.
- (5.6) D. Banerjee, T. K. Nandy, A. K. Gogia and M. Muraleedharan, Proc. 6th World Conference on Titanium, Part II, 1988, p.1092.
- (5.7) Annual Book of ASTM standards, Vol. 03.01, Section 3, Standard Procedure for Fatigue Crack Growth Testing, E-647-88, 1992.